THERMAL AND HYDRAULIC PERFORMANCE COMPARISON OF CARBON BASED AND METAL BASED NANOFLUIDS IN FLAT PLATE SOLAR COLLECTOR: A CFD ANALYSIS

2022

الجامعـــة الإسلاميـــة للتكنولوجيا
UNIVERSITE ISLAMIQUE DE TECHNOLOGIE
ISLAMIC UNIVERSITY OF TECHNOLOGY
DHAKA, BANGLADESH
ORGANISATION OF ISLAMIC COOPERATION

THERMAL AND HYDRAULIC PERFORMANCE COMPARISON OF CARBON BASED AND METAL BASED NANOFLUIDS IN FLAT PLATE SOLAR COLLECTOR: A CFD ANALYSIS

A Thesis by

Mashrur Muntasir Nuhash (170011011)
Md. Ibthisum Alam (170011012)
Ananta Zihad (170011028)

Department of Mechanical and Production Engineering

Islamic University of Technology

May (2022)

THERMAL AND HYDRAULIC PERFORMANCE COMPARISON OF CARBON BASED AND METAL BASED NANOFLUIDS IN FLAT PLATE SOLAR COLLECTOR: A CFD ANALYSIS

Mashrur Muntasir Nuhash, Student ID: 170011011, Session: 2020-21
Md. Ibthisum Alam, Student ID: 170011012, Session: 2020-21
Ananta Zihad, Student ID: 170011028, Session: 2020-21

Submitted in Partial Fulfillment
of the Requirements
for the Degree of

Bachelor of Science in Mechanical Engineering

DEPARTMENT OF MECHANICAL AND PRODUCTION ENGINEERING

May (2022)

CERTIFICATE OF RESEARCH

This thesis titled "Thermal and Hydraulic Performance Comparison of Metal and Carbon Based Nanofluids in Flat Plate Solar Collector: A CFD Analysis" submitted by Mashrur Muntasir Nuhash (170011011), Md. Ibthisum Alam (170011012) and Ananta Zihad (170011028) have been accepted as satisfactory in partial fulfillment of the requirement for the Degree of Bachelor of Science in Mechanical Engineering.

Supervisor

Dr. Md. Rezwanul Karim

Associate Professor

Head of the Department

Prof. Dr. Md. Anayet Ullah Patwari

Professor

Department of Mechanical and Production Engineering (MPE)

Islamic University of Technology (IUT)

DECLARATION

I hereby declare that this thesis entitled "Thermal and Hydraulic Performance Comparison of Metal and Carbon Based Nanofluids in Flat Plate Solar Collector: A CFD Analysis" is an authentic report of study carried out as requirement for the award of degree B.Sc. in Mechanical Engineering at Islamic University of Technology, Gazipur, Dhaka, under the supervision of Dr. Md. Rezwanul Karim, Associate Professor, MPE, IUT in the year 2020-2021.

The matter embodied in this thesis has not been submitted in part or full to any other institute for award of any degree.

Mashrur Muntasir Nuhash

Mashrur Muntasir Nuhash
Student ID: 170011011

Ibthisum Alam

Md. Ibthisum Alam
Student ID: 170011012

Ananta Zihad

Ananta Zihad
Student ID: 170011028

ACKNOWLEDGEMENT

In the Name of Allah, the Most Beneficent, the Most Merciful.

First of all, we are grateful to ALLAH (SWT), the most benevolent and kind to provide us the strength and ability to complete the project and write this dissertation amidst all the challenges and hardship during our student life. Then, we would like to thank our supervisor Dr. Md. Rezwanul Karim, Associate Professor, MPE Department whose expertise and guidance was invaluable to us. His patient support throughout our final year has enabled us to overcome many obstacles in our thesis. We would also like to thank Dr. Arafat Ahmed Bhuiyan, Associate Professor, MPE Department and Mr. Md. Jahid Hasan, Research Assistant, MPE Department for their valuable guidance. Their informative remarks encouraged us to sharpen our thoughts and raise the quality of our work. Finally, we would like to thank our family and friends for their continuous support of our journey.

ABSTRACT

The constant rise in global temperature and the need to reduce fossil fuel consumption has made renewable energy sources desirable, especially solar energy systems. Flat plate solar collector (FPSC) is one of the most established solar energy technologies for lower to medium heat applications. FPSC has a wide range of implications because of their beneficiary of simple structure and low maintenance although the low thermal efficiency of the conventional system hinders their further development. The utilization of nanofluid as the heat transfer fluid in FPSC has been a popular trend for the last decades and significant improvements in the performance using this technique have been observed. Due to their better thermo-physical properties, carbon-based nanofluid possesses greater prospects compared to metal-based nanofluid. However, this subject matter has not been explored further yet. This study develops a CFD model to assess the performance of a metal-based based nanofluid (Al_2O_3/water) and two carbon-based nanofluids (SWCNT/water and MWCNT/water) at volume concentrations up to 1% in a simple FPSC. Based on thermal-hydraulic properties, a detailed comparison among these three nanofluids is made. The observation was, that, with the elevation of Reynolds number (Re) and volume concentrations the outlet temperature decreases and among the nanofluids Al_2O_3/water showed the lowest reduction. The types of nanofluids do not influence the friction factor. It was noticed that the friction factor decreases with the increase of Re while higher volume concentration necessitates greater pumping power. SWCNT/water nanofluid showed the best results in terms of heat transfer coefficient and Nusselt number followed by Al_2O_3/water and MWCNT/water. For enhancing both the Re and volume concentration the heat transfer coefficient is boosted. But for the Nu, the values rose with the higher Re while it deteriorated with the increasing volume concentration. The highest Stanton number was achieved for greater volume concentration and smaller Re. In the case of the thermal-hydraulic performance parameter (THPP) the values increased with higher volume concentrations although the Re had a negligible impact on it. The analysis indicates the SWCNT/water is the best performing nanofluid but requires a higher pumping power. This study concludes that carbon-based nanofluid outperforms metal-based nanofluid at both inlet temperatures of 303K and 313K. These findings from the study will be beneficial in future design of efficient solar thermal applications.

Keywords: Flat plate solar collector, Al_2O_3/water nanofluid, SWCNT/water nanofluid, MWCNT/water nanofluid, Thermal-hydraulic performance.

TABLE OF CONTENTS

LIST OF FIGURES

LIST OF TABLES

NOMENCLATURE

C_p = Specific heat

d = Diameter

dw = Distilled water

f = Friction factor

h = Heat transfer coefficient

k = Thermal Conductivity

K_B = Boltzmann constant

L = Riser tube length

n = Shape factor

Nu = Nusselt number

ΔP = Pressure drop

q^w = Heat flux on the tube wall

Re = Reynolds number

St = Stanton number

T= Temperature

v = Velocity

Abbreviations:

CFD = Computational fluid dynamics

FPSC = Flat plate solar collector

MWCNT = multi-wall carbon nanotube

SWCNT = single wall carbon nanotube

THPP = Thermo-hydraulic performance parameter

Greek Letters:

θ = Inclination angle

ρ = Density

ϕ = volume concentration

μ = Dynamic viscosity

Subscripts:

n_p = Nano-particle

b_f = Base-fluid

n_f = Nanofluid

CHAPTER 1. INTRODUCTION

A flat plate solar collector is a device that collects solar energy by absorbing solar radiation and transferring it into the working fluid for heating applications. Water has been utilized as the working fluid in FPSC traditionally. However, nanofluid has shown good prospects in the recent past and is now considered an alternative. Nanofluid is the fluid where solid nanoparticles are below 100 nm and are suspended in a base fluid [1], [2]. It is the high surface area and high thermal conductivity of nanoparticles that augments the heat exchange capability; exhibits excellent performance in FPSC [3].

1.1 BACKGROUND OF THE STUDY

The continuous growth in power demand calls for more sustainable means of extracting energy that leaves no environmental impact unlike the burning of fossil fuels. The report produced by Intergovernmental Panel on Climate Change (IPCC) forewarns a drastic rise in global warming between 2030 and 2052 ranging from 274.5 to 274.7 K, which was kept down to about 273 to 274.3 K above pre-industrial times [4]. This constant rise in global temperature enforces the reduction of fossil fuel consumption and emphasizes using renewable energy sources efficiently. Solar energy, abundant in almost all parts of the world is widely considered one of the best renewable sources compatible with fossil fuels. Solar collector and solar photovoltaic cells are the two most prominent systems to extract solar energy and use it in other desired forms of applications. Among solar collectors, FPSC is a low-cost, environment-friendly device used for low to medium-temperature domestic applications.

FPSCs are generally placed at the top of the facility and do not require any tracking system as both beam and diffuse radiation is absorbed by them [5]. In FPSCs, solar radiation transfers through the transparent glass envelop, then transferred to a high absorption surface [6][7]. A mixture of conduction and convection mechanisms then transfers the heat from the absorber plate to the working fluid running via the riser tubes [8]. This augments the temperature of the operating fluid at the tube outlet. FPSCs are mainly used for lower to moderate temperature applications (30 - 100˚C) like water and space heating for domestic and industrial applications [9]. Hybrid PV/T collectors are another exciting prospect that utilizes solar energy more efficiently by integrating

photovoltaic devices and FPSC, producing both electrical energy and thermal energy concurrently using same space [10]. But the low efficiency and low heat transfer of FPSC have always been the major barriers to the wide application of this technology [11][12].

Figure 1.1 Experimental FPSC setup by Yousefi et al. [13].

Differrent techniques have been used to enhance the efficiency of FPSCs. Among them, changing the design parameters and applying novel working fluids with better thermal conductivity and higher heat capacity are among the popular choices [14]. In conventional FPSC water, oil, or ethylene glycol are frequently used as working fluids, among them water is the most accepted. However, the disadvantage of the conventional working fluids is inferior thermo-physical properties, low convective heat transfer coefficient between the absorber and working fluids and low thermal efficiency. For improving the effectiveness of FPSCs, implementation of nanofluids with superior thermo-physical properties is an exciting prospect [15]–[17]. Among the nanofluids, metal-based nanofluids have been meticulously investigated. But due to their superior thermal performance, carbon-based metal nanofluids can be a much better eco-friendly alternative.

1.2 PROBLEM STATEMENT

There have been significant works on determining the compatibility of metal-based nanofluids in FPSC, both experimentally and analytically. The implication of carbon-based nanofluids in FPSC is comparatively a recent phenomenon and has not been explored to the required state. Some experimental works have been conducted, and very few numerical studies are available in the literature. Because of the improved conductivity, carbon-based nanofluids are an exciting prospect to augment the performance of the FPSC system. Nonetheless, superior thermo-physical properties of carbon-based nanofluids over metal-based nanofluids is laboratory established; there is a lack of study which investigate both types of nanofluid performance in FPSC together. Therefore, a study must be conducted that takes account of prominent metal-based and carbon-based nanofluids in FPSC and provide a compact performance analysis in terms of thermal-hydraulic parameters. The present work is focused on connecting this research gap which generates a detailed comparative study of metal-based and carbon-based nanofluids in FPSC using the computational technique.

1.3 GOAL AND OBJECTIVES

To analyze the performance of metal-based and carbon-based nanofluids in FPSC, change in thermal-hydraulic parameters during the heat transfer process need to be calculated. The aim of this investigation is to construct and develop a computational model which will generate the numerical results to calculate the necessary thermal-hydraulic parameters for analysis in detail. From the comparison of the thermal-hydraulic performances, the superior performance of metal-based or carbon-based nanofluids will be determined. Also, from the analysis, suitable nanofluids with concentration will be recommended for different operating conditions.

This study embarks on the following objectives:

i. Performance analysis of Al_2O_3/water (metal-based), SWCNT/water and MWCNT/water (carbon-based) nanofluids with concentrations of 0.025, 0.05, 0.075, 0.1, 0.5, and 1% were conducted at Re range of 1000 to 2000, operating at an inlet temperature of 303K and 313K.

ii. Determination of seven thermal-hydraulic properties - outlet temperature, friction factor, relative pumping power, heat transfer coefficient, Nusselt number (Nu), Stanton number (St) and thermal-hydraulic performance parameter (THPP) at each concentration of the selected nanofluid.

iii. Selection of best performing nanofluid from the comparison of the thermal-hydraulic properties.

1.4 METHODOLOGY OF THE STUDY

a) Data Collection On Nanofluid Properties:

Nanoparticle properties like particle diameter, density, thermal conductivity and specific heat capacity were collected from the literature review. In the analysis, considering water as the base fluid thermo-physical characteristics of the nanofluids were computed by applying empirical equations. The shape factors were considered in these equations, due to the spherical shape of metal-based nanofluids and the cylindrical shape of carbon-based nanofluids.

b) Development of a CFD Model for The FPSC:

A basic model of a FPSC was selected from literature analysis and CAD model was generated. To simplify the computational complexity, a simplified geometry was created. Then a CFD model was developed via the software ANSYS FLUENT for further analysis of the collector. The design condition was laminar flow, mixed convention and heat and mass transfer model. The model generated in this study can be applied for future analysis.

c) Validation of the numerical data with experimental results:

Results were simulated through the CFD model and were compared to the verified experimental work. The error limit generated should be less than 5%.

d) Analysis of thermal-hydraulic properties of the nanofluids:

In the next step, each concentration of the nanofluids was utilized at the predetermined Reynolds (Re) number range and the results of seven thermal-hydraulic properties were produced. The trend of the parameters at changing concentrations and Re were observed and suitable graphs were plotted.

e) Selection of the best performing nanofluid:

Finally, a comparative study of thermal-hydraulic performances among the nanofluids was made and the best performing nanofluid is chosen for the future solar flat plate collector applications.

1.5 ORGANIZATION OF THE THESIS

This study is mainly arranged into five chapters. Chapter 1 gives an idea of the FPSC system and applications of nanofluids in FPSC. The main goals and objectives of this study are also described in the first chapter. Literature review section is in Chapter 2 where major works in the FPSC system are briefly discussed. This chapter is divided into multiple subsections to distinguish between the application of carbon-based and metal-based nanofluids in FPSC. Chapter 3 describes the methodology of this research, where physical and mathematical models, necessary equations, boundary conditions, mesh generation process, and validation of the generated model are explained in different subsections. In Chapter 4, first the changes in nanofluids' properties are discussed. Then the seven selected thermo-physical properties are analyzed to obtain the best performing nanofluid for FPSC application. In the final chapter, Chapter 5, the whole study is summarized and the potential future research scope is highlighted.

CHAPTER 2. LITERATURE REVIEW

In this section, a detailed review of established literature has been performed about nanofluid applications in FPSC. The first two sections are about the application of metal-based and carbon-based nanofluids in FPSC. The third section focuses on the existing comparative study between metal-based and carbon-based nanofluids. The final section gives a detailed overview of the numerical models developed for FPSC.

2.1 REVIEW OF METAL-BASED NANOFLUIDS IN FPSC

The metal oxide-based nanofluids - Al_2O_3/water, CuO/water, ZnO/water, MgO/water, TiO_2/water etc. nanofluids are mainly selected as the working fluid as they provide relatively low density [18]. Gupta et al. [19] evaluated the inclusion of thin-film Al_2O_3/water nanofluid in a low-temperature direct absorption solar collector. In comparison with water, at a 2 L/min flow rate, the collector efficiency was increased by 22.1%, 39.6%, 24.6%, and 18.75% for 0.001, 0.005, 0.01, and 0.05% volume concentration, respectively.

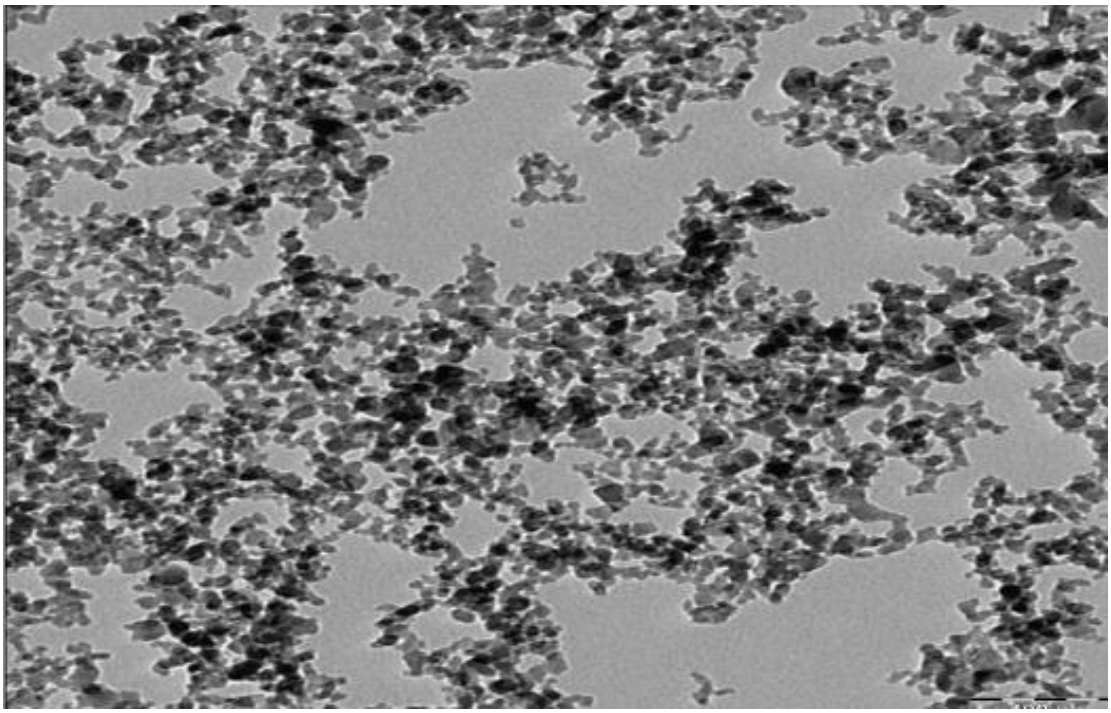

Figure 2.1 Transmission electron microscopy (TEM) image of Al_2O_3/water nanofluid [20].

Verma et al. [12] applied MgO/water nanofluid of 0.25, 0.5, 0.75, 1.0, 1.25, and 1.5% volume concentration at 0.5, 1.0, 1.5, 2.0, and 2.5 L/min flow rates in a FPSC. In contrast to water, the maximum energy and exergetic efficiency enchancement were 9.34% and 32.23%, respectively, for 0.75% particle concentration and 1.5 L/min flow rate. At that operating condition, the maximum Bejan number of 0.96 was obtained. A 6.84% increase in pressure drop was observed for 0.75% concentration at 1.5 L/min, which became higher for increased concentration value. Applying MgO nanofluid at a 0.75% concentration, 12.5% of the conventional solar collector's surface area could be reduced.

In a FPSC, the effect of Al_2O_3/water nanofluid at 0.1% concentration was investigated by Mirzaei et al. [21]. At a 2 L/min flow rate the highest enhancement of average efficiency was 23.6%. Applying Al_2O_3 nanofluid at 1, 2 and 4 L/min flow rates increased the temperature of water in a storage tank by 7.1%, 8.4% and 7.5%, respectively.

In experimental work, Sharafeldin et al. [22] integrated CeO_2/water nanofluid to augment the energy efficiency of FPSC. 0.0167%, 0.033%, and 0.066% volume concentrations of CeO_2 were incorporated with different mass flow rates including 0.015, 0.018, and 0.019 kg s^{-1} m^{-2}. In contrast to water, the highest enhancement in efficiency recorded 10.74% at zero reduced temperature parameter for a 0.066% volume fraction at a mass flow rate of 0.019 kg s^{-1} m^{-2}. They concluded that a nanoparticle volume concentration of 0.033% was preferable as it presented better efficiency in a wide range.

The impact of SiO_2/deionized water nanofluid in FPSC was inquired experimentally and analytically by Jouybari et al. [23]. SiO_2 nanoparticles diameter of 20-30 nm and concentrations up to 0.6% were examined in the study. Both experimental and analytical results indicated that silica nanoparticles provide significant improvement despite lower thermal conductivity.

An experiment by Stalin et al. [24] evaluated the performance of FPSC using a series of volume concentrations of CeO_2/water nanofluid at various flow rates. The outcome showed 28.07% enhanced efficiency from the base fluid when 0.05% CeO_2/water at 2

L min^{-1} was employed. The maximum exergy increment of 5.8% was reported at 0.05% volume concentration. In comparison to the conventional collector, CeO_2/water utilized FPSC allowed 24.52% collector area reduction for the same capacity.

Moravej et al. [25] conducted an experiment where water was replaced by surfactant-free rutile TiO_2/water nanofluid. Their experimental study shows that the collector gives better performance for increased nanoparticle concentration. At a flow rate of 0.050467 L/s, the efficiency was improved by 17.41%, 27.09%, and 33.54% for 1 wt%, 3 wt%, and 5 wt% nanoparticle concentrations of TiO_2.

Water-based Cu nanofluid was used to examine the heat transfer, friction factor along with efficiency of FPSC, with the addition of twisted tape inserts [26]. In that experiment, the FPSC with twisted tape inserts (H/D = 5) increased the Nu up to 46.90% when 0.3% volume concentrations of Cu nanofluid were used. At this condition, collector efficiency was measured as 64%, compared to the 52% efficiency with water in the plain collector. The report suggested that a 25% reduction in collector size was possible using Cu nanofluid in this altered collector design.

An experimental study found that 0.2-1 vol% of ZnO nanofluid with water:EG (50:50) base fluid can be stable for more than 25 days [27]. In this concentration range, the maximum thermal efficiency in FPSC (69.24%) was noted for 1 vol% ZnO nanofluid operating at 60 LPH volumetric flow rate. This was 19.2% higher than the water:EG (50:50) base fluid. At this operating condition, an 18% increase in absorbed energy parameter and a 62.5% decrease in removed energy parameter were observed.

Choudhary et al. [28] evaluated the stability issue and thermal performance in a FPSC for EG:Water based MgO nanofluid. They found nanofluid up to 0.2 vol% concentration, in addition to CTAB surfactant was capable of remaining stable for more than 15 days. According to the work, the highest thermal efficiency of the collector (69.1%) was gained by applying 0.2 vol% MgO nanofluid at 1.5 L/min. The efficiency enhancement was 1.167-times than the EG:Water based fluid. The study showed a 16.74% increase in the absorbed energy parameter and a 52.2% decrease in the heat loss parameter at this identical condition.

Okonkwo et al. [29] used Al_2O_3 and hybrid Al_2O_3-Fe/water based nanofluid in FPSC. The parametric study showed that 0.1% Al_2O_3/water nanofluid improved the energy and exergy performance of FPSC in contrast to hybrid water nanofluid. A 2.16% increase of the thermal efficiency was reported for Al_2O_3/water nanofluid, where implying hybrid nanofluid decreased the efficiency by 1.79%. But in terms of exergetic efficiency hybrid nanofluid enhanced the efficiency by 6.9% compared to the 5.7% for Al_2O_3/water nanofluid.

An experimental evaluation on stability and performance in FPSC was conducted for Fe_3O_4 ethylene glycol-distilled water (50:50) based nanofluid [30]. In the study, 1 vol % Fe_3O_4 with a 30 L/h mass flow rate exhibited the highest outlet temperature and highest efficiency in the collector. At this condition, improvement in the thermal efficiency and heat absorption parameter, $F_R(\tau\alpha)$ was achieved by 15.27% and 17.05% consecutively.

The experimental study of Farhana et al. [31] was focused on improving the efficiency of FPC via utilizing metal oxide (Al_2O_3) and biodegradable (Crystal nano-cellulose, CNC) nanofluid as working fluids. Volume fractions of 0.3% and 0.5% were used for each nanofluid in this investigation. The outlet temperature enhanced maximum by 4.4% for using 0.5% Al_2O_3 nanofluid instead of water. The highest efficiency increment was reported 2.48% for 0.5% Al_2O_3 and 8.46% for 0.5% CNC nanofluids.

In their experimental study, Alklaibi et al. used 0.2, 0.4, 0.6, 0.8 and 1.0% volume concentrations of nanodiamond (ND) nanoparticles in water for FPSC [32]. The result showed that 1.0 vol% ND/water nanofluid provided the maximum collector efficiency of 69.85%, an increase of 12.7% from the conventional FPSC.

CuO+Al_2O_3/water hybrid nanofluid was utilized in an energy storage system coupled with FPSC [33]. The result depicted an increase in heat capacity of the energy storage system and recommended the use of hybrid nanofluid over pure water in FPSC.

2.2 REVIEW OF CARBON-BASED NANOFLUIDS IN FPSC

In recent times carbon-based nanofluids like Multiwall Carbon Nanotubes (MWCNT), Single Wall Carbon Nanotubes (SWCNT), Graphene Nano Palettes (GNP), Graphene Oxide (GO) etc [34] gained significant attention. The carbon-based nanofluids provided better thermal conductivity and lower density than metal-based nanofluids. The impact of MWCNT/water on FPSC was investigated by Yousefi et al. [35]. Without surfactant 0.2 wt.% MWCNT/water lessened the efficiency, but using Triton X-100 surfactant with the same nanofluid provided better efficiency compared to water. Without surfactant 0.4 wt.% MWCNT provided higher efficiency than both water and 0.2 wt.% MWCNT.

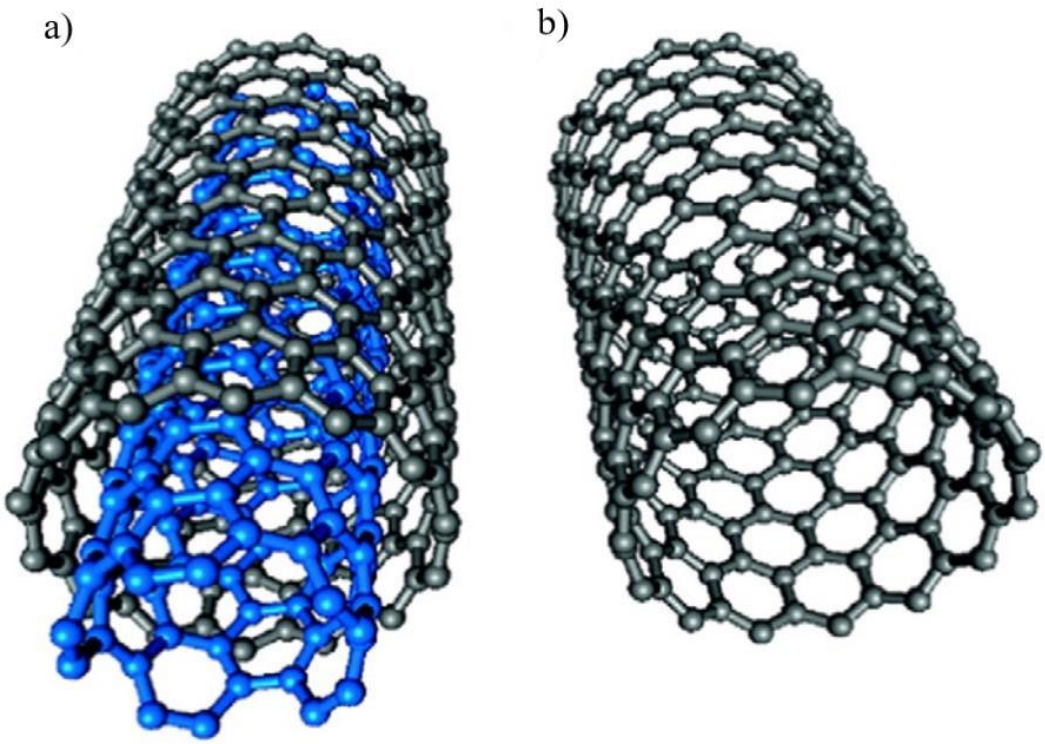

Figure 2.2 Structural image of a) MWCNT and b) SWCNT [36].

In another investigation, the thermal efficiency, overall heat transfer coefficient, and friction factor of a FPSC were determined by applying three mass concentrations of graphene oxide (GO), which were 0.005, 0.01, and 0.02%, without any surfactant by Vincely et al. [37]. 0.0067, 0.01, 0.0133, and 0.0167 kg/s mass flow rates were used to perform this experiment. The FPSC efficiency improved with the flow rate and mass fraction of nanofluid. The GO nanofluid of 0.02 mass fraction at 0.0167 kg/s showed

an enhancement of 7.3% in efficiency in contrast to deionized water. 8%, 10.9%, and 11.5% improvements in heat transfer coefficient were observed using 0.005, 0.01, and 0.02 mass fractions of GO nanofluid, respectively.

Vakili et al. [38] investigated the effect of graphene nanoplatelets-deionized water nanofluid in a volumetric solar collector. The maximum zero efficiency was 83.5%, 89.7%, and 93.2% at a 0.015 kg/s flow rate for 0.0005, 0.001, and 0.005 wt.% concentrations, respectively, whereas the base fluid had a zero efficiency of 70%. The maximum heat loss coefficient was associated with 0.005 wt.% at 0.0075 kg/s.

The effectiveness of nanographene with a mixture of water and ethylene glycol (70:30 wt.%) as the working fluid was investigated by Bioucas et al. [39]. In the indoor experiment with the highest concentration of 0.10 wt.%, a 1.84˚C higher outlet temperature was obtained than the base fluid. With 0.10 wt.% nanographene in the outdoor setup, the efficiency increased by 5.90% than the base fluid.

Eltaweel et al. [40] suggested implying MWCNT/water nanofluid in thermosiphon mode in FPSC as a viable solution to augment the energy and exergy efficiency. Their experimental work depicted a 34.13% efficiency increase and 34% collector area decrease compared to water by using 0.1 wt% of MWCNT in thermosiphon mode. A further 6.21% enhancement of the thermal efficiency was observed applying a 1.5 L/min volumetric flow rate for the same concentration; the results presented that nanofluid in thermosiphon provided better results compared to the water in forced circulation.

The effect of clove treated GNP-water nanofluid on FPSC was investigated for three different mass fractions at three different mass flow rates [41]. The maximum 78% collector efficiency was generated for mass fraction of 0.1% at a 0.0260 kg s^{-1} m^{-2} flow rate. This accounted 18.2% increase in the efficiency than the base fluid under the same condition. The maximum increase in heat absorbed factor and heat removal factor of 22.30% and 26.79%, respectively, was reported for the same input parameter.

Alawi et al. [42] implied pentaethylene glycol-treated graphene nanoplatelets (PEG-GNP) while water was used as the working fluid in FPSC. The experimental outcome

indicated a 32.4% enhancement in collector efficiency for 0.1 wt % PEG-GNP at a 0.025 kg s^{-1} flow than water. At this condition, an increment in heat absorption factor and heat removal factor was observed by 12.79% and 6.40%, respectively.

Gupta et al. [43] analyzed the performance of FPSC under the volumetric direct absorption mode at 30, 40, and 60 L/h flow rates using Al_2O_3 based nanofluid with a 0.02% concentration and without nanofluid. With nanofluid, the outlet temperature of the FPSC was 5-10˚ C higher than without nanofluid at the specified flow rates. The thermal efficiency of the collector was increased by 9-40% using nanofluid. The maximum efficiency for both with nanofluid and without nanofluid was achieved at a flow 60 L/h.

Covalently functionalized GNPs with triethanolamine (TEA-GNPs), for different surface areas, were synthesized in concentrations ranging up to 0.1% to apply in the FPSC [44]. The experimental results found a 0.1% weight concentration of water-based nanofluid with TEA-GNP nanoparticles as the best alternative nanofluid for enhanced performance. Using this nanofluid, the efficiency of the collector gain was 10.53% in comparison to the water. A code was constructed and developed using MATLAB in the study to evaluate the measured data and it showed acceptable accordance with the experimental results.

Hybrid nanofluid of CF-MWCNT and CF-GNP with h-BN was the working fluid in FPSC to measure the thermal performance improvement [45]. Tw-80 surfactant was used to prepare this water-based hybrid nanofluid. From the conducted experimental, it was observed the hybrid nanofluid provides significantly better performance in FPSC than the nanofluid in isolation. The maximum collector efficiency of 85% was obtained using 0.10 wt% of hybrid nanofluid at 4 L/min flow rate which was 20% better than using the base fluid.

2.3 REVIEW OF THE COMPARISON OF METAL-BASED AND CARBON-BASED NANOFLUIDS IN FPSC

Researchers also tried to compare the performance of metal oxide and carbon-based nanofluids performance in FPSC [46]. Verma et al. [47] compared the energetic and

exergetic efficiency of six different nanofluids: SiO_2/water, TiO_2/water, CuO/water, Al_2O_3/water, Graphene/water, and MWCNTs/water using six different particle volume concentrations (0.25, 0.5, 0.75, 1, 1.25, and 2%) with varying mass flow rates. The optimum values of concentration and mass flow rate were obtained in the range of 0.75-1% and 0.03 kg/s, respectively. The maximum increase in energetic efficiency was observed to be 23.47% greater than the base fluid for MWCNTs at a 0.75% volume concentration and a 0.025 kg/s mass flow rate. Graphene, CuO, Al_2O_3, TiO_2, and SiO_2 nanofluids also increased the energy efficiency by 16.93%, 12.64%, 8.28%, 5.09%, and 4.08%, respectively. At the same optimum concentration and mass flow rate, MWCNTs nanofluid enhanced 29.32% exergetic efficiency compared to the base fluid, followed by 21.46%, 16.67%, 10.86%, 6.97%, and 5.74% enhancement for Graphene, CuO, Al_2O_3, TiO_2, and SiO_2 nanofluids, respectively. Variation of pumping power loss and Bejan number with the volume concentration were also shown in the study. The MWCNTs/water nanofluid reached the highest Bejan number of 0.97 and had a 19.11% surface area reduction possibility.

The experimental work by Tong et el. [48] compared the performance of Al_2O_3, CuO, MWCNT, Fe_3O_4, WO_3 and CeO_2 water-based nanofluids in FPSC under different operating conditions. The results showed that the efficiency was highest (87%) for MWCNT nanofluid and the heat loss coefficient was lowest (7.86) for WO_3 nanofluid. The influence of nanofluid concentration on collector performance was highest (11.2%) for CeO_2 and lowest (2.5%) for Fe_3O_4. Deviation from optimal solar concentration has the biggest impact on MWCNT (53%) nanofluid and the smallest (23.2%) on CuO nanofluid. For enhancing the temperature gradient eight times, the efficiency reduction was 45.7% for 0.005 vol% MWCNT nanofluid and 21.7% for 1.0 vol% Al_2O_3 nanofluid. In terms of nanoparticle size, CuO showed the most sensitivity, decreasing the efficiency by 7.9% for increasing the nanoparticle size by five times from that showing the maximum efficiency.

2.4 REVIEW OF THE NUMERICAL METHODS DEVELOPED USING NANOFLUID IN FPSC

Many researchers also tried to define specific numerical models for FPSC using different nanofluids. From numerical and literature study, the efficiency, cost and

embodied energy savings, size and weight reduction of a FPSC were estimated for CuO, Si_2O, TiO_2, and Al_2O_3 nanofluids by Faizal et al. [49]. Compared to water, the efficiency was enhanced by 38.5% for CuO and 28.8% for Si_2O, TiO_2, and Al_2O_3 nanofluids. Size reduction was 25.6%, followed by 21.6%, 22.1%, and 21.5% for CuO, Si_2O, TiO_2, and Al_2O_3 nanofluids, respectively. Solar collectors using nanofluids had an average payback period of 2.4 years and an average value of embodied energy savings of 220 MJ, compared to water as the working fluid. Nanofluids reduced CO_2 emissions by an average of 170 kg compared to traditional collectors, which eventually reduced the total damage cost.

Nasrin et al. [50] compared the 2D and 3D models using the finite element method for Cu/water nanofluid employed in FPSC. The results showed an increase of 8% thermal efficiency for Cu/water nanofluid in the 3D simulation, which was 5% higher than the efficiency in the 2D simulation.

Farajzadeh et al. [51] evaluated the efficiency of the FPSC experimentally and numerically using nanofluids- Al_2O_3-H_2O (0.1 wt.%), TiO_2-H_2O (0.1 wt.%), and their mixture having an equal ratio (0.1 and 0.2 wt.%). 19%, 21%, and 26% higher efficiency was achieved than the base fluid using Al_2O_3, TiO_2, and mixed nanofluid at 0.1 wt.%, respectively. In the experiment, compared to the 1.5 L/min volume flow rate, the efficiency increased by about 8% and 5% for 2.0 L/min and 2.5 L/min volume flow rates, respectively. Increasing the concentration of mixed nanofluid from 0.1 wt.% to 0.2 wt.% enhanced the efficiency by about 3-5%. Compared to the experimental results, the numerical modelling showed a 3% higher efficiency for water and a 5% lower efficiency for mixed nanofluid at 0.1 wt.%.

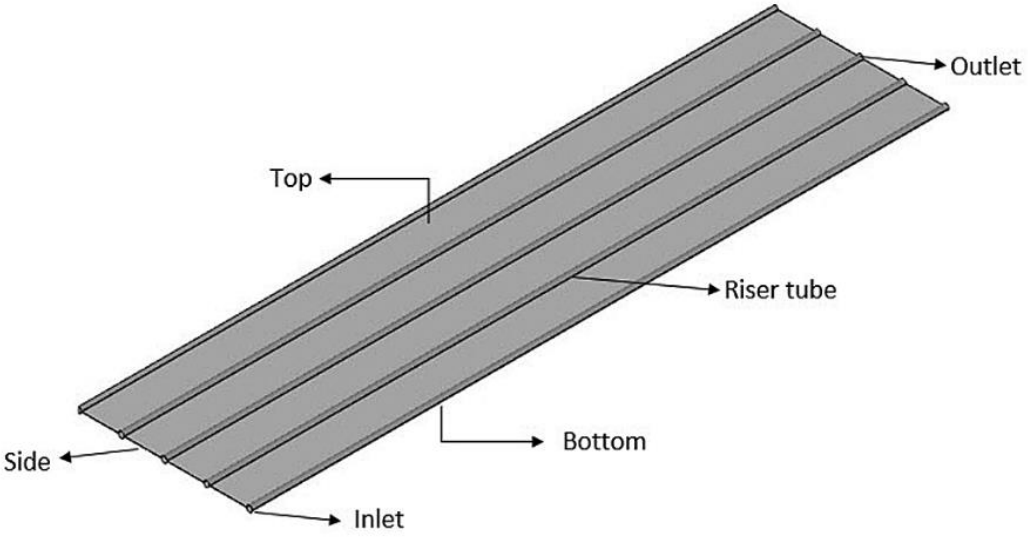

Figure 2.3 Boundary conditions of FPSC from the study of Farajzadeh et al. [51].

A theoretical study was performed to analyze CuO/water as the operating fluid in FPSC [52]. The results concluded that nanoparticle volume concentration impacted the collector efficiency more strongly than the nanoparticle size. It was observed that up to volume concentration of 2% CuO the heat removal factor increased and the overall heat loss coefficient decreased. A 5% increase in collector efficiency was achieved using the CuO nanoparticle size of 25 nm at the optimal 2% volume concentration.

Hawwash et al. [1] evaluated the impact of Alumina nanofluids on the efficiency of FPSC experimentally and numerically. The volume fraction of the nanofluid was in the range of 0.1-3% and a 5.5 L/min flow rate was applied. The efficiency increased up to 0.5% of the volume concentration, but then the efficiency started to decrease. Using Alumina nanofluid at low temperature and high temperature differences, 3% and 18% improvements in efficiency were observed, respectively, than double distilled water. Increasing the volume fraction of the nanofluid from 0.1% to 3% enhanced the pressure drop by about 28 Pa.

Shamshirgaran et al. [53] developed a MATLAB code to evaluate the performance of CuO/water in a FPSC under steady state, laminar conditions. The CuO nanofluid had a positive impact on the energetic efficiency and decreased the total entropy generation. Using 25 nm copper nanoparticles at a 4% volume concentration improved the energetic efficiency of the FPSC from 70.3% to 72.1%. At a specific volume

concentration, the larger size of copper nanoparticles reduced the thermal efficiency and increased the total heat generation than the 25 nm nanoparticles.

A numerical method was implemented to analyze the turbulent three-dimensional flow inside the collector pipe with a twisted tape insert [54]. Al_2O_3/water nanofluid was used as the working fluid in the FPSC to simulate the results. The realizable k-ε model was considered to model the steady three-dimensional flow in the turbulent regime and final sets of equations were solved via FVM in Ansys Fluent. The outcome indicated that with increasing diameter ratio (D*) and no. of revolutions (N) turbulent intensity inside the pipe intensifies, which simultaneously provided a better Nu and a larger pressure loss.

In their numerical study, Saffarian et al. [55] implemented three different flow path shapes in FPSC with addition to Al_2O_3/water and CuO/water to investigate the change of heat transfer characteristics. Flow path of U-shaped, wavy and spiral pipes with identical pipe lengths were designed. Nanofluids of volume fractions 1% and 4% were applied to track the results in these arrangements. The numerical output showed that the heat transfer coefficient and Nu increased significantly in wavy and spiral pipes. It was noticed that wavy pipe generated the highest pressure drop among these flow path shapes. The output indicated that the utilization of nanofluid increased the heat transfer coefficient but not the Nu except for CuO 4%. It was revealed that CuO/water nanofluid with a volume fraction of 4% in a wavy pipe arrangement enhanced the heat transfer coefficient up to 78.25%.

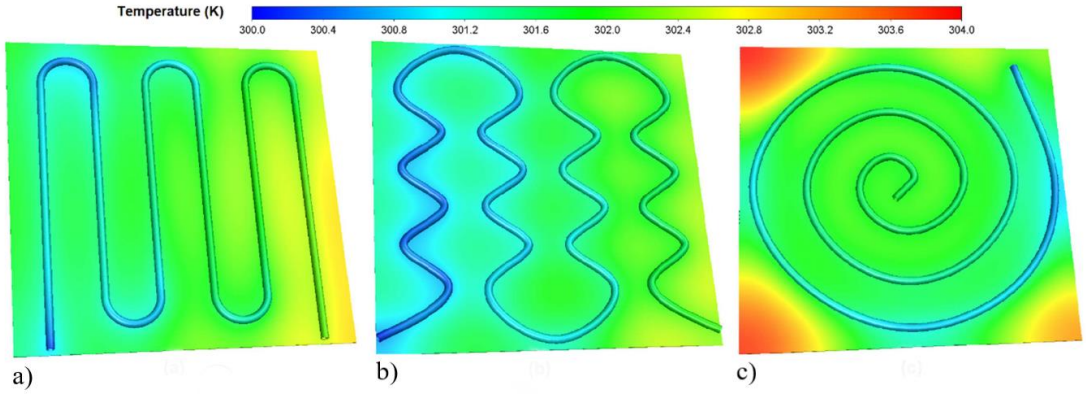

Figure 2.4 Temperature distribution in a) U-shaped, b) wavy and c) spiral pipe designs from Saffarian et al. [55].

Darcy-Brinkman model was used to assess the thermal performance of hybrid (copper and alumina) water-based nanofluid in FPSC [56]. The results indicated that in a constant volume fraction of nanoparticles, the hybrid nanofluid of copper and alumina with equal fractions provides better heat transfer characteristics than the pure alumina particles and there was a very small difference with pure copper nanoparticles.

The energetic and exergetic performance of heat pipe FPC operating with nanofluids were characterized numerically by applying a one-dimensional transient heat transfer model [57]. CuO, Al_2O_3, and TiO_2 nanoparticles in the concentration range of 0-3% with water were compared for various operating parameters. The output showed the highest energetic and exergetic efficiencies for 3% CuO/water. In comparison to water, it enhances the energetic and exergetic efficiencies by 2.7% and 11.1% respectively. Among the studied working fluids, CuO nanofluid was guilty of generating the largest pressure drop across the collector. At the concentration of 3% CuO, the increase in pressure drop was estimated 13.26% from the water base fluid.

Bezaatpour et al. [58] investigated the effects of rotary pipes and Fe_2O_3-water in FPSC. This numerical study was conducted using the SIMPLE algorithm and the finite volume method with upwind procedure. Four rotary pipes were used in this design with a 2% volume fraction of Fe_2O_3/water at a flow rate ranging from 0.424-2.544 L/min. Both nanofluid and rotary pipes helped to restore energy loss by 1.65% and 10.44%, respectively, resulting in 120.16 W more energy storage than the conventional design. The energy and exergy efficiency enhancements were observed to be 5.83% and 3.21%, respectively. In another numerical study, the same authors proposed a modified design using the same nanofluids of the same concentration by adding a magnetic field inducer to the rotary pipes [59]. The magnetic inducer restored an additional 27.8% of the lost energy. At a magnetic field intensity of 10 mT and a rotational speed of 0.15 rad/s, the maximum first law efficiency was achieved to be 61.7%, which is 39% higher than the efficiency of a collector without the rotary pipes and magnetic inducer. The exergetic efficiency improved only at low volume flow rates.

H. Nabi et al. [60] developed a CFD model of a U-shaped FPSC integrated with turbulators and hybrid nanofluids. A 3D, FEM based simulation was performed using

Ansys Fluent where three different geometries of turbulence prompting pipes were simulated alongside the base pipe between Re 4000 and Re 20000 and a 31.31% increase in heat transfer coefficient was observed for the third variation of geometry at Re 10000. Furthermore, SWCNT-CuO/water and MWCNT-CuO/water were employed with particle concentration of 1-5% in the best performing geometry. Among the nanofluids, SWCNT-CuO/water showed better performance with an 8.79% increase in heat transfer coefficient at Re 4000.

2.5 CONCLUSIONS FROM THE LITERATURE REVIEW

Despite numerous studies on the effects of metal-based nanofluids in FPSC, the use of carbon-based nanofluids is a relatively new trend. Researchers are focusing on experimental studies on carbon-based nanofluid applications in FPSC, but there are only a few numerical studies in the literature. From the literature review, it can be understood that the better thermophysical properties of carbon-based nanofluids over metal-based nanofluids are experimentally evaluated. But there are inadequent numerical studies which compare the performance of both these types of nanofluids in FPSC. This study intends to fill this research gap by developing a CFD model that can compare the thermo-physical properties of both carbon-based and metal-based nanofluids in FPSC applications.

CHAPTER 3. METHODOLOGY

This chapter explains the overall computational methodology of the simulation of the FPSC. In the first section, the physical model of this study is described. The following sections consist of mathematical modelling, governing equations, performance parameters and equations for calculating the thermo-physical properties of nanofluids. Subsequently, the mesh generation process and boundary condition of the numerical study is discussed followed by a representation of the numerical methodology. Finally, the validation of the computational method is presented.

3.1 PHYSICAL MODEL

A three-dimensional laminar heat transport model in a FPSC has been computationally simulated in this study via Ansys Fluent 2019 R2. The full and sliced geometry of the FPSC is displayed in Figure 3.1 which comprises a copper made absorber, a welded joint and a copper riser tube. The dimensions of the collector are extracted from established literature which consists of two header tubes and four riser tubes [4]. Due to the presence of symmetry and also to reduce the computational effort, a single riser tube was selected for the investigation instead of the full geometry (Figure 3.2).

Table 3.1 exhibits the specifications of the geometry. The computational domain is split into multiple zones consisting of fluid domain, absorber plate, and riser tube and welded joint.

Fluid domain: This portion involves the fluid volume passing through inner tube alongside the inlet and outlet of the pipe. In the inlet boundary, a laminar flow with initial velocity and temperature is applied. Atmospheric pressure is considered as the fluid domain pressure outlet.

Absorber Plate: The FPSC consists of a copper absorber which is situated at the top of the geometry. The top of the absorber surface receives incident radiation from the sun. The side and bottom walls of the absorber are considered adiabatic.

Welded joint: A copper welded junction connects the riser tube and the absorber surface.

Riser Tube: Thin copper riser tube is situated underneath the welded joint.

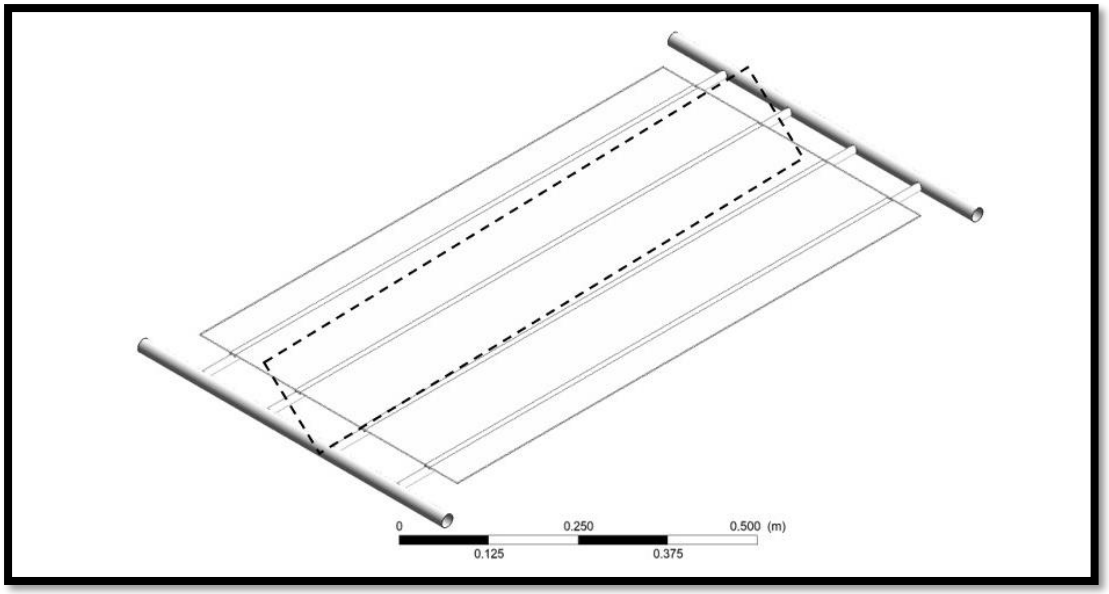

Figure 3.1 Full geometry of the FPSC with header and riser.

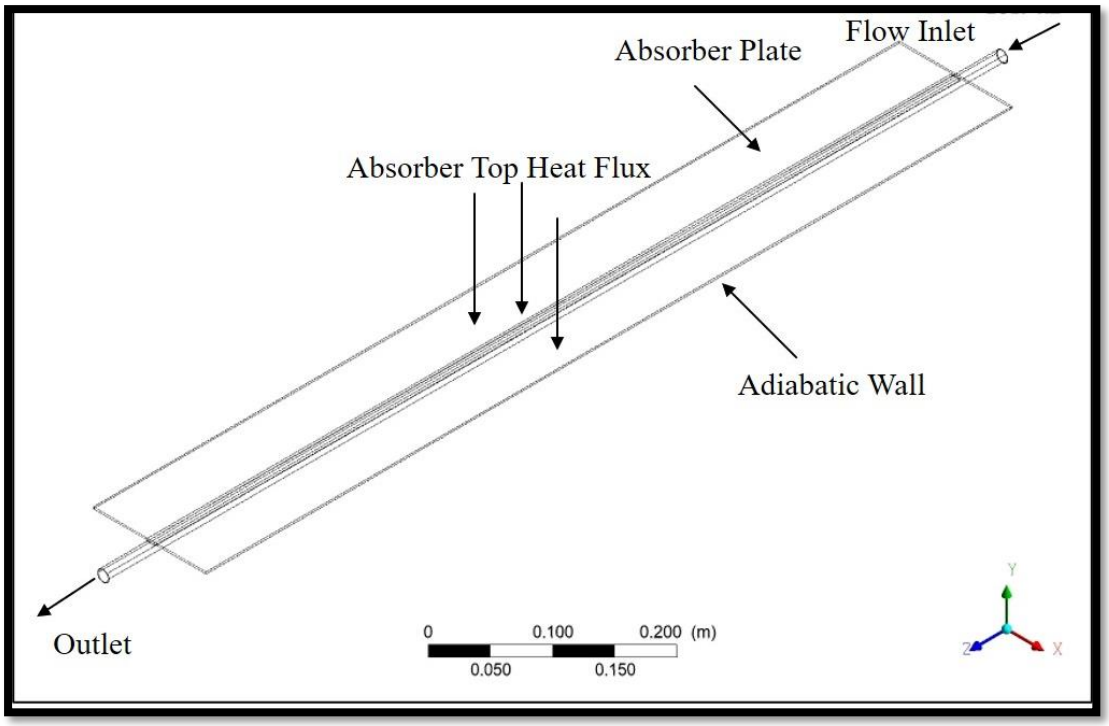

Figure 3.2 Sliced section of the geometry consisting of a single riser tube, absorber and welded joint.

Table 3.1 Geometric dimensions of the FPSC

Specification	Dimension	Unit
Absorber length	914.4	mm
Absorber width	128	mm
Absorber Thickness	2	mm
Riser tube length	1020	mm
Outer tube diameter	12.7	mm
Tube thickness	1.1	mm
Inclination angle	30	Degree

3.2 MATHEMATICAL MODEL

This study computationally investigates a FPSC with an inclination angle of 30-degree, operating in a three-dimensional laminar heat transfer model. The FPSC consists of a copper made absorber and riser tube along with a welded joint attaching the absorber plate with the riser tube. A constant initial temperature along with velocity profile is exerted at the inlet of the tube. Three nanofluids are considered for this investigation which are Al_2O_3/water, SWCNT/water and MWCNT/water nanofluids with volume concentrations ranging between 0.025% to 1% at Re reaching 1000-2000. Distilled water is selected as the base fluid for the nanofluids. The top of the absorber surface is subjected to a constant heat flux while the adiabatic condition is applied at the side and bottom walls. At the boundary wall of the riser pipe, the no-slip condition was subjected and the three-dimensional fluid flow is treated to be steady while the compressibility and radiation effects are ignored. Gravitational effects work both in the normal and flow directions.

3.3 GOVERNING EQUATIONS

The steady, three-dimensional governing equations of this investigation are addressed in tensor forms as follows:

Continuity:

$$\frac{\partial}{\partial x_i}(\rho u_i) = 0 \tag{1}$$

Momentum:

$$\frac{\partial}{\partial x_j}(\rho u_i u_j) = \frac{\partial p}{\partial x_i} + \frac{\partial}{\partial x_j}(v\left(\frac{\partial u_i}{\partial x_j} + \frac{\partial u_j}{\partial x_i}\right) - u_i' u_j') \quad (2)$$

Energy:

$$\frac{\partial \rho c_p u_j T}{\partial x_j} = \frac{\partial}{\partial x_j}\left(k\frac{\partial T}{\partial x_j} - \rho c_p \overline{u_j T}\right) + S_t \quad (3)$$

Here, i = 1, 2. 3 and u_i = u, v, w velocity vectors.

3.4 PERFORMANCE PARAMETERS

In this section, the required expression for analyzing the performance of the FPSC is described. Base fluid, nanofluid, and nanoparticle are represented by the subscripts bf, nf, and np, respectively.

The Reynolds number is represented by the following equation, which is the ratio of the inertial forces due to the momentum of the fluid and the viscous forces of the fluid, is defined by the following expression [61]:

$$Re = \frac{\rho V_{inlet} D_h}{\mu} \quad (4)$$

In which, the inlet velocity (ms^{-1}), the hydraulic diameter is (m), density (kg/m^3) and viscosity (Pa s) are expressed as V_{inlet} and D_h, ρ and μ respectively.

Due to the presence of inclination angle, the gravitational force (ms^{-2}) has components in the y and z-direction [62].

$$g_y = g\cos\theta \quad (5)$$

$$g_z = -g\sin\theta \quad (6)$$

Here θ is 30 degrees, the inclination angle of the FPSC.

The friction factor of the base fluid and nanofluid is calculated below [63].

$$f = \frac{\Delta P}{(\frac{L}{D_h})(\frac{\rho V_{inlet}{}^2}{2})} \tag{7}$$

In which, the length (m) of the riser tube is denoted by L and ΔP is the pressure drop (Pa) across the riser tube which is characterized as the subtraction between the area average of outlet pressure and inlet pressure.

$$\Delta P = P_{outlet} - P_{inlet} \tag{8}$$

The pumping power of the collector is given by the below equation [64].

$$Pumping\ Power = (\frac{\dot{m}}{\rho})\Delta P \tag{9}$$

The relative pumping power of the FPSC can be calculated by the given expression [65]:

$$Relative\ Pumping\ Power = \frac{Pumping\ Power_{nf}}{Pumping\ Power_{bf}} \tag{10}$$

In addition, the heat transfer coefficient (W/m^{2}K) is evaluated as [66]:

$$h = \frac{q^w}{T_{wall} - T_{fluid}} \tag{11}$$

Where q^w, T_{wall} and T_{fluid} are heat flux acting on the tube wall (W/m^2), averaged temperature of the tube wall (K) and averaged fluid temperature (K) respectively.

Furthermore, the Nusselt Number (Nu), which is the ratio of convective to conductive heat transfer at the boundary of the fluid domain, can be read as [67]:

$$Nu = \frac{hD_h}{k} \tag{12}$$

Here, the thermal conductivity (W/m.K) of the fluid is denoted by k.

The Stanton Number (St) denotes the ratio between heat transfer coefficient and heat capacity of the fluid. It can be computed as [68]:

$$St = \frac{h}{\rho C_p v_{avg}} \tag{13}$$

Here, C_p represents the heat capacity of the fluid (J/kg.k).

Thermo-hydraulic performance parameter (THPP) calculates the thermal heat capacity of fluid by including the St and friction factor of the fluids, which can be acquired by the following equation [69]:

$$THPP = \frac{(St_{nf}/St_{dw})^3}{(f_{nf}/f_{dw})} \tag{14}$$

3.5 THERMO-PHYSICAL PROPERTIES

The thermophysical characteristics of the nanofluids are obtained employing the following empirical correlations.

The density of the nanofluid can be estimated using [70]:

$$\rho_{nf} = (1-\varphi)\rho_{bf} + \varphi\rho_{np} \tag{15}$$

Where φ is the particle concentration of the nanofluid.

The heat capacity of the nanofluid is evaluated by the following expression [71], [72]:

$$C_{\rho,nf} = \frac{C_{\rho,bf}\rho_{bf}(1-\varphi) + C_{\rho,np}\rho_{np}\varphi}{\rho_{nf}} \tag{16}$$

The thermal conductivity of the nanofluids is obtained by using the modified Li-Qu-Feng model that considers the aggregation and Brownian motion of the nanoparticles along with the shape factor of the nanoparticles [73].

$$k_{nf} = \frac{k_{np} + (n-1)k_{bf} + (n-1)\varphi(k_{np} - k_{bf})}{k_{np} + (n-1)k_{bf} - \varphi(k_{np} - k_{bf})}k_{bf} + \frac{\rho\varphi C_p}{2}\sqrt{\frac{K_B T_{avg}}{3\pi r_c \mu_{nf}}} \tag{17}$$

In the modified Li-Qu-Feng model, the thermal conductivity (W/m k) is denoted as k, n is the empirical shape factor (n=3 for spherical nanofluids and n=6 for cylindrical nanofluids), μ is the dynamic viscosity (mPa s), K_B is the Boltzmann constant (K_B = 1.3806505 × 10^{-23} J/K), T_{avg} is the average temperature (K) of the fluid and r_c is the average radius (m) of the nanoparticles.

To calculate the viscosity of the nanofluids, the following correlation is used [74].

$$\mu_{nf} = \frac{1}{1 - 34.87\left(D_{np}/D_{bf}\right)^{-0.3}\varphi^{1.03}}\mu_{bf} \tag{18}$$

In which the nanoparticle diameter (m) and the equivalent base fluid particle diameter (m) are represented by d_{np} and d_{bf} respectively. The diameter of the base fluid is calculated by the following equation [74]:

$$d_{bf} = 0.1\left(\frac{6M}{N\pi\rho_{bf0}}\right)^{1/3} \tag{19}$$

Where, M, N and ρ_{bf0} are the molecular weight of the base fluid, Avogadro number and density of the base-fluid calculated at 293K respectively.

The properties of distilled water and the nanoparticles collected from available literature [35], [75]–[78] are presented in Table 3.2.

Table 3.2 Thermo-physical properties of water and nanoparticles

Thermo-physical properties	**ρ (Kg/m^3)**	**C_p (J/Kg.K)**	**k (W/m.K)**	**μ (mPa.s)**	**D_p (nm)**
Water (303K) [75]	995.5075	4145.5976	0.5927	0.7955	-
Water (313K) [75]	992.4082	4141.2634	0.6115	0.6527	-
Al_2O_3 [76]	3690	773	40	-	20
MWCNT [35]	2600	710	3000	-	7
SWCNT [77]	1400	1380	3500	-	2

3.6 MESH GENERATION

Figure 3.3 represents the overall mesh arrangement of the computational body. To obtain better quality and control of mesh generation, the fluid domain was divided into 12 bodies and the riser pipe was split into 8 bodies. Grids were generated using structured method. Closer to the tube wall, the mesh concentration was increased for capturing the wall effects. Edge sizing was applied at the outer edges of the fluid domain to create concentrated mesh near the tube wall. Figure 3.4 represents the front view of the mesh where the concentration of mesh around the tube wall is visible.

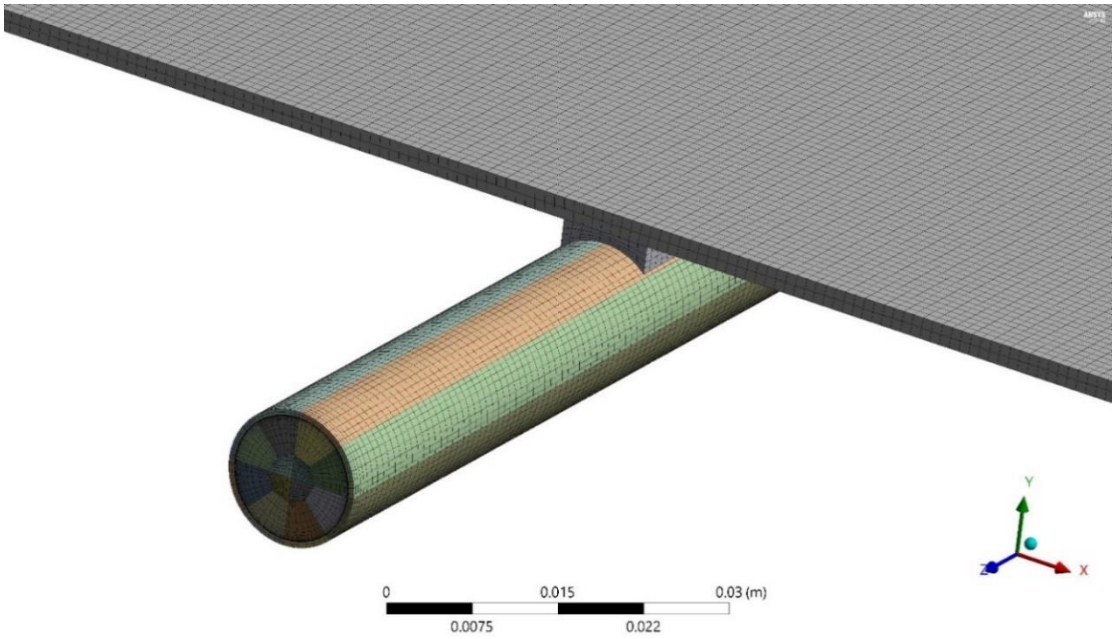

Figure 3.3 Mesh layout of FPSC.

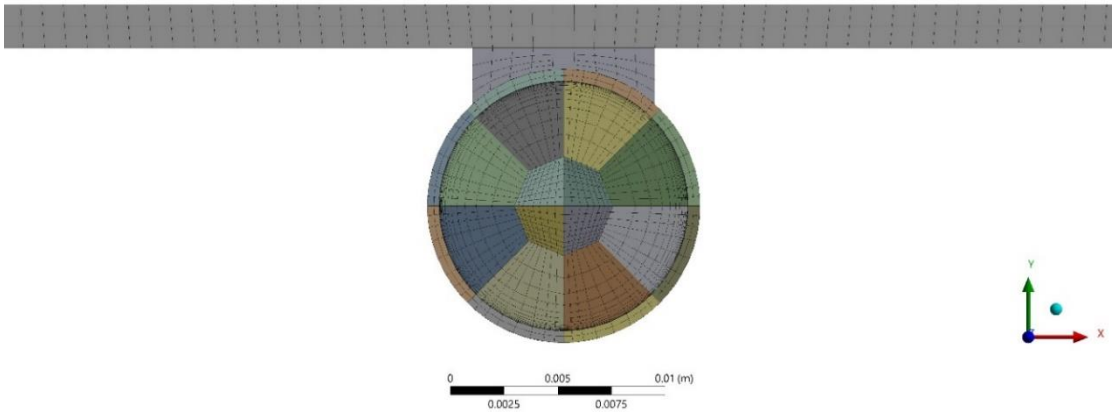

Figure 3.4 Front view of mesh arrangement.

To check the dependency of the generated mesh and computed results, a mesh independence study was conducted comprising four different element numbers. To run this mesh independence study, a heat flux of 900 W/m^2 was applied at the top of the absorber with an inlet temperature of 303 K and a Re of 1000 for water. The deviation in the results of the computational procedure was analyzed and an optimum cell number of 1,583,276 was considered for this study. Table 3.3 represents the results and deviation in the mesh sensitivity analysis.

Table 3.3 Mesh independence study

Number of cells	Nu	% Diff Nu
242,529 (coarse)	8.529	1.88
521,444 (intermediate)	8.69	1
1,583,276 (fine)	8.775	0.1
2,434,716 (very fine)	8.766	-

3.7 BOUNDARY CONDITIONS

This section addresses the required boundary condition for the computational method. Figure 3.2 shows the employed boundary condition for this investigation.

Inlet of the riser tube:

Velocity inlet boundary condition is used at the inlet with constant temperature and uniform velocity. The direction of velocity is in the stream wise z-direction. Initial velocity is laminar, ranging between Re 1000 and Re 2000 with an inlet temperature of 303 K and 313 K.

Absorber Plate:

The top edge of the absorber plate is subjected to a heat flux of 900 W/m^2 which works as the incident solar radiation at the absorber plate. The lateral side and the bottom of the absorber plate are kept insulated as no heat loss occurs from these sections. Hence, adiabatic conditions are applied. Heat dissipates to the riser tube from the absorber plate through the welded joint.

Riser tube outlet:

The riser tube outlet consists of pressure outlet boundary conditions where the outlet pressure is kept as atmospheric pressure.

3.8 NUMERICAL METHODOLOGY

For pressure velocity coupling and the discretization of convection and diffusion terms, SIMPLEC method with second-order upwind scheme was employed for both momentum and energy. The solving process is presumed to be converged when the residuals are under 10^{-4} for continuity and momentum equation while 10^{-8} for energy equation and it took around 1000-1500 iterations for solution to converge.

3.9 VALIDATION

In order to evaluate the precision of the developed computational model, the current study was compared to a previously published experimental study [4]. The experimental study demonstrated outlet temperatures of riser tubes of a FPSC at flow rates of 0.8 L/min, 1.2 L/min and 1.5 L/min, at weight concentrations of 0.025%, 0.05% and 0.01% of graphene nanoplatelets. Outlet temperature was preferred for validation purposes as the thermal-hydraulic performance of the fluids depends substantially on the fluid temperature. To compare the results of the experimental investigation with the current numerical model, a similar boundary condition working under the laminar heat transfer model was applied to the present geometry, which consists of identical dimensions to the experimental study. At the inlet domain, uniform velocity and initial temperature is applied according to the flow rates and conditions of the experiment. The applied heat flux at the top of the absorber is 877 W/m^2 and a heat transfer coefficient is employed at the bottom of the absorber. Instead of an adiabatic condition like the current investigation, a heat transfer coefficient was applied at the absorber bottom to replicate the heat loss coefficient of the FPSC used in the experiment as the adiabatic condition indicates no heat loss from the FPSC. The thermo-physical properties of nanofluids used for validation purposes are extracted from the data given in the experimental study. The computational model shows acceptable agreements with the experimental results as presented in Figure 3.5, which shows the variation of outlet temperature with flow rates for three different volume concentrations of graphene nanoplatelets. As illustrated, both experimental and numerical results show a similar trend in all of the volume concentrations. Numerical results presented better accuracy at higher flow rate and volume concentrations. The highest deviation of the numerical

results from the experimental data is around 0.4% at a flow rate of 0.8 L/min and a volume concentration of 0.025%.

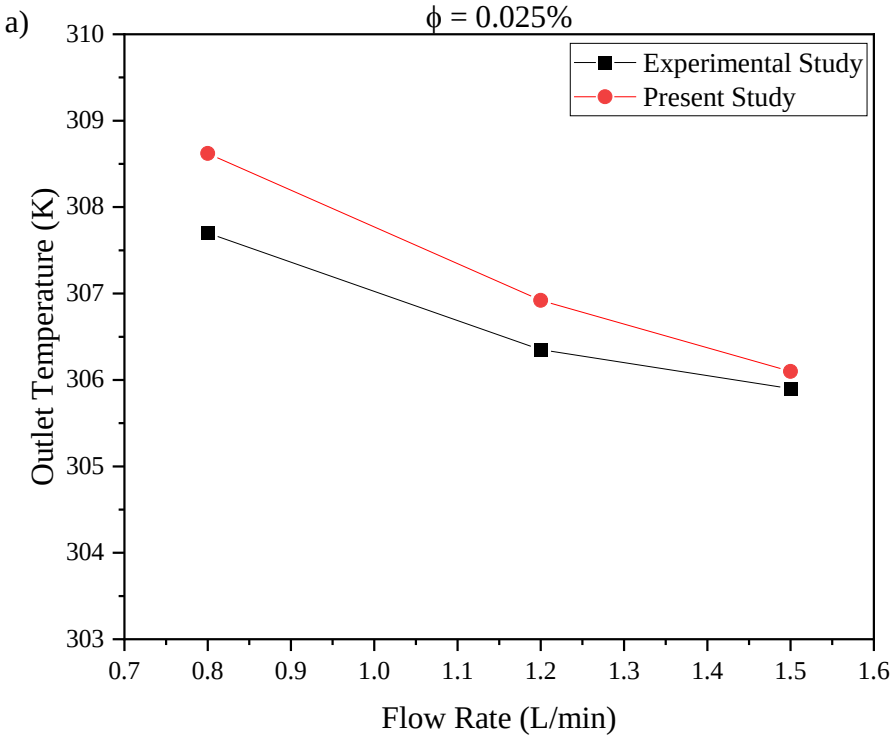

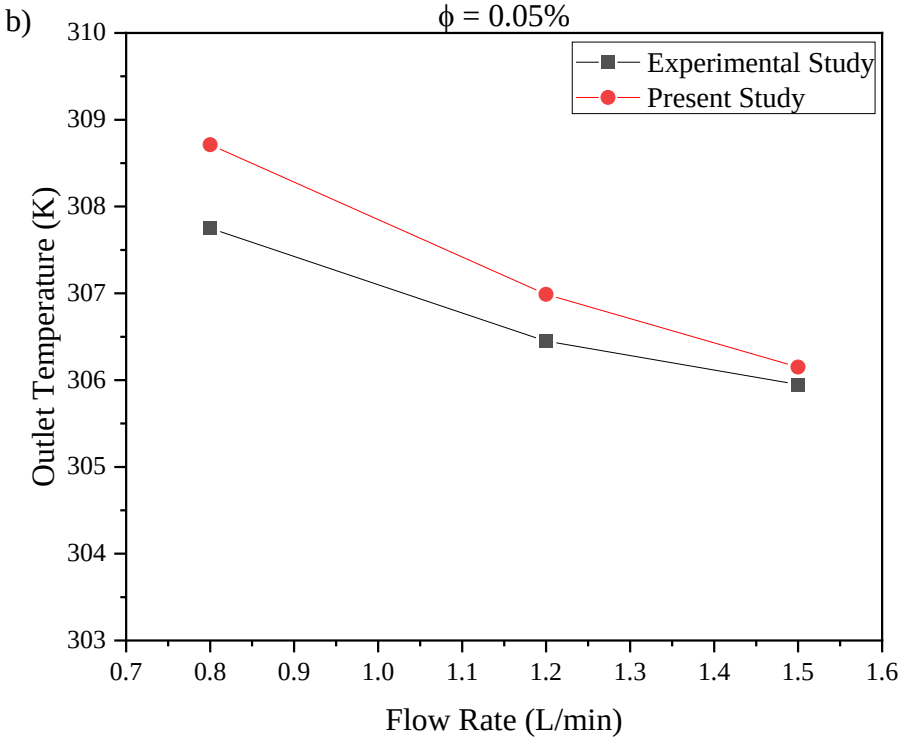

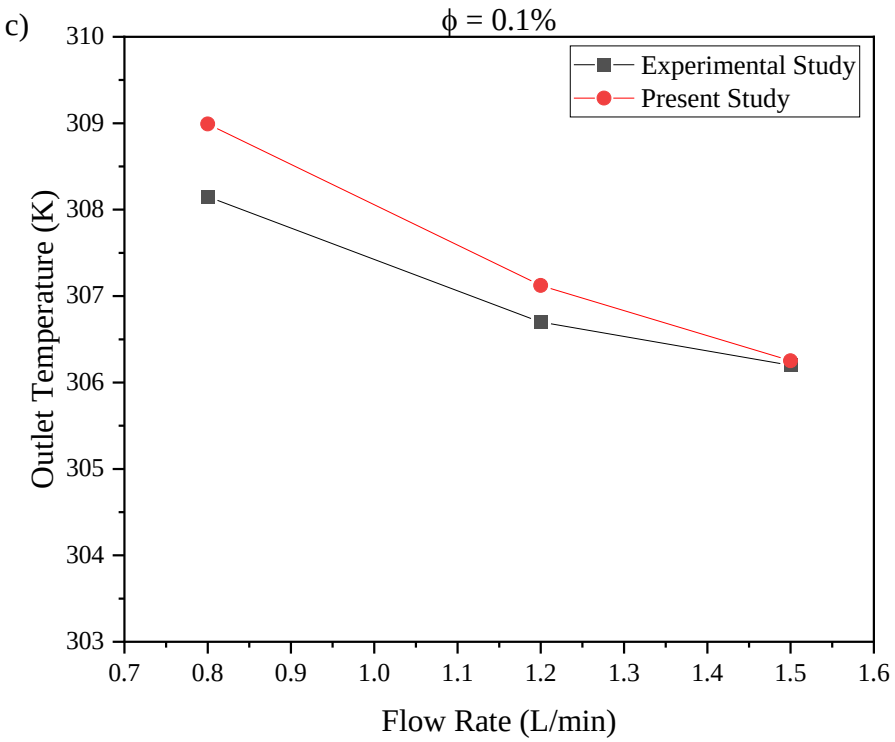

Figure 3.5 Validation of outlet temperature by Ref. [4] at three different volume concentration. a) ϕ = 0.025%, b) ϕ = 0.05% and c) ϕ = 0.1%

3.10 CONCLUSIONS FROM METHODOLOGY

This chapter addressed the investigation's methodology, correlations, and data gathering. The computational domain design, required boundary conditions, and mesh sensitivity analysis were discussed, followed by required parameters for FPSC performance and nanofluid thermo-physical characteristics. The established numerical technique agreed with a previously published experimental investigation, which is provided at the end of this chapter.

CHAPTER 4. RESULTS AND DISCUSSION

In this study, steady three-dimensional laminar heat transfer flow has been simulated for FPSC using Ansys Fluent. The thermal-hydraulic performance comparison between carbon-based and metal-based nanofluids is the topic of investigation. In this chapter, firstly, the variation of thermo-physical properties with concentration was shown. These properties were calculated by applying empirical equations mentioned in Chapter 3. Among the thermo-physical properties density, thermal conductivity, and viscosity increased with increasing nanofluid concentration, but specific heat decreased.

Then, in the later sections, seven thermal-hydraulic performance parameters- outlet temperature, friction factor, relative pumping power, heat transfer coefficient, Nu, St, THPP of Al_2O_3/water, SWCNT/water, and MWCNT/water nanofluids are compared and the reasons behind their changes are discussed. The variation of outlet temperature, friction factor, heat transfer coefficient, Nu, and St is plotted against the Re. Their changes with volume concentration at a fixed Re can also be observed from the graphs. The variation of relative pumping power and THPP with concentration are also discussed. Finally, the better performing nanofluid is selected based on its superior thermal-hydraulic performance.

4.1 THERMO-PHYSICAL PROPERTIES OF THE NANOFLUIDS

4.1.1 Density of the Nanofluids

Figure 4.1 and Figure 4.2 show the variation of nanofluid density with particle volume concentrations. According to the figures, nanofluid density gradually increases with volume concentration. For both temperatures, Al_2O_3/water exhibited a higher density than other nanofluids. It is because of higher particle density of Al_2O_3/water than SWCNT and MWCNT nanoparticles (Table 3.2). Between MWCNT/water and SWCNT/water nanofluids, higher density is observed for MWCNT/water which is also due to higher nanoparticle density.

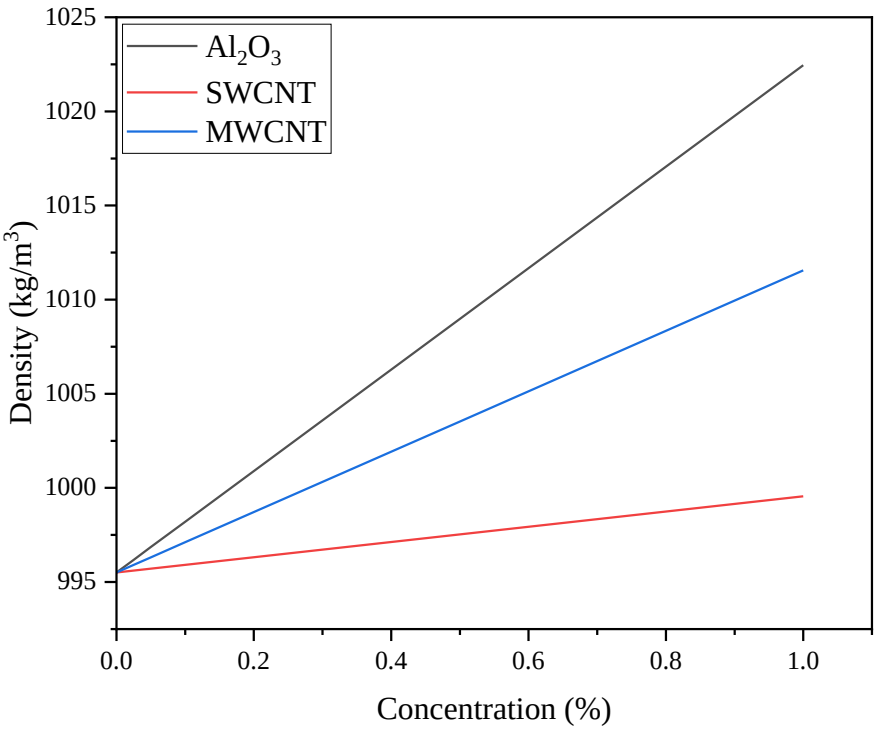

Figure 4.1 Variation of the density of nanofluids with volume concentrations at 303K.

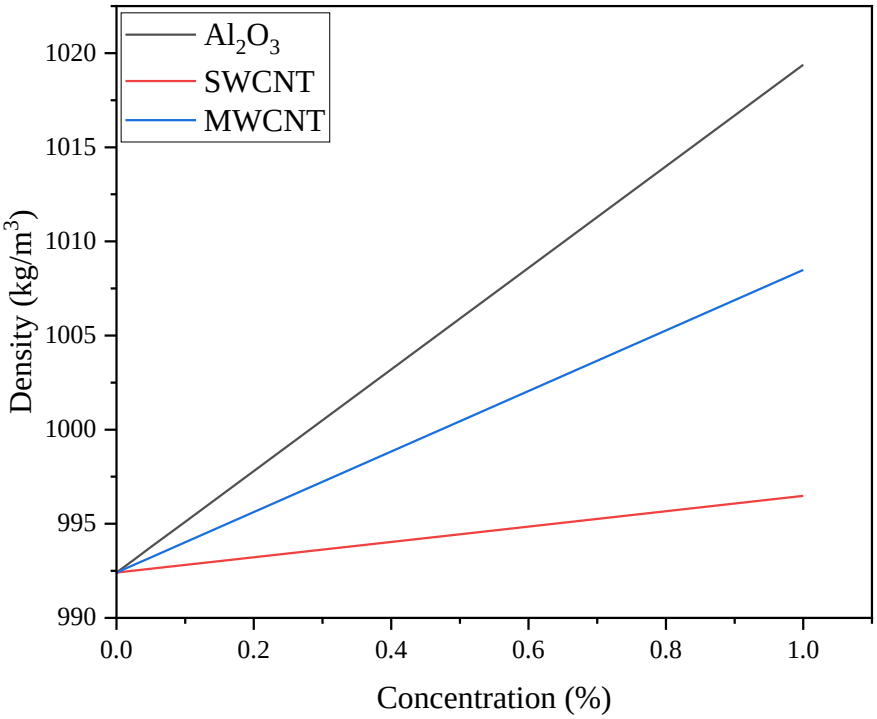

Figure 4.2 Variation of the density of nanofluids with volume concentrations at 313K.

4.1.2 Thermal Conductivity of the Nanofluids

Thermal conductivity displays a proportional relation with the volume concentration of the nanoparticles which is displayed in Figure 4.3 and Figure 4.4 . As the volume concentration increases, more solid particles are mixed in water greatly enhancing the heat conduction performance of the nanofluids [79]. Furthermore, a higher thermal conductivity of the nanofluids is observed at 313 K. With the increase in temperature, the water particles and nanoparticles dissolved, water gets energized resulting in higher thermal conductivity.

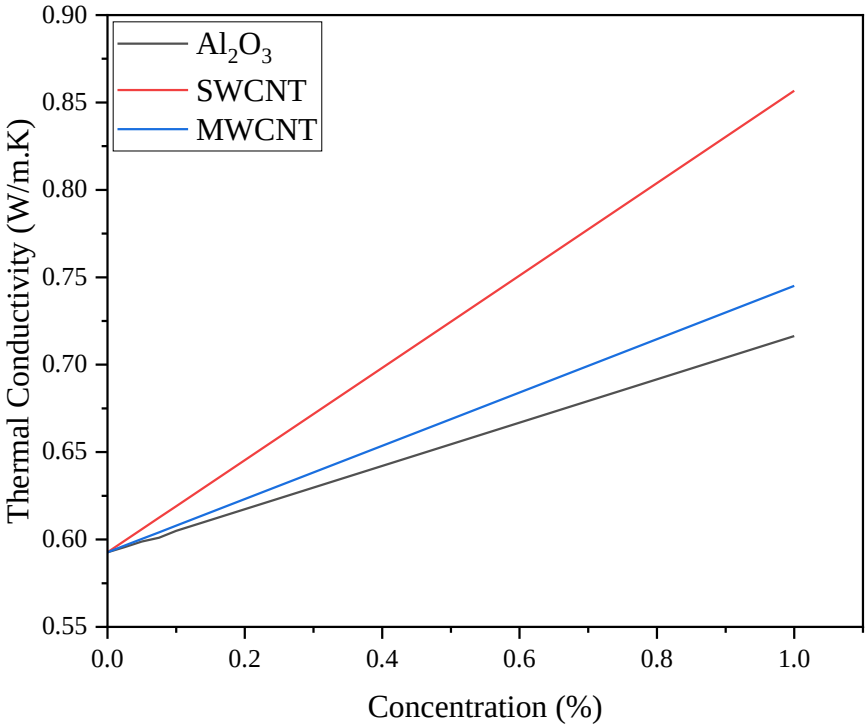

Figure 4.3 Variations of thermal conductivity with volume concentration at 303K.

Among the nanofluids, SWCNT/water displayed the highest increment of thermal conductivity because of low particle size, followed by MWCNT/water. MWCNT particles have lower particle diameter and very high thermal conductivity than Al_2O_3 particles, MWCNT/water displays moderately higher enhancement of thermal conductivity than Al_2O_3/water nanofluid.

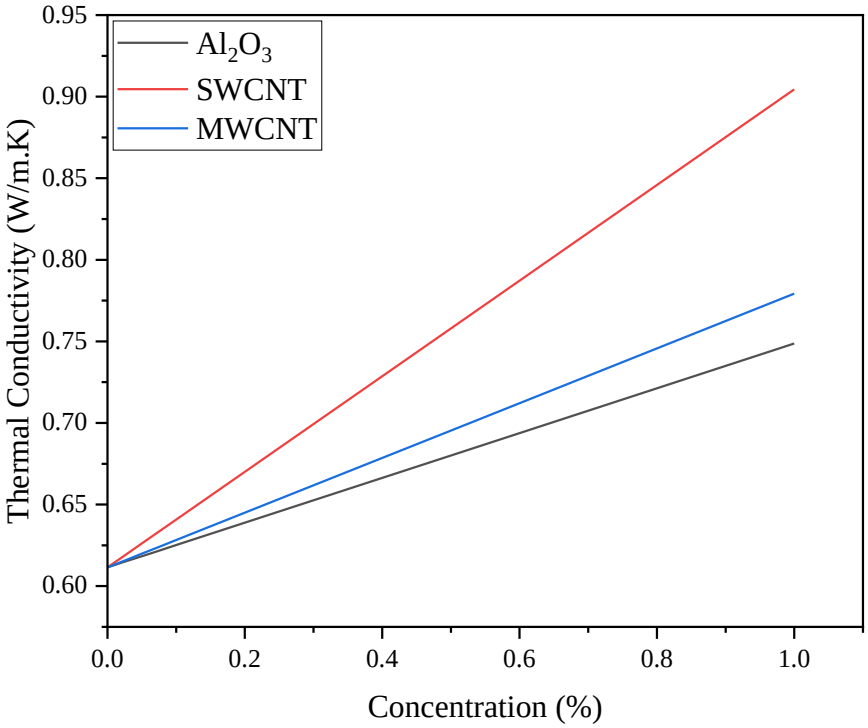

Figure 4.4 Variations of thermal conductivity with volume concentration at 313K.

4.1.3 Viscosity of the Nanofluids

As illustrated in Figure 4.5 and Figure 4.6, the viscosity of the nanofluids shows an almost linearly proportional relationship with particle volume concentration. An increase in volume concentration also increases the friction between water particles and nanoparticles which increases the fluid viscosity. Also, friction between the nanoparticles themselves provides a significant effect [80], [81]. However, the viscosity significantly reduces when the operating temperature is augmented to 313 K as the intermolecular and inter-particle adhesion forces plummet.

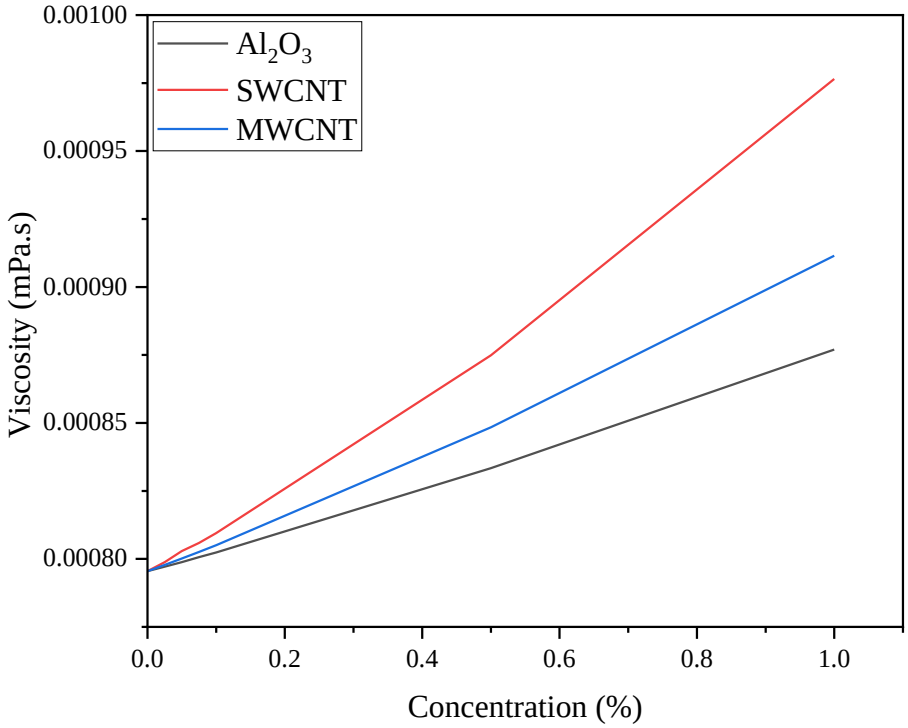

Figure 4.5 Variation of viscosity with volume concentration at 303K.

Among the three nanofluids, SWCNT/water shows the biggest increment in viscosity followed by MWCNT/water and Al_2O_3/water. It can be described via the expression of nanofluid viscosity (equation 18) from which it's observed that viscosity is inversely proportional to the nanoparticle diameter. Hence, as SWCNT has the lowest diameter of 2 nm, it displayed the highest increment in viscosity. Al_2O_3 has the highest diameter among the nanofluids hence it showed the least rise in viscosity.

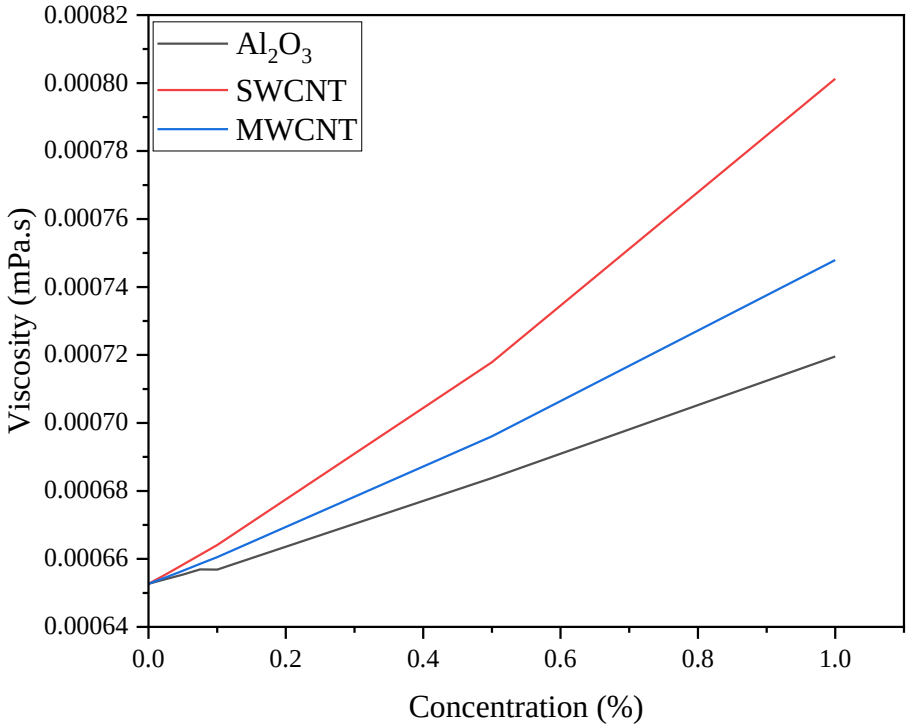

Figure 4.6 Variation of viscosity with volume concentrations at 313K.

4.1.4 Specific Heat of the Nanofluids

As displayed in Figure 4.7 and Figure 4.8, specific heat is inversely proportional to volume concentration and it shows negligible changes with an increase in temperature. Among the three nanofluids, Al_2O_3/water shows a greater reduction of specific heat with volume concentration, followed by MWCNT/water and SWCNT/water.

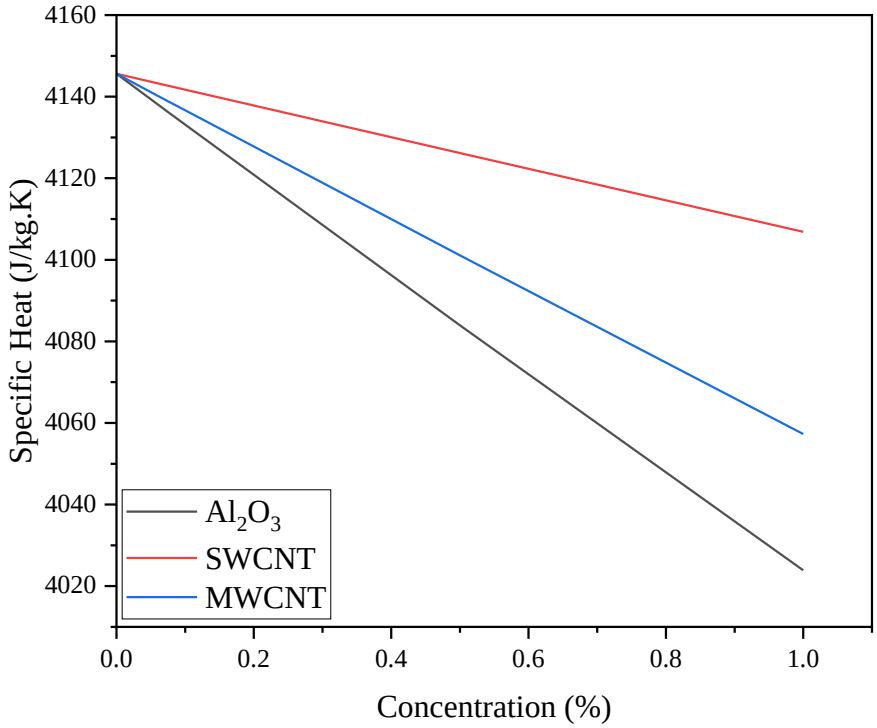

Figure 4.7 Variation of specific heat with volume concentrations at 303K.

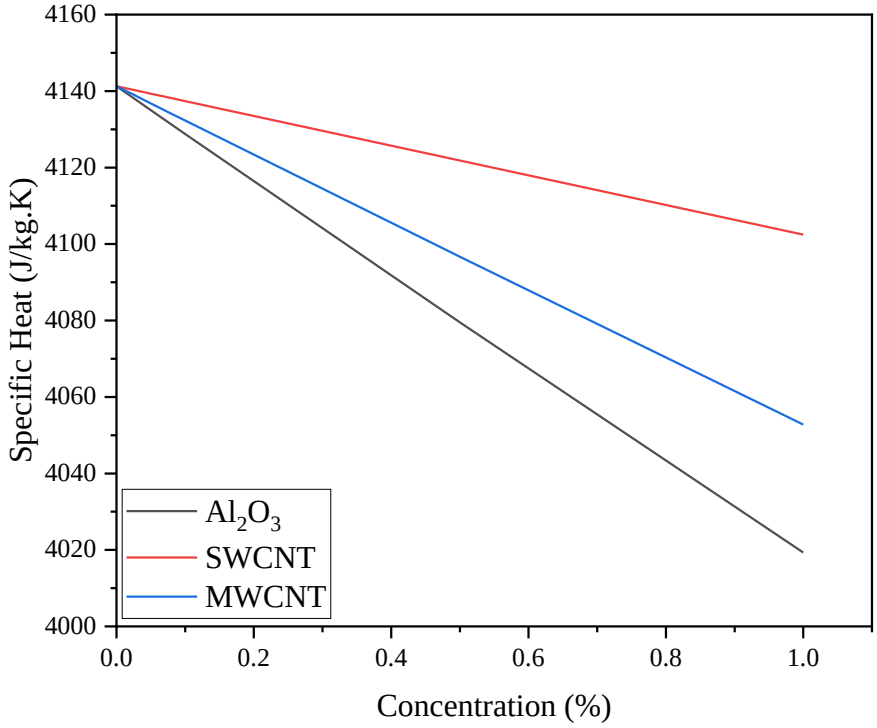

Figure 4.8 Variation of specific heat with volume concentrations at 313K.

4.2 OUTLET TEMPERATURE

Figure 4.9 and Figure 4.10 exhibit the impact of the Re on the outlet temperature at different volume concentrations for Al_2O_3/water, SWCNT/water and MWCNT/water at an inlet temperature of 303 K and 313 K, respectively. The outlet temperature of FPSC falls with the augmentation of the Re for all the nanofluids which can be explained by the definition of the Re. The average velocity of the fluid increases with the Re which reduces the time available for heat exchange between the wall and fluid. Hence, outlet temperature reduces with the Re. Furthermore, at a specific Re, an increase in volume concentration diminishes the outlet temperature. Figure 4.5 and Figure 4.6 display the increment of viscosity with particle concentration. Hence at a specific Re, because of an increment in viscosity, the velocity of the fluid augments. Therefore outlet temperature diminishes when opposed to increasing particle concentration. The outlet temperature curve of nanofluids is almost identical to the outlet temperature curve of water at lower volume concentrations (ϕ = 0.025, 0.05, 0.075, 0.1%). Significant changes in the outlet temperature curves of nanofluids and water can be observed at higher concentrations (ϕ = 0.5 and 1%). In both operating temperatures, SWCNT/water at 1% volume concentration shows the lowest temperature. As SWCNT/water has the highest increment of viscosity it also reaches the highest fluid velocity. Hence it shows the lowest outlet temperature among the nanofluids. Among the three nanofluids, at 1% volume concentration, Al_2O_3/water exhibited the highest outlet temperature as it has the lowest viscosity among the nanofluids.

a)

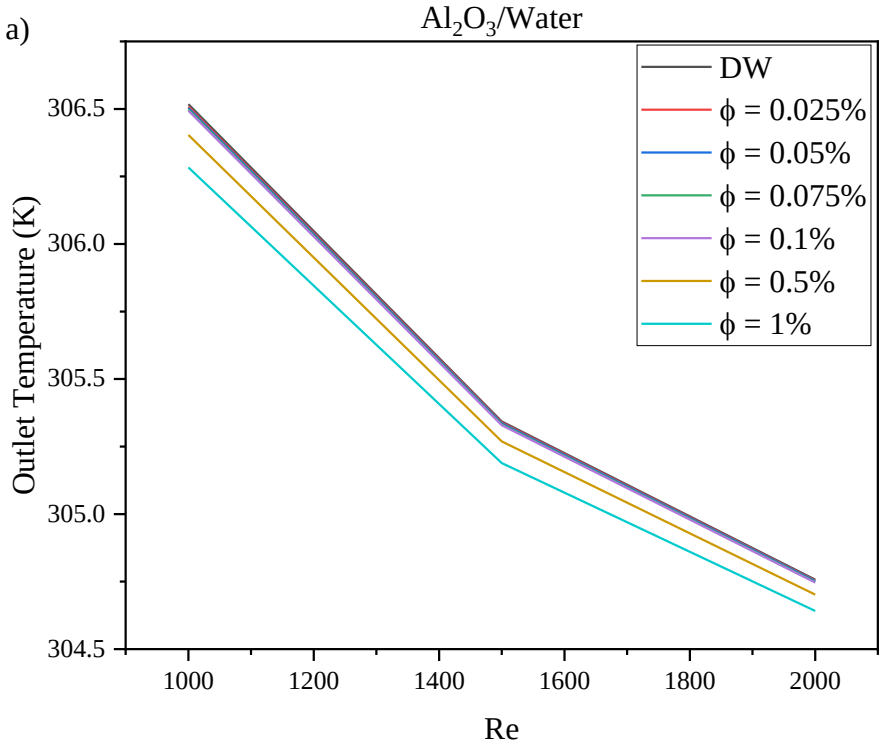
Al2O3/Water
DW
ϕ = 0.025%
ϕ = 0.05%
ϕ = 0.075%
ϕ = 0.1%
ϕ = 0.5%
ϕ = 1%
Outlet Temperature (K)
306.5
306.0
305.5
305.0
304.5
1000
1200
1400
1600
1800
2000
Re

b)

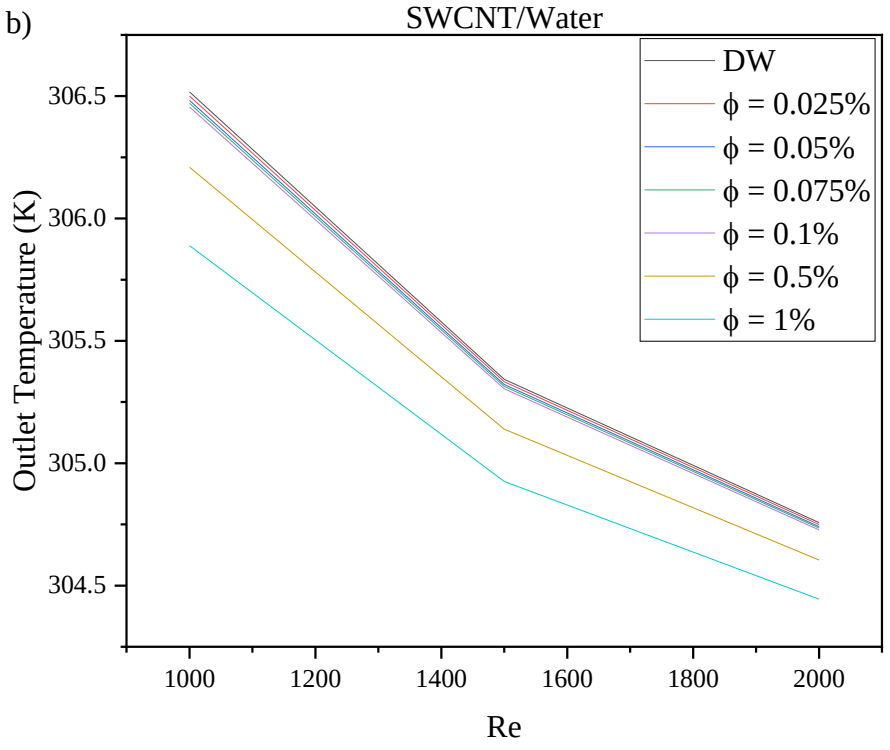
SWCNT/Water
DW
ϕ = 0.025%
ϕ = 0.05%
ϕ = 0.075%
ϕ = 0.1%
ϕ = 0.5%
ϕ = 1%
Outlet Temperature (K)
306.5
306.0
305.5
305.0
304.5
1000
1200
1400
1600
1800
2000
Re

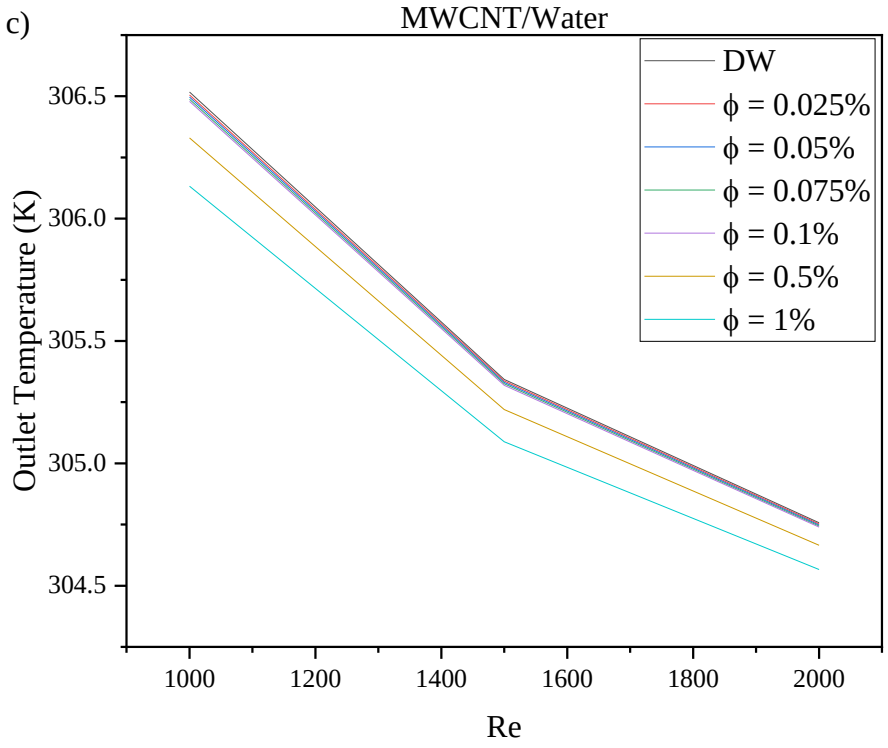

Figure 4.9 Variation of outlet temperature with Re at 303K. a) Al_2O_3/water, b) SWCNT/water, and c) MWCNT/water

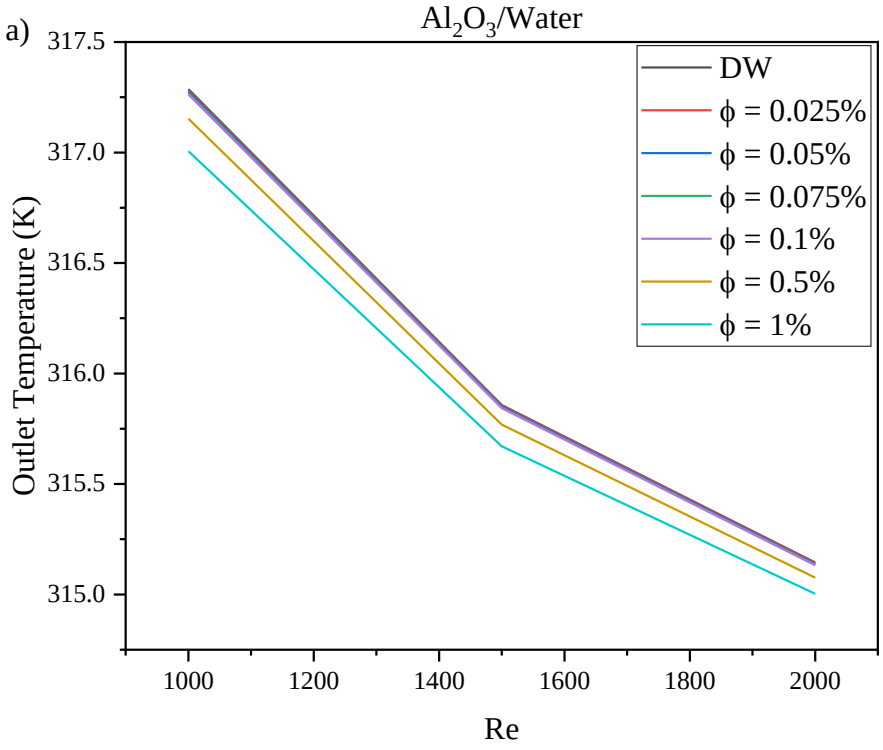

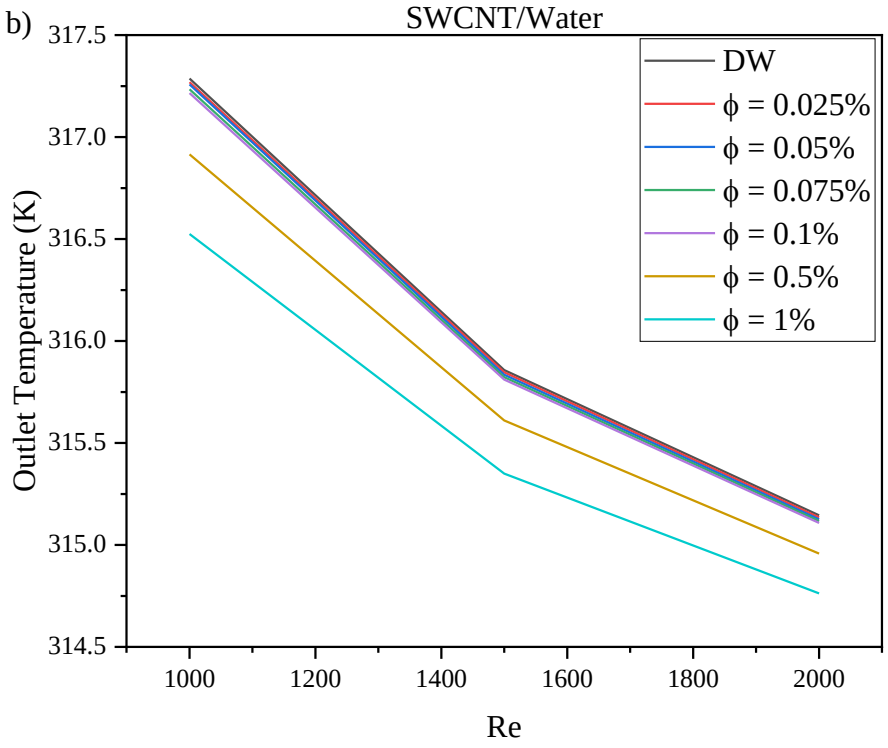

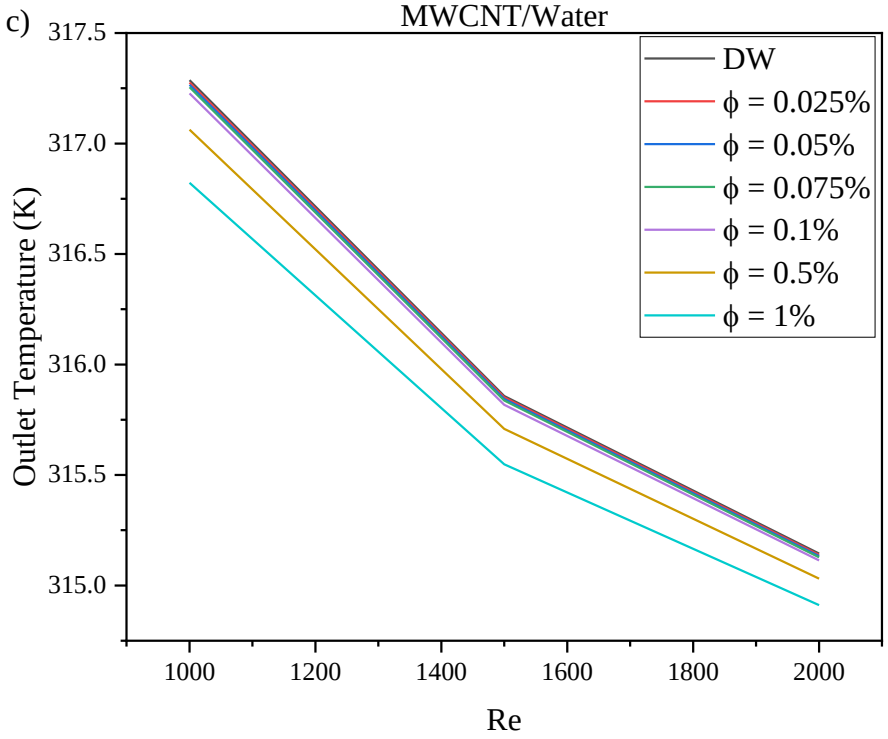

Figure 4.10 Variation of outlet temperature with Re at 313K. a) Al_2O_3/water, b) SWCNT/water, and c) MWCNT/water

4.3 FRICTION FACTOR

Figure 4.11 and Figure 4.12 depict the change of friction factor with the Re for Al_2O_3/water, SWCNT/water and MWCNT/water nanofluids at inlet temperatures of 303 K and 313 K respectively. As illustrated, an increase of the Re results in declination in the friction factor. From the expression of friction factor (equation 7), it is evident that velocity and friction factor has an inversely proportional relationship. Therefore, the friction factor falls with an increment in the Re. It is also apparent that volume concentration has a negligible impact on the values of the friction factor which shows similar results to previous studies [9]. At an unchanging Re, the friction factor shows very little to no alternation when opposed to a change in nanoparticle concentration. For increasing inlet temperature from 303 K to 313 K, the friction factor increases marginally provided that the Re and the nanoparticle concentrations are kept constant. Furthermore, comparing the friction factor values for the three nanofluids it is distinguished that changing nanofluid at a specific concentration and Re does not have any significant effect.

At a fixed Re, the augmentation of pressure drop diminishes the increase of density and velocity at higher volume concentration. Subsequently, the friction factor changes negligibly with volume concentration. The same rate of change of pressure drop, density and velocity occurs for every nanofluid. Therefore, the friction factor is independent of the type of nanofluid used.

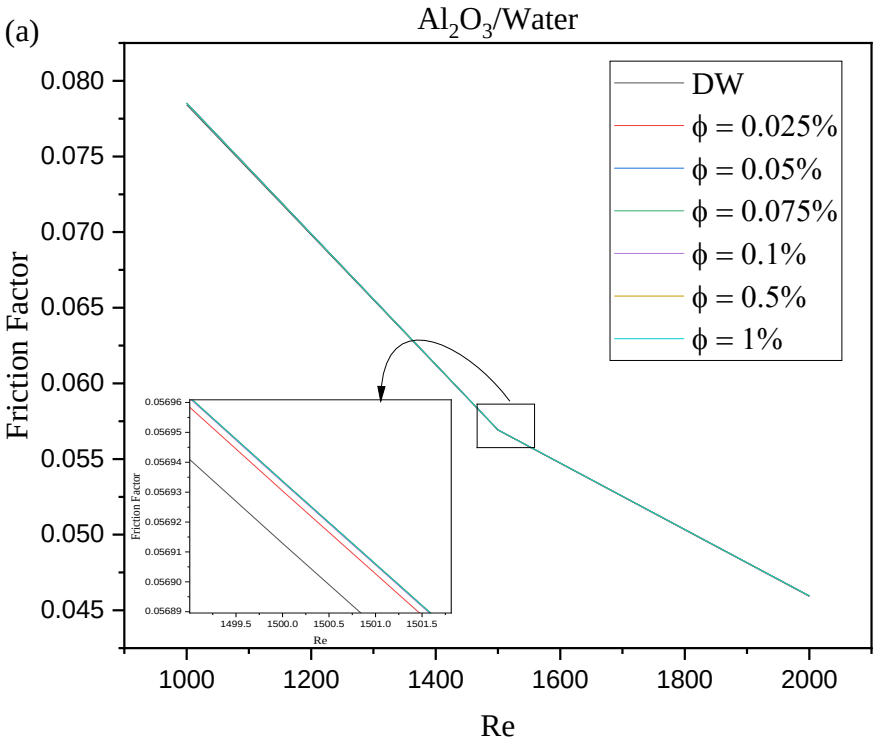
(a)
Al2O3/Water
Friction Factor
Re
DW
ϕ = 0.025%
ϕ = 0.05%
ϕ = 0.075%
ϕ = 0.1%
ϕ = 0.5%
ϕ = 1%
0.080
0.075
0.070
0.065
0.060
0.055
0.050
0.045
1000
1200
1400
1600
1800
2000
0.05696
0.05695
0.05694
0.05693
0.05692
0.05691
0.05690
0.05689
1499.5
1500.0
1500.5
1501.0
1501.5

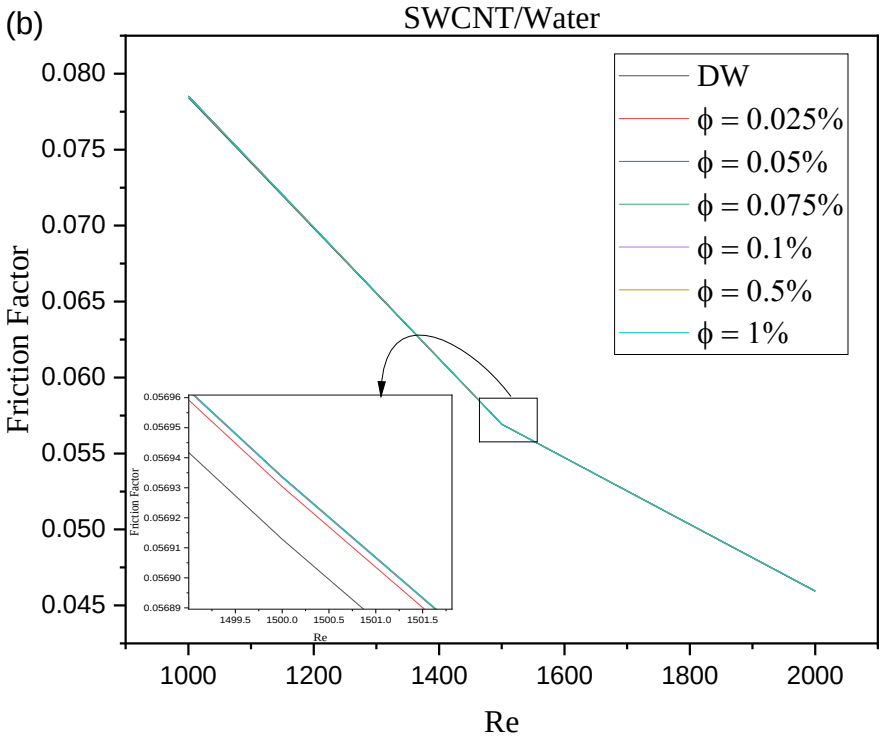
(b)
SWCNT/Water
Friction Factor
Re
DW
ϕ = 0.025%
ϕ = 0.05%
ϕ = 0.075%
ϕ = 0.1%
ϕ = 0.5%
ϕ = 1%
0.080
0.075
0.070
0.065
0.060
0.055
0.050
0.045
1000
1200
1400
1600
1800
2000
0.05696
0.05695
0.05694
0.05693
0.05692
0.05691
0.05690
0.05689
1499.5
1500.0
1500.5
1501.0
1501.5

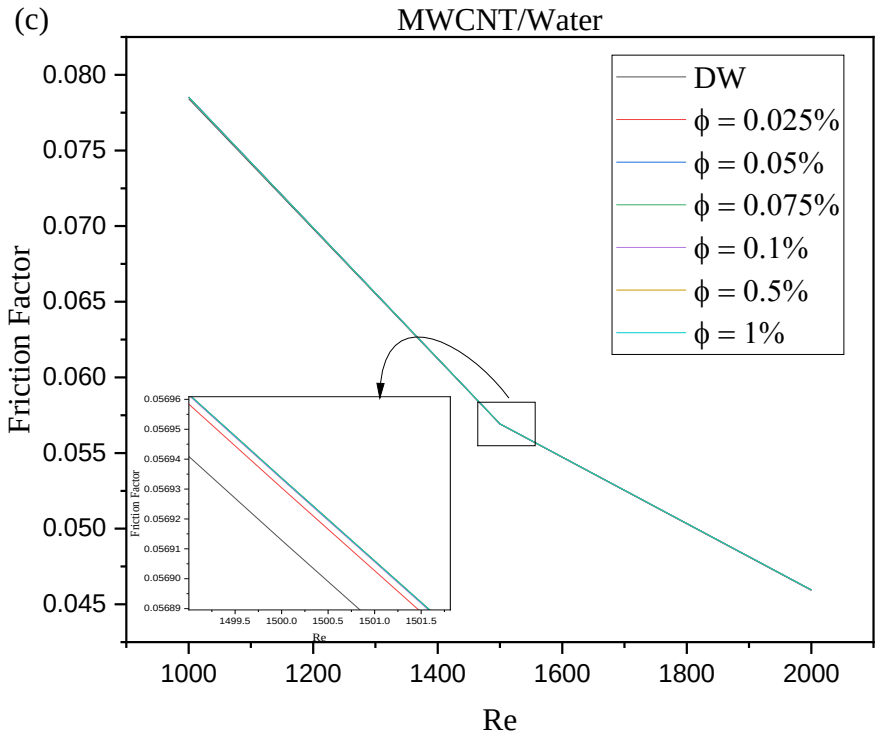

Figure 4.11 Variation of friction factor versus the Re for three different nanofluids at 303K. a) Al_2O_3/water, b) SWCNT/water, and c) MWCNT/water

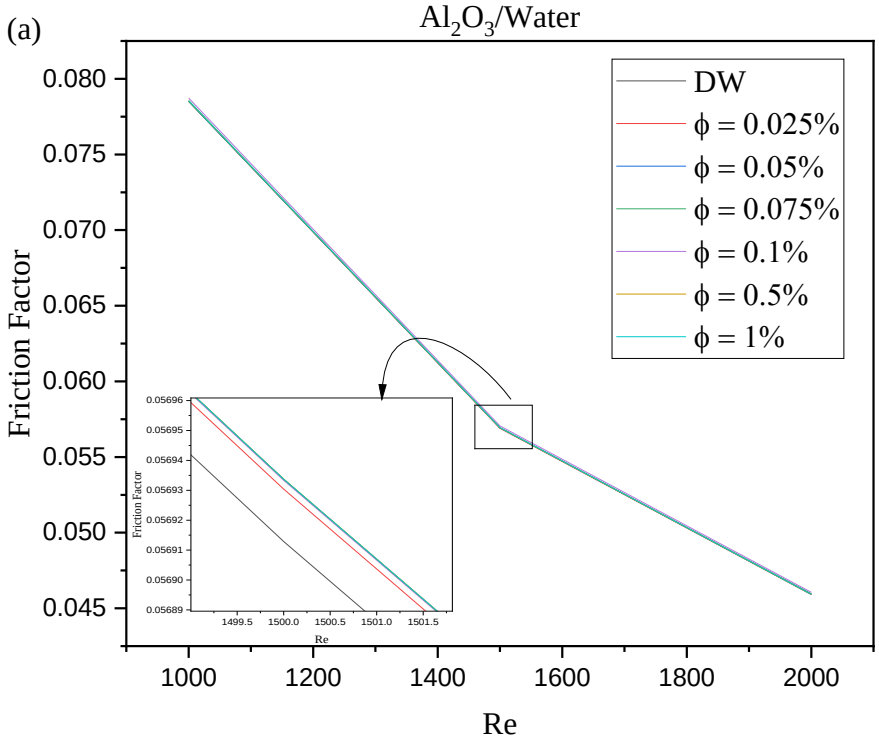

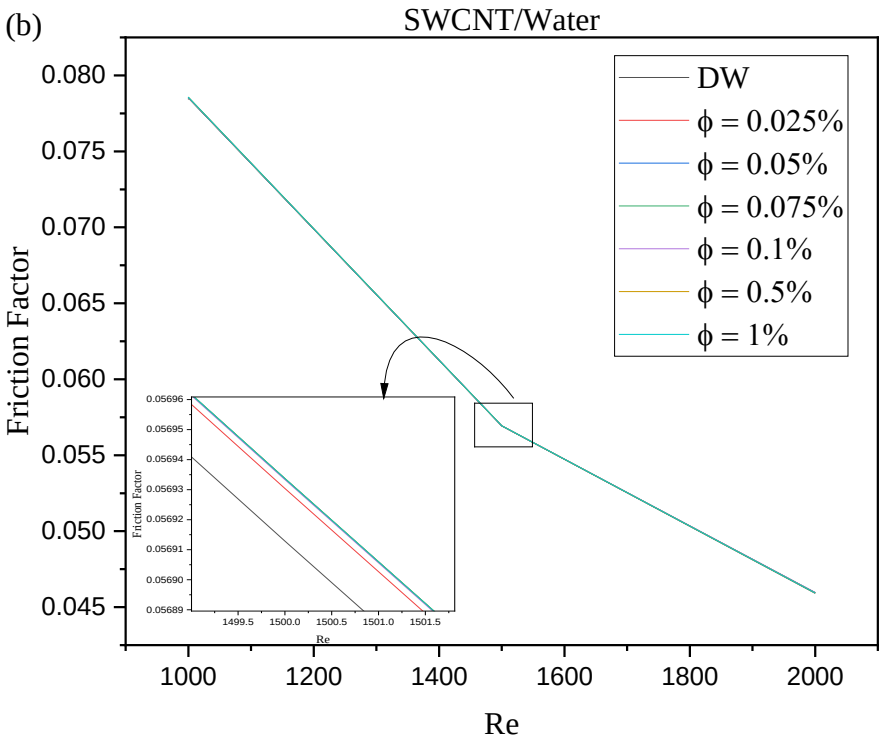

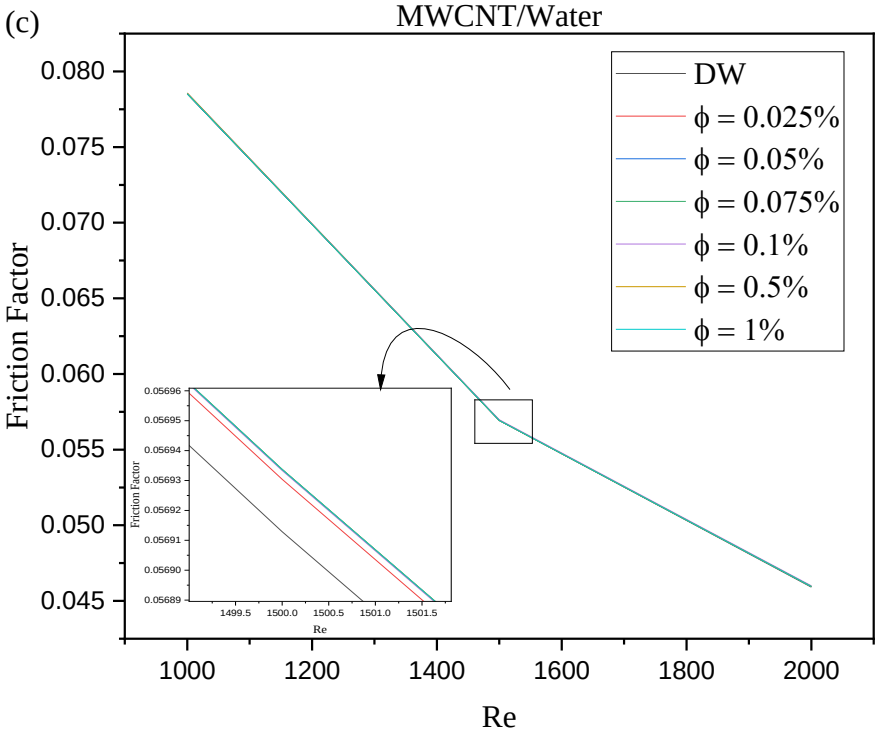

Figure 4.12 Variation of friction factor versus the Re for three different nanofluids at 313K. a) Al_2O_3/water, b) SWCNT/water, and c) MWCNT/water

4.4 RELATIVE PUMPING POWER

Variations of relative pumping power with the nanofluid concentrations at Re of 1000, 1500 and 2000 are shown in Figure 4.13 and Figure 4.14 for inlet temperatures of 303 K and 313 K respectively. It is observed that relative pumping power elevates with the addition of nanoparticle concentration. The viscosity of the nanofluids increments at higher nanoparticle concentration, resulting in higher relative pumping power. Re and temperature have very little effect on the pumping power values and can be considered negligible. Changing the Re poses no effect on the viscosity of the nanofluids and hence, relative pumping power remains the same. The pressure drop and velocity soar with an increase in particle concentration. Therefore, the relative pumping power of the FPSC increases at higher volume concentrations.

Among the three nanofluids, SWCNT shows the biggest increment followed by MWCNT and Al_2O_3. At 1% of volume concentration, SWCNT/water requires 1.83 times more pumping power than water whereas, MWCNT/water has a relative pumping power of 1.45 and 1.27 for Al_2O_3/water. Among the nanofluids, SWCNT/water shows the highest rise of viscosity with volume concentration. Therefore, it creates a higher pressure drop hence higher relative pumping power. Al_2O_3/water shows the minimum rise in viscosity and pressure drop. Subsequently, it requires the lowest pumping power among the nanofluids.

(a)

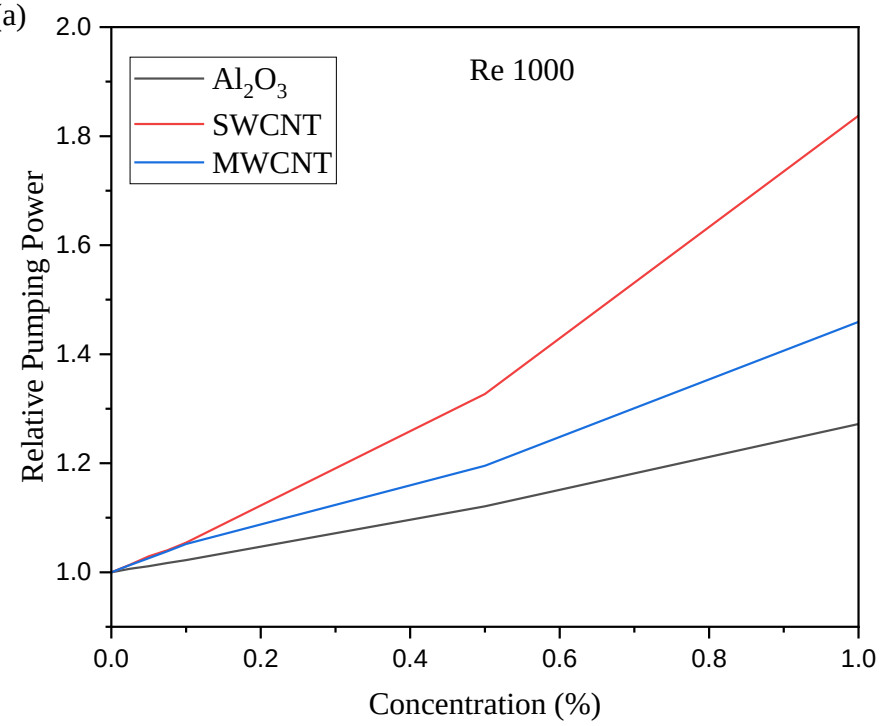
Re 1000
Al2O3
SWCNT
MWCNT
Relative Pumping Power
Concentration (%)
2.0
1.8
1.6
1.4
1.2
1.0
0.0
0.2
0.4
0.6
0.8
1.0

(b)

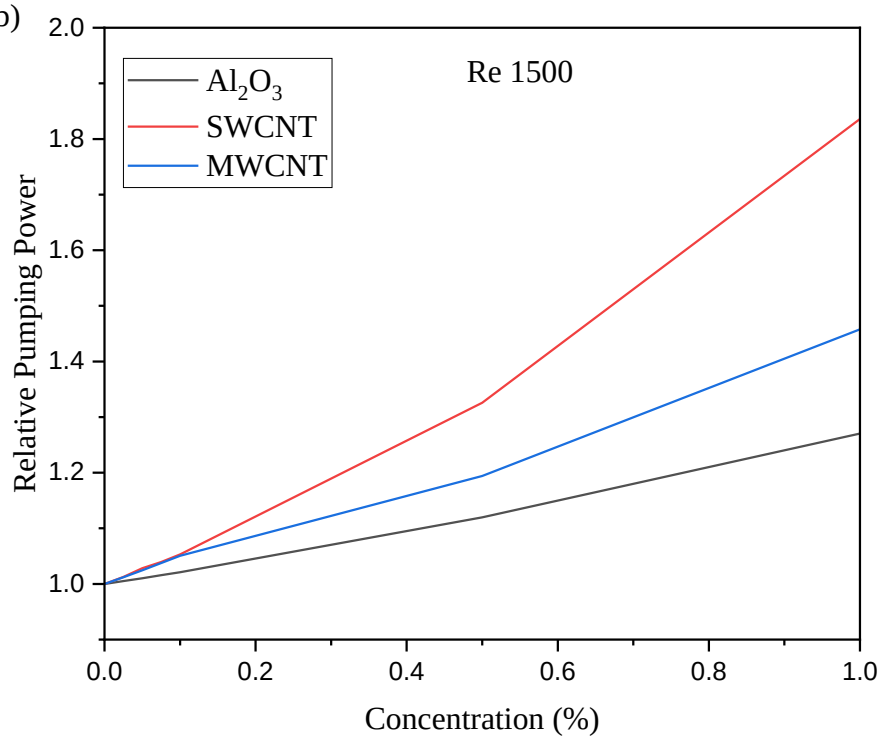
Re 1500
Al2O3
SWCNT
MWCNT
Relative Pumping Power
Concentration (%)
2.0
1.8
1.6
1.4
1.2
1.0
0.0
0.2
0.4
0.6
0.8
1.0

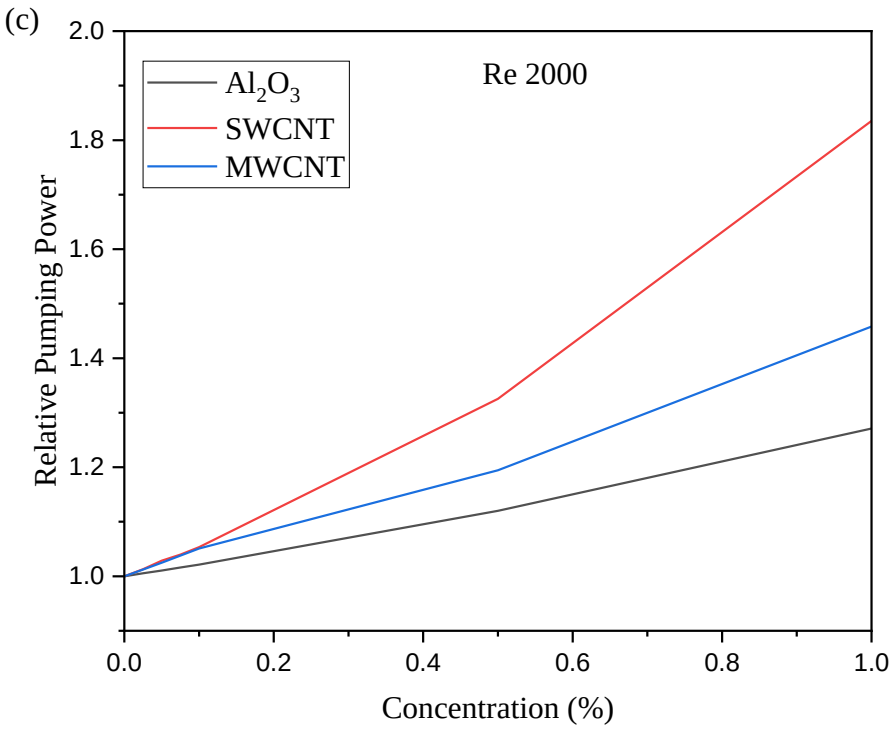

Figure 4.13 Variation of relative pumping power versus the volume concentration at three different Re for an inlet temperature of 303K. a) 1000 Re, b) 1500 Re and c) 2000 Re

(a)

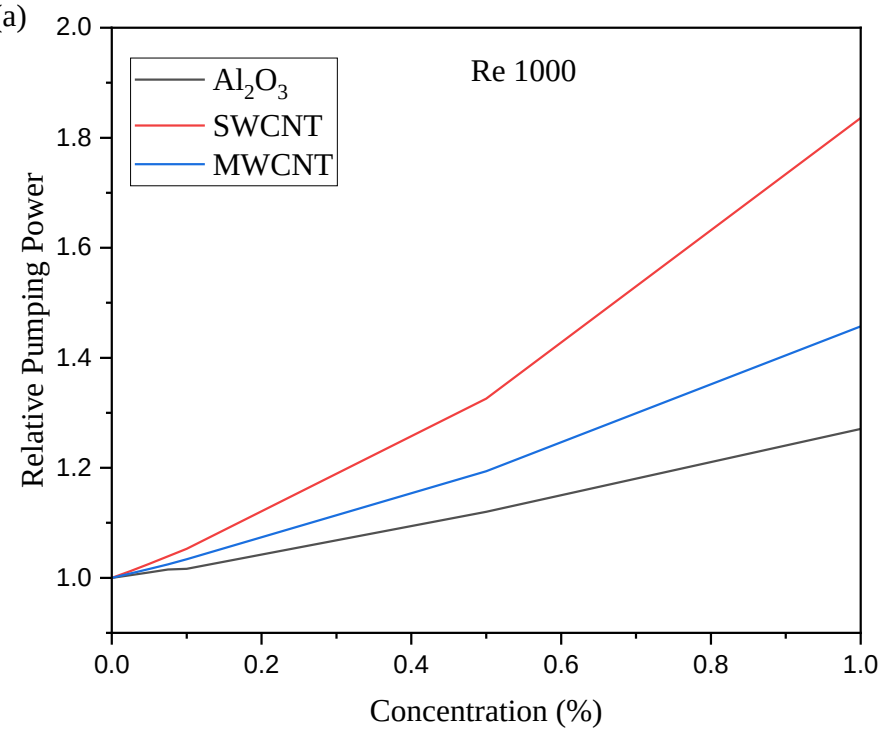
Re 1000
Al2O3
SWCNT
MWCNT
Relative Pumping Power
Concentration (%)
2.0
1.8
1.6
1.4
1.2
1.0
0.0
0.2
0.4
0.6
0.8
1.0

(b)

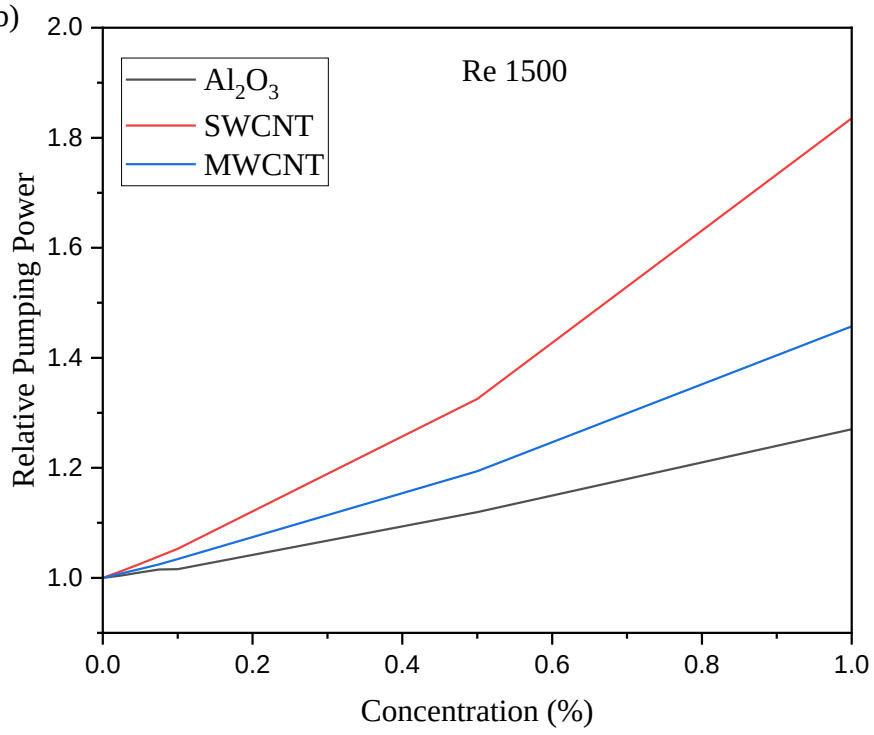
Re 1500
Al2O3
SWCNT
MWCNT
Relative Pumping Power
Concentration (%)
2.0
1.8
1.6
1.4
1.2
1.0
0.0
0.2
0.4
0.6
0.8
1.0

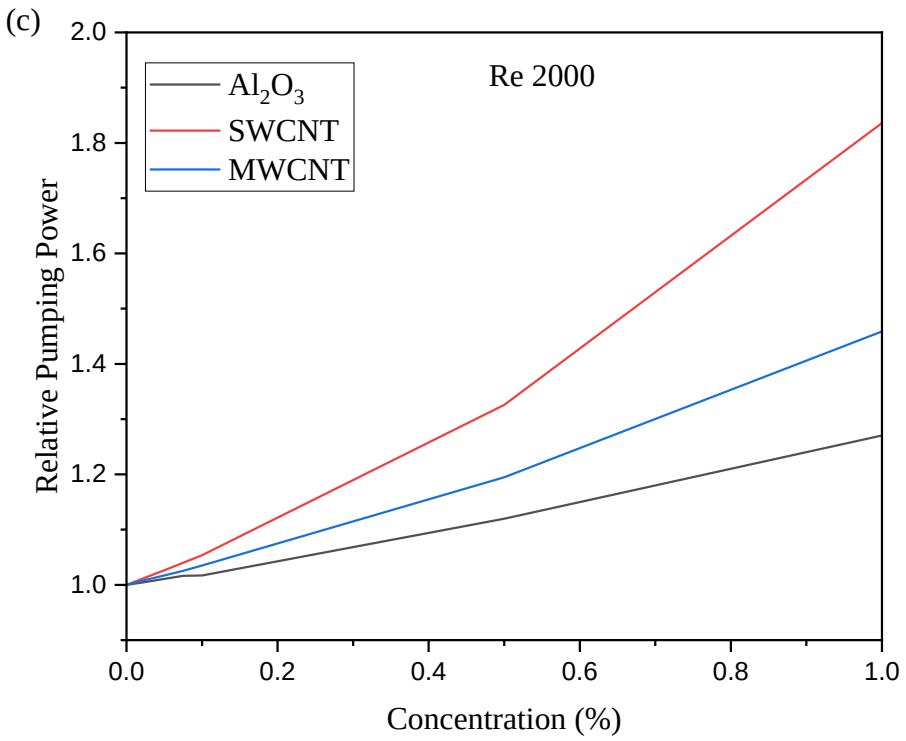

Figure 4.14 Variation of relative pumping power versus the volume concentration at three different Re for an inlet temperature of 313K. a) 1000 Re, b) 1500 Re and c) 2000 Re

4.5 HEAT TRANSFER COEFFICIENT

The graph of heat transfer coefficient versus Re is plotted in Figure 4.15 and Figure 4.16. As inferred in the figures, the heat transfer coefficient shows a rising trend when opposed to increasing Re at a constant particle concentration. Furthermore, at a specific Re, the heat transfer coefficient soars at a higher particle concentration. The difference between the riser tube wall temperature and the averaged fluid temperature diminishes with an increase in the Re. Similar phenomena occur when the particle concentration is increased which soars the thermal conductivity. Therefore, the heat transfer coefficient of the nanofluid improves for both circumstances.

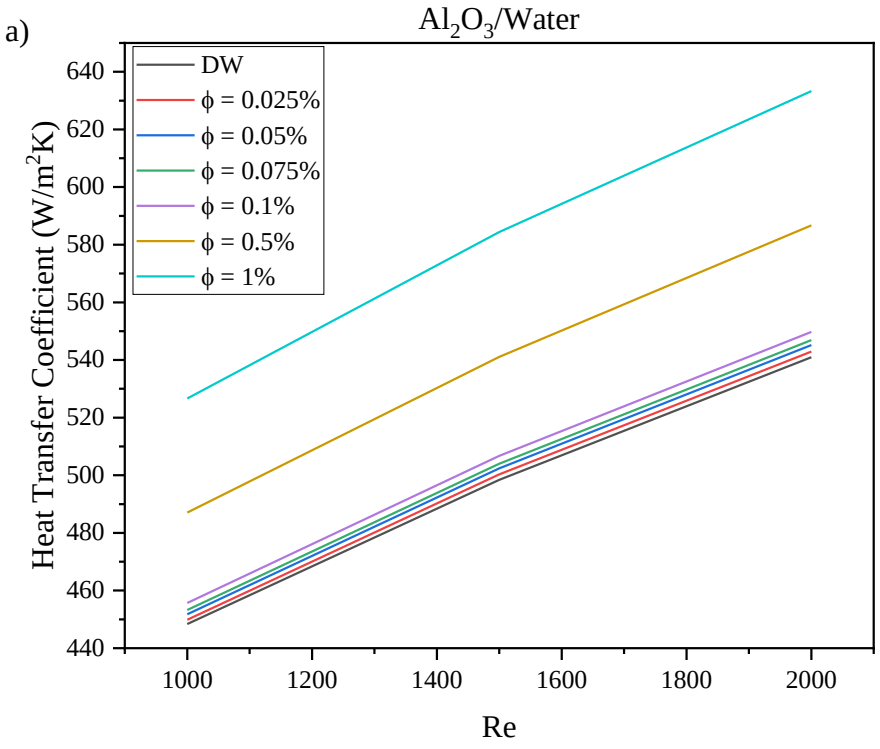

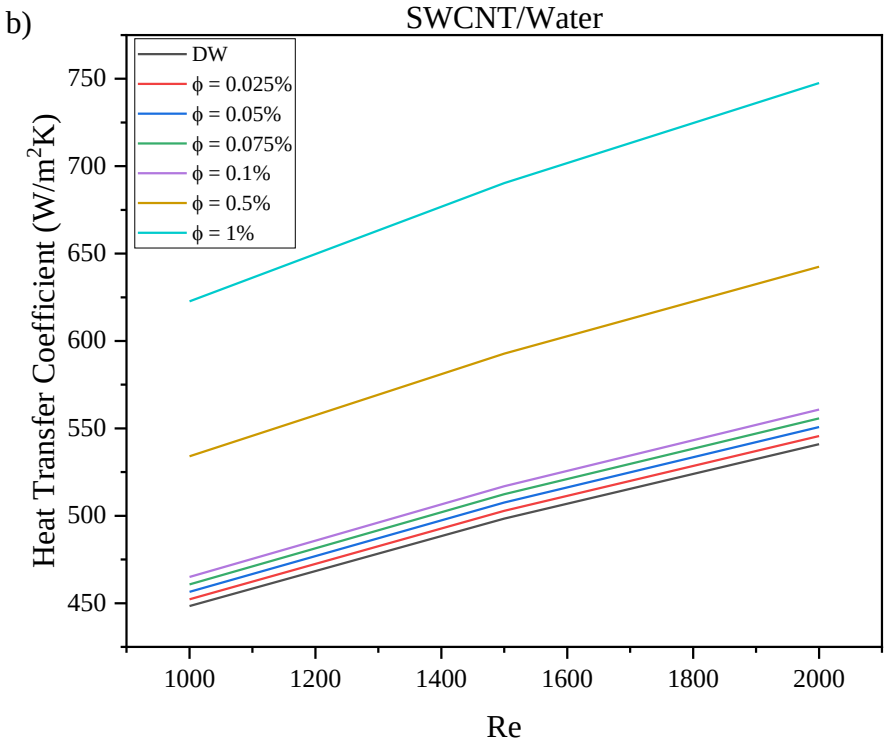

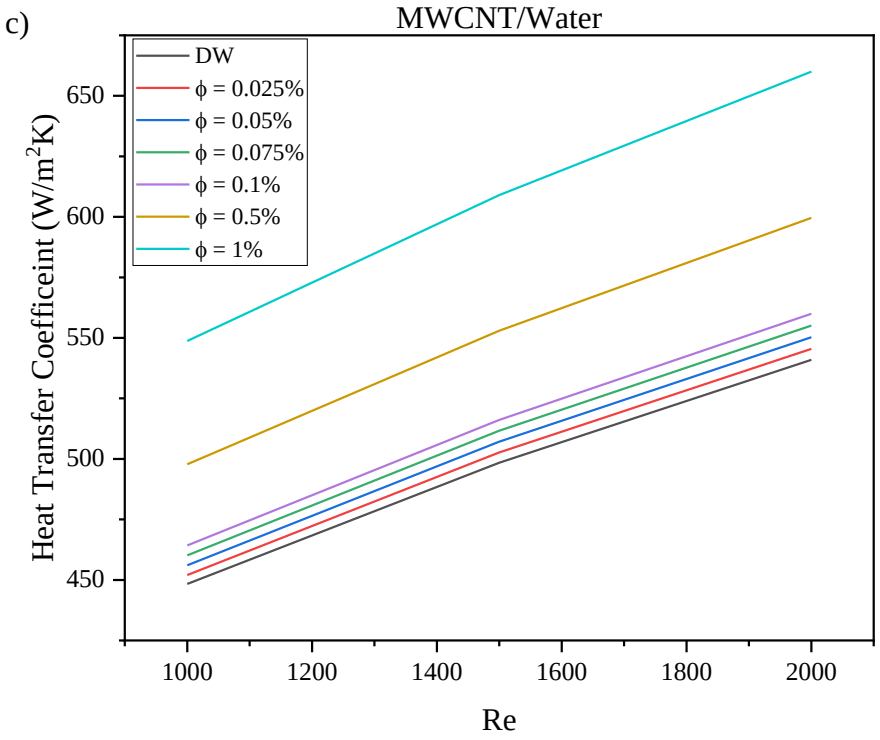

Figure 4.15 Variation of heat transfer coefficient with Re at 303K. a) Al_2O_3/water, b) SWCNT/water, and c) MWCNT/water

At 303 K inlet temperature, the highest increase of heat transfer coefficient is generated for SWCNT/water at ϕ = 1% and Re of 2000, reaching 747 W/m^{2}K, followed by MWCNT/water at 659 W/m^{2}K and Al_2O_3/water at 633 W/m^{2}K. The heat transfer coefficient magnitudes for SWCNT/water, MWCNT/water, and Al_2O_3/water at 313 K initial temperature were 741 W/m^{2}K, 649 W/m^{2}K, and 622 W/m^{2}K, respectively, at ϕ = 1% and Re of 2000. Figure 4.3 and Figure 4.4 indicate the biggest improvement in heat transfer coefficient for SWCNT/water due to its high thermal conductivity.

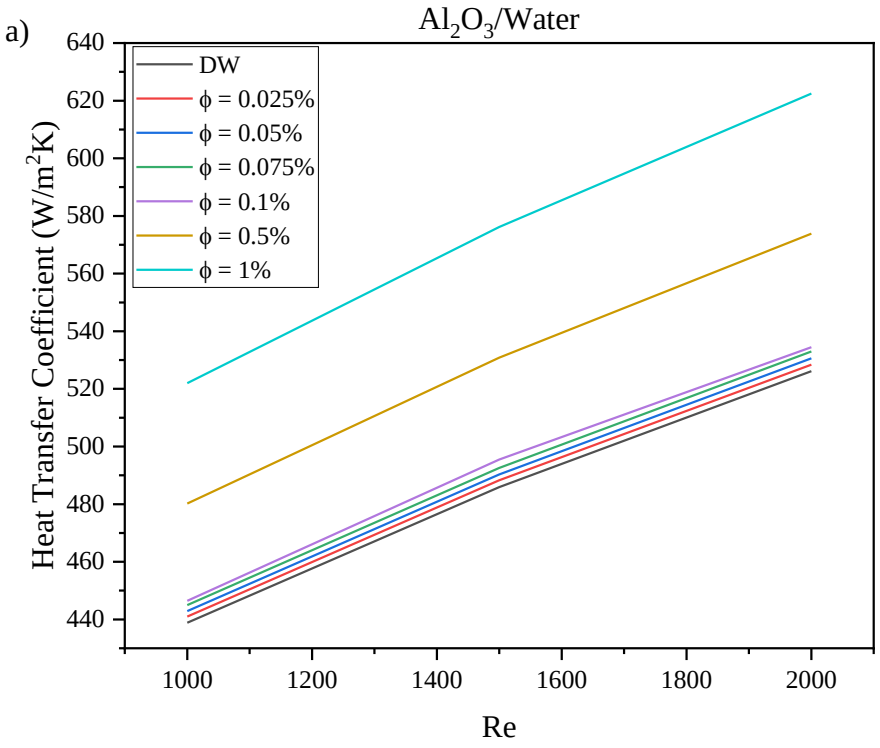

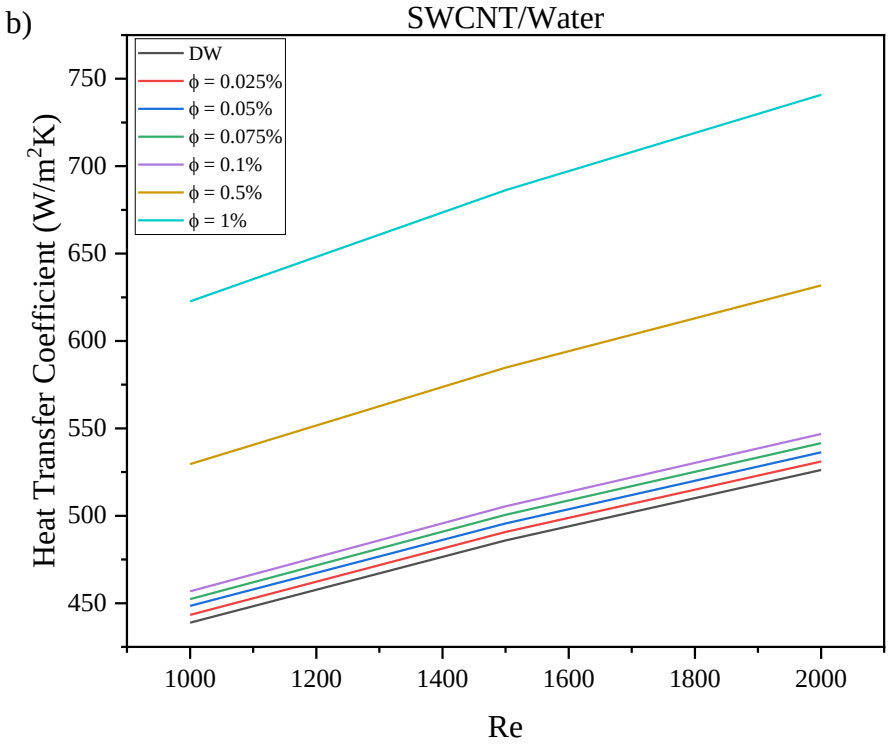

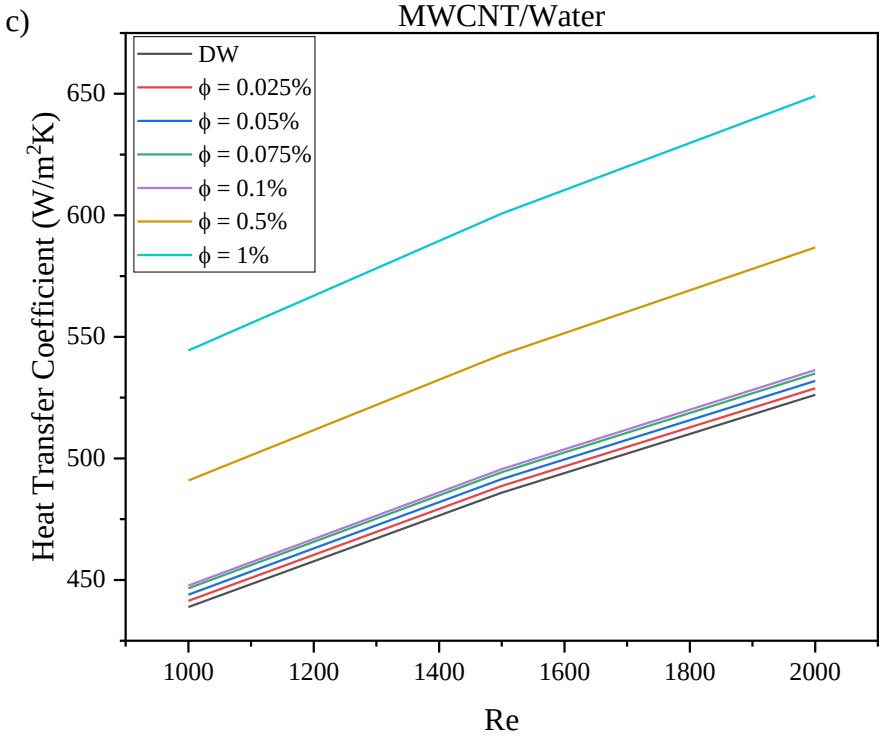

Figure 4.16 Variation of heat transfer coefficient with Re at 313K. a) Al_2O_3/water, b) SWCNT/water, and c) MWCNT/water

4.6 NUSSELT NUMBER

Figure 4.17 and Figure 4.18 depicts the variation of the Nu when opposed to the Re for Al_2O_3/water, SWCNT/water and MWCNT/water nanofluids at different particle concentrations with inlet temperatures of 303 K and 313 K respectively. From the graph, it is evident that for a fixed concentration the Nu improves as the Re rises, while for a fixed Re it diminishes with the addition of particle volume concentrations. As inferred in the figures, the heat transfer coefficient augments at a higher Re when volume concentration is kept constant. From the expression of the Nu (equation 12), it's evident that the Nu and the heat transfer coefficient share a directly proportional relationship. Therefore, the heat transfer coefficient and the Nu both increase with the Re. However, with the increase in particle concentration, the thermal conductivity of the nanofluid soars which is inversely proportional to the Nu. Furthermore, thermal conductivity shows a greater rate of increment than the heat transfer coefficient in this case. Therefore, with volume concentration, the Nu plummets. At low Re and high volume concentration, SWCNT/water generates the largest reduction in Nu followed by Al_2O_3/water and MWCNT/water. At inlet conditions of 303 K, for Re of 1000 and volume concentration of 1%, Nu of SWCNT/water decreased to 8.43 from 8.77 of water. At the same operating condition for Al_2O_3/water and MWCNT/water, the Nu values were recorded 8.52 and 8.54. For 313 K inlet temperature, the Nu resulted for SWCNT/water, Al_2O_3/water and MWCNT/water were 7.98, 8.09 and 8.10 respectively compared to the Nu of 8.32 for water. This also suggests the depletion of the Nu with a gain in inlet temperature.

(a)

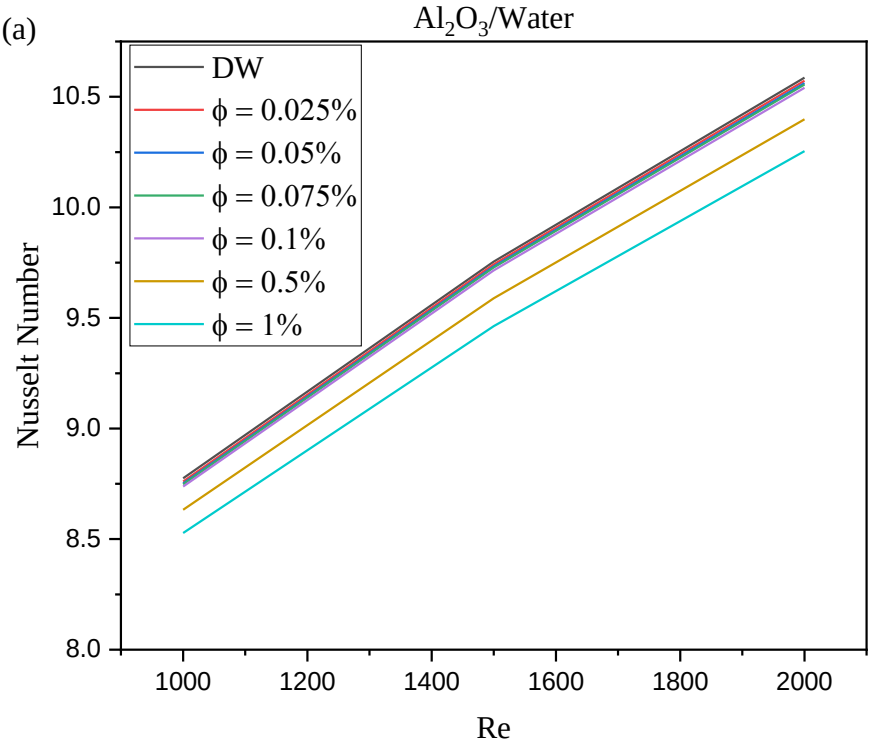
Al2O3/Water
DW
ϕ = 0.025%
ϕ = 0.05%
ϕ = 0.075%
ϕ = 0.1%
ϕ = 0.5%
ϕ = 1%
Nusselt Number
Re
8.0
8.5
9.0
9.5
10.0
10.5
1000
1200
1400
1600
1800
2000

(b)

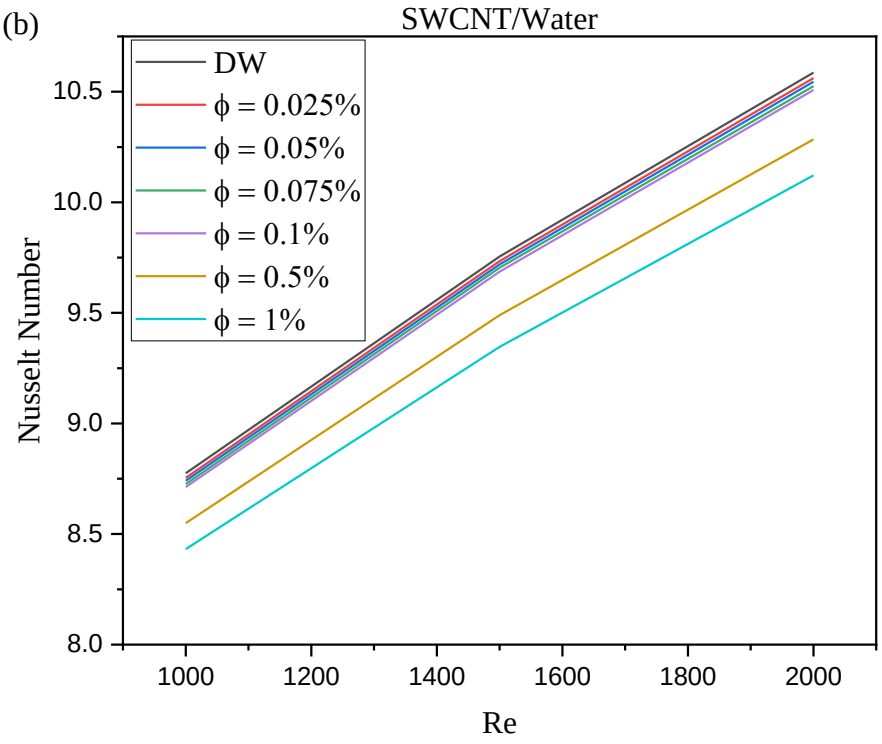
SWCNT/Water
DW
ϕ = 0.025%
ϕ = 0.05%
ϕ = 0.075%
ϕ = 0.1%
ϕ = 0.5%
ϕ = 1%
Nusselt Number
Re
8.0
8.5
9.0
9.5
10.0
10.5
1000
1200
1400
1600
1800
2000

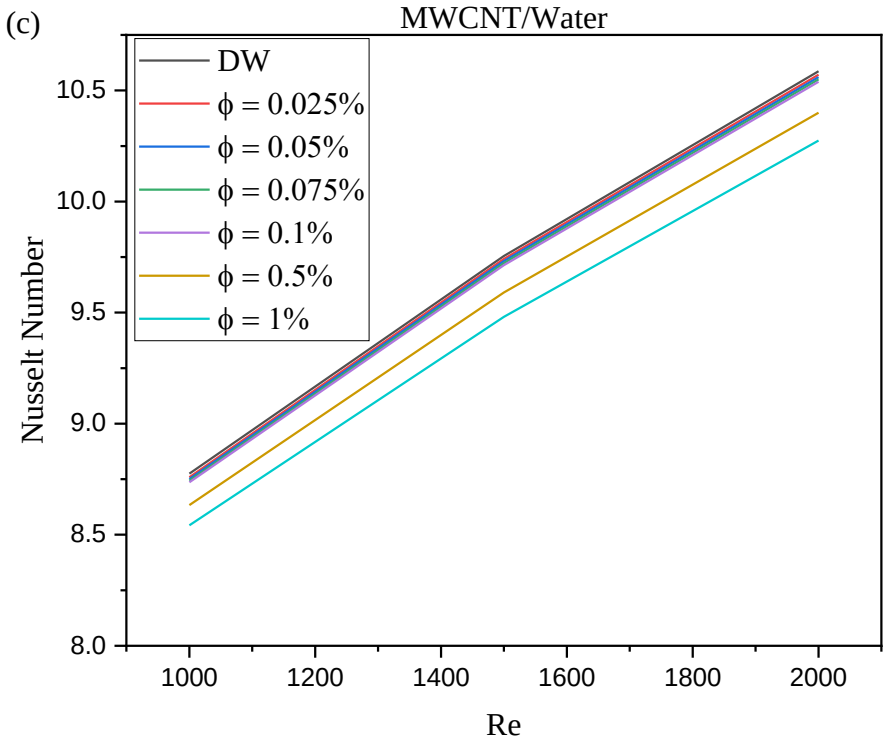

Figure 4.17 Variation of Nu versus the Re for three different nanofluids at 303K. a) Al_2O_3/water, b) SWCNT/water, and c) MWCNT/water

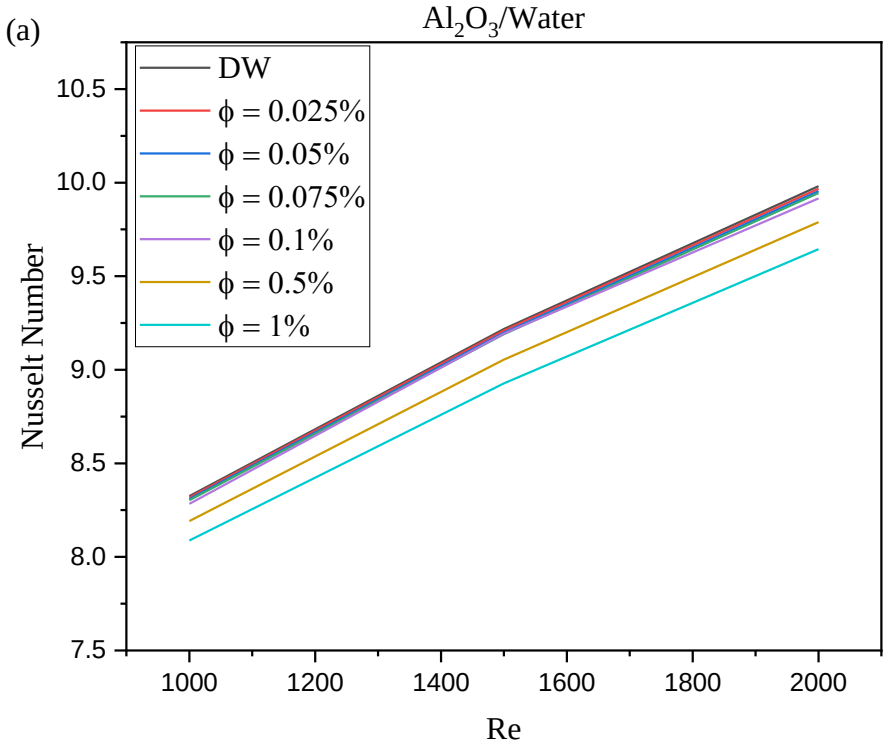

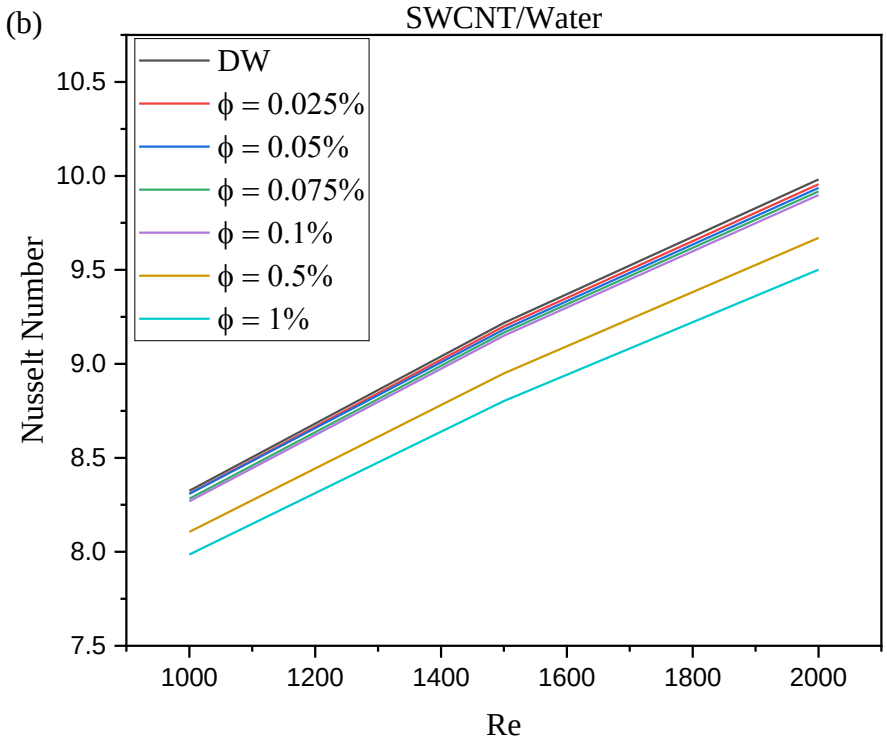

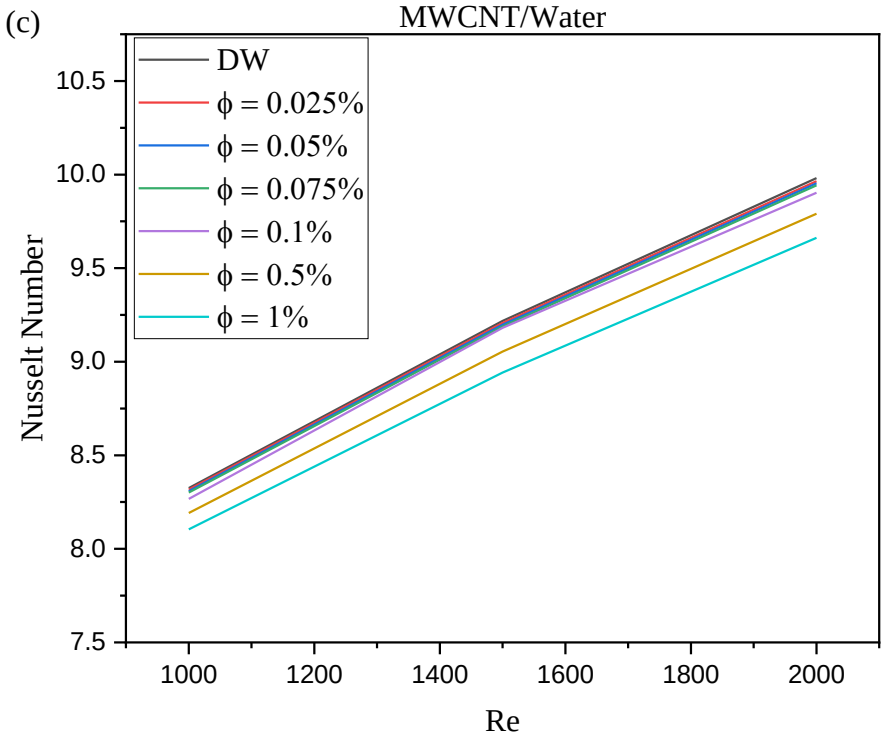

Figure 4.18 Variation of Nu versus the Re for three different nanofluids at 313K. a) Al_2O_3/water, b) SWCNT/water, and c) MWCNT/water

4.7 STANTON NUMBER

St is a dimensionless number that reflects the quantity of heat transferred by the fluid when there is heat transmission between a solid surface and a fluid. The change of St with Re is exhibited in Figure 4.19 and Figure 4.20. These graphs represents that the St diminishes with the surge of the Re but soars with the rise of volume concentration at a specific Re. The velocity of the nanofluids rises with the Re when the volume concentration is fixed. From the expression of the St (equation 13), it's evident that St is inversely proportional to the velocity. Subsequently, at a higher Re, the St drops. However, as volume concentration increases, the heat transfer coefficient, which is proportional to the St, increases. Therefore, the St increases with volume concentrations.

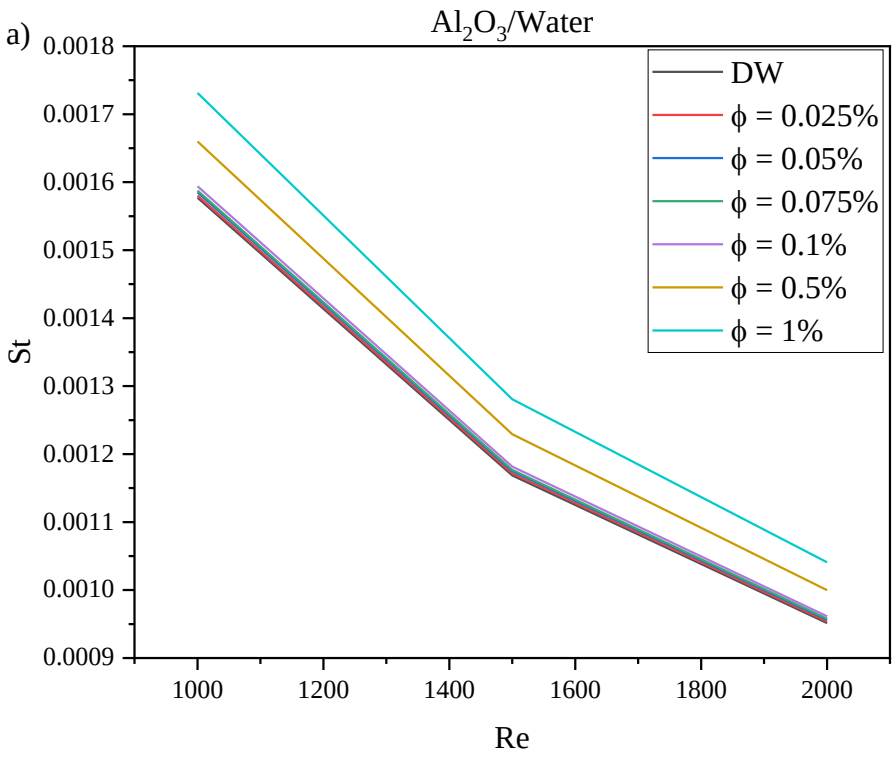

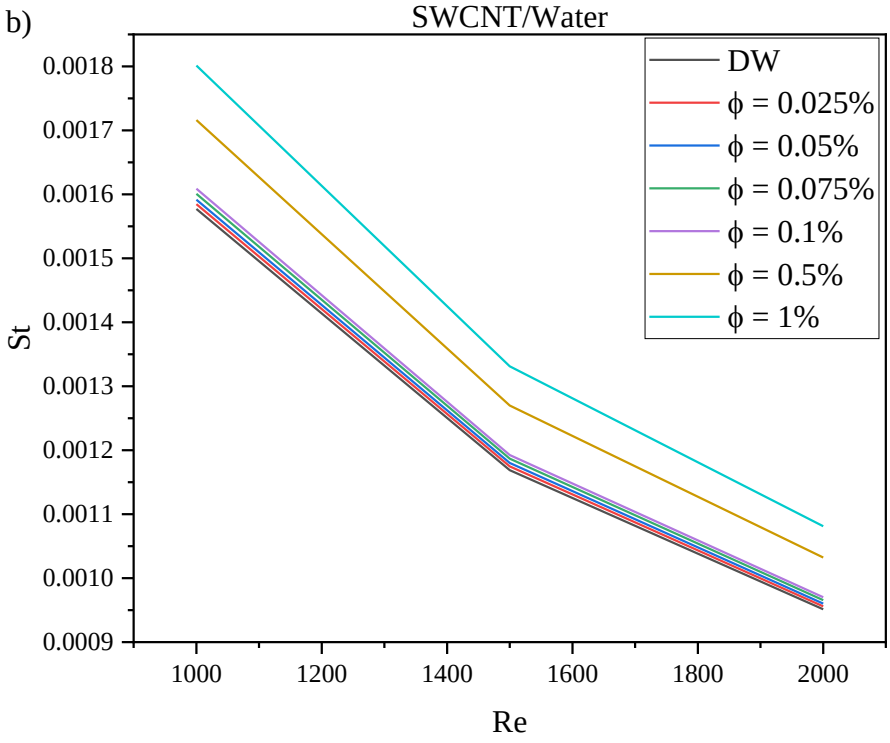

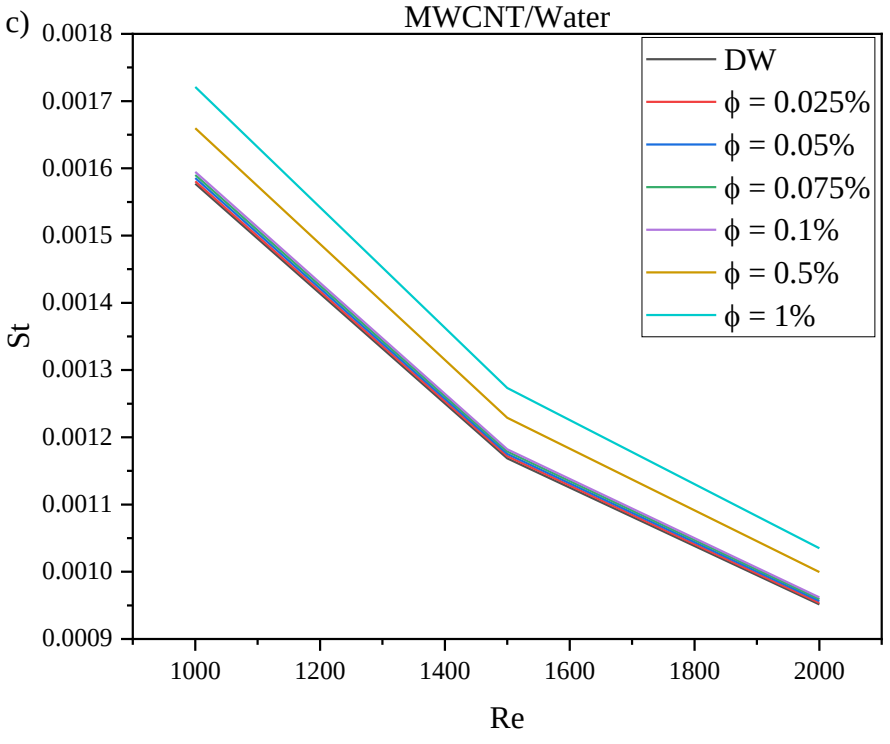

Figure 4.19 Variation of St with Re at 303K. a) Al_2O_3/water, b) SWCNT/water, and c) MWCNT/water

For 303K inlet temperature, at 1000 Re and 1% volume concentration, maximum St of 0.001801 was obtained for SWCNT/water nanofluid, whereas Al_2O_3/water and MWCNT/water obtained 0.001731 and 0.001721, respectively, at the same condition. Again, at 313 inlet temperature, SWCNT/water showed a highest St of 0.002197 followed by 0.002093 of Al_2O_3/water and 0.002083 of MWCNT/water at the lowest Re and highest volume concentration. Because of its higher heat transfer coefficient and lower density, SWCNT/water displays a higher St. Although Al_2O_3/water shows a lower heat transfer coefficient at any volume concentration than MWCNT/water, it generates a higher St. It occurs due to the lower viscosity of Al_2O_3/water than MWCNT/water. Because of its low viscosity, Al_2O_3/water has a lower velocity than MWCNT/water at a specific Re subsequently generating a higher St.

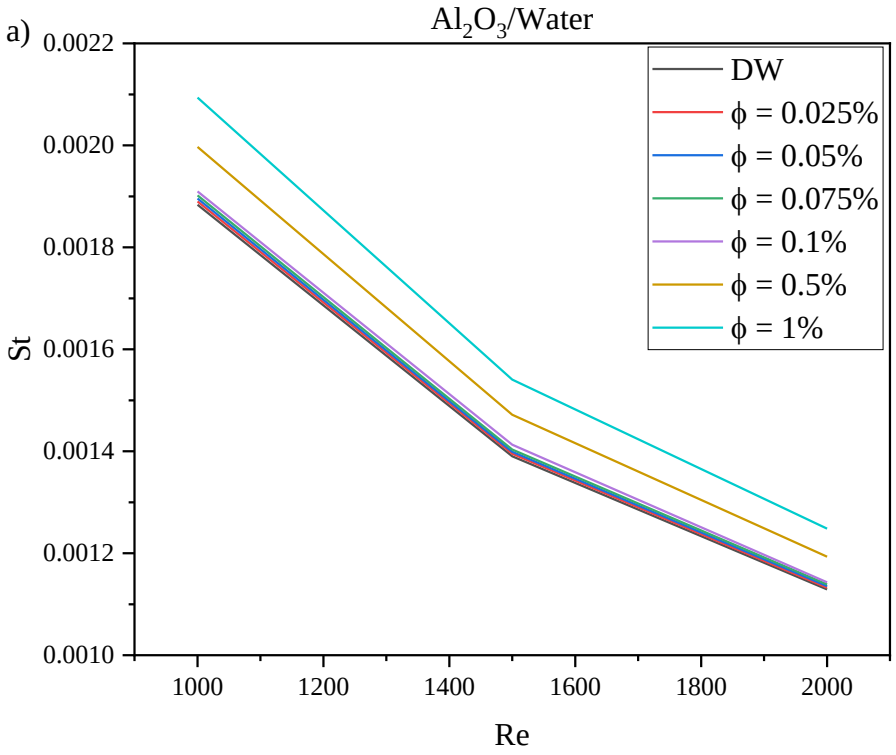

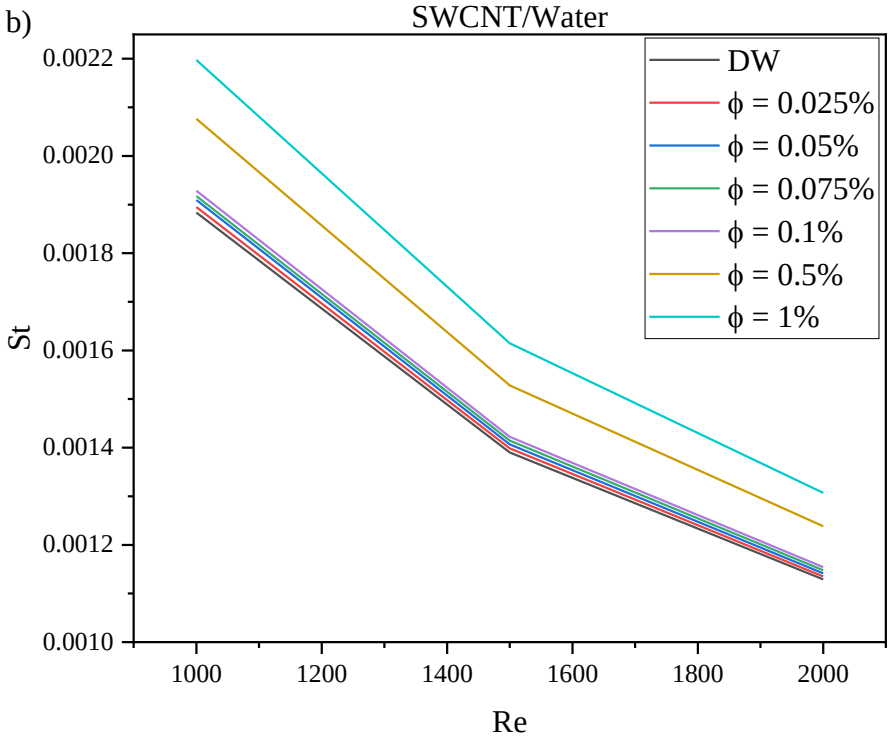

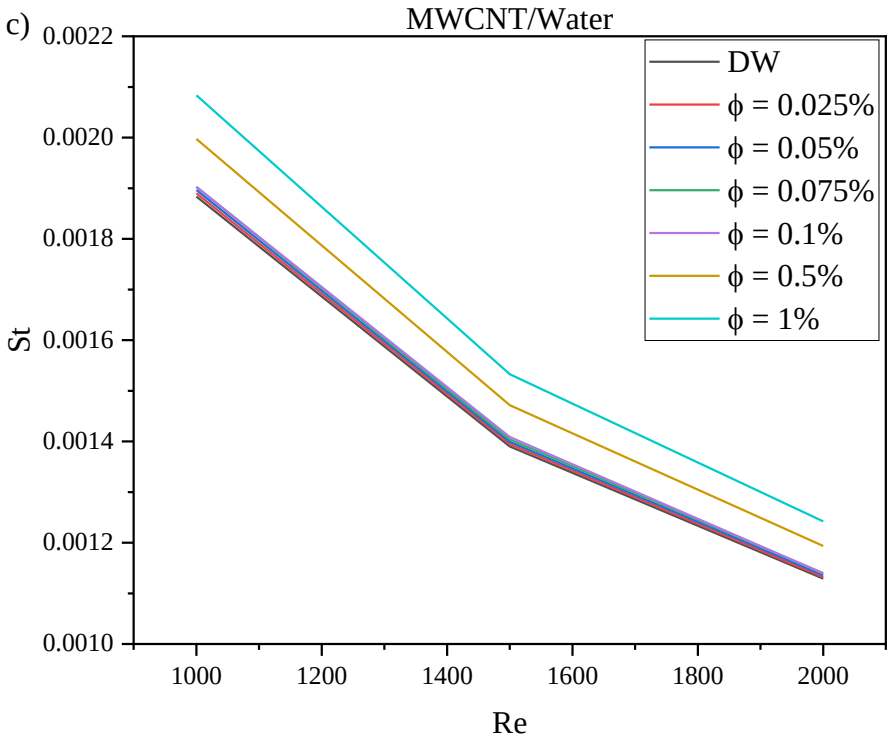

Figure 4.20 Variation of St with Re at 313K. a) Al_2O_3/water, b) SWCNT/water, and c) MWCNT/water

4.8 THERMO HYDRAULIC PERFORMANCE PARAMETER

A THPP vs concentration graph is presented in Figure 4.21 and Figure 4.22. THPP increases as the particle concentration increases. At a constant Re, an increment of the St results in a higher THPP value at higher particle concentration. However, the ratio of change in St for base fluid and nanofluid is similar to the Re. Therefore, the variation of THPP at different Re is almost negligible.

For an inlet condition of 303K, SWCNT/water indicates the highest THPP of 1.48 at ϕ = 1%, followed by Al_2O_3/water and MWCNT/water of 1.32 and 1.29, respectively. However, at concentrations lower than 0.05%, MWCNT/water results in higher THPP than Al_2O_3/water. At 313K, SWCNT/water displayed the maximum THPP of 1.59 at ϕ = 1%. The THPP curve for the Al_2O_3/water and MWCNT/water is almost similar up to 0.5% volume concentration. At higher volume concentrations, Al_2O_3/water was better than MWCNT/water.

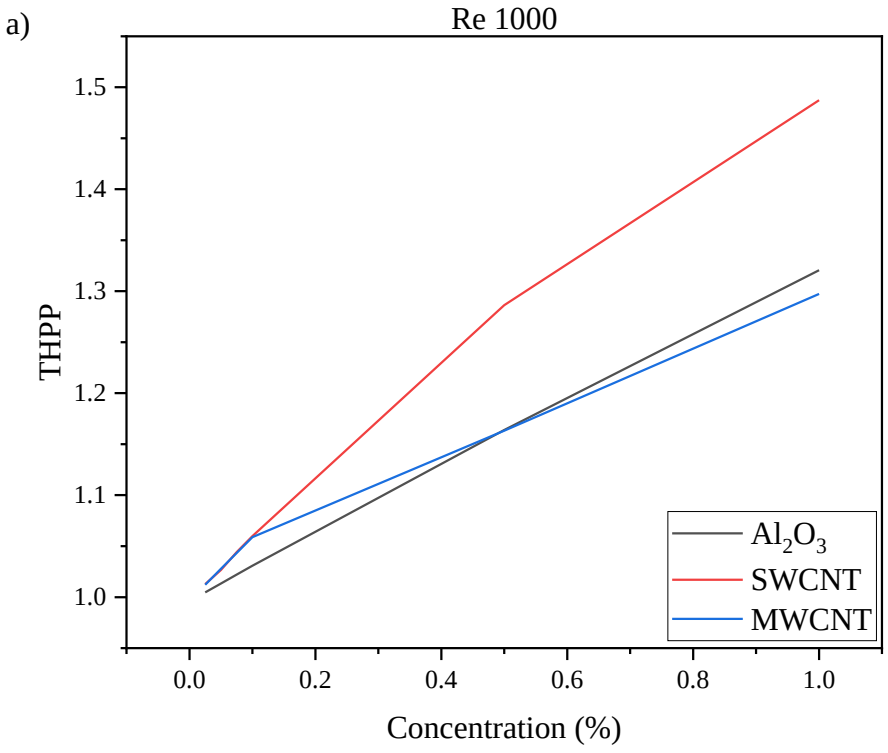

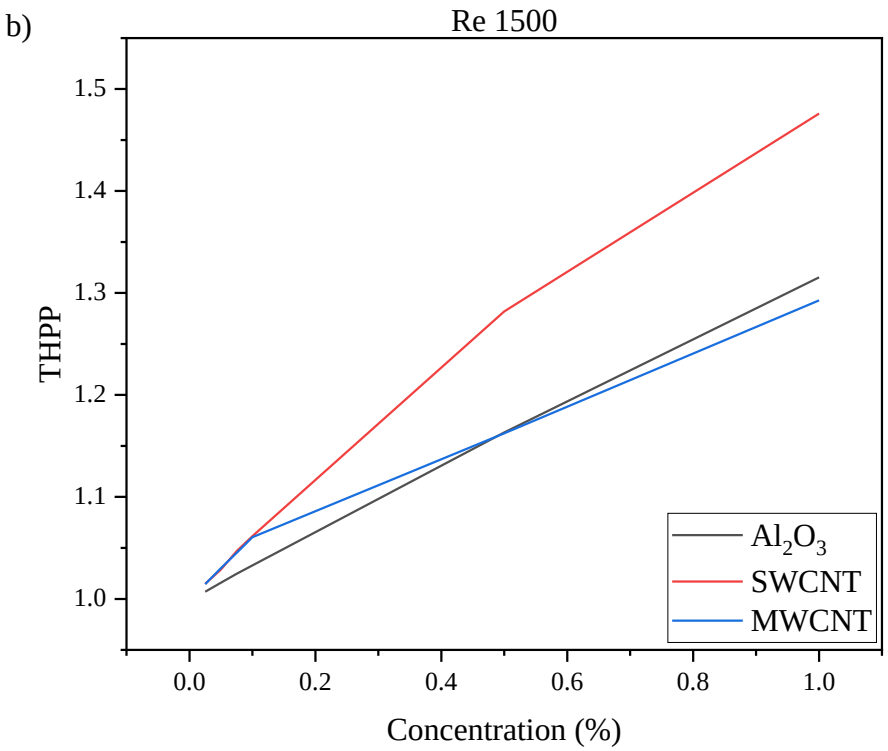

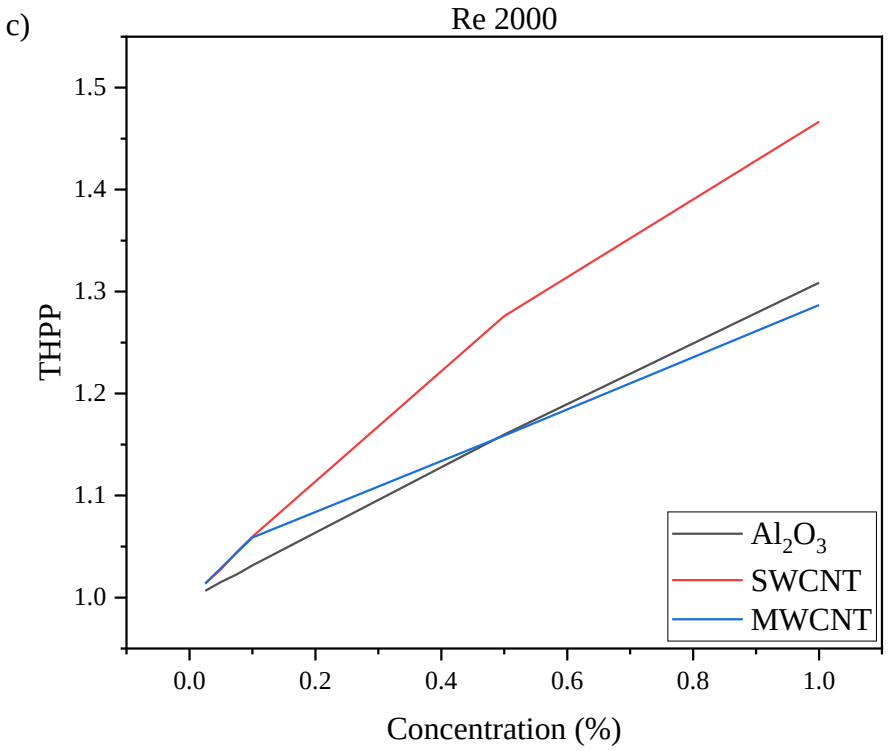

Figure 4.21 Variation of THPP with concentration at 303K. a) 1000 Re, b) 1500 Re and c) 2000 Re

a)

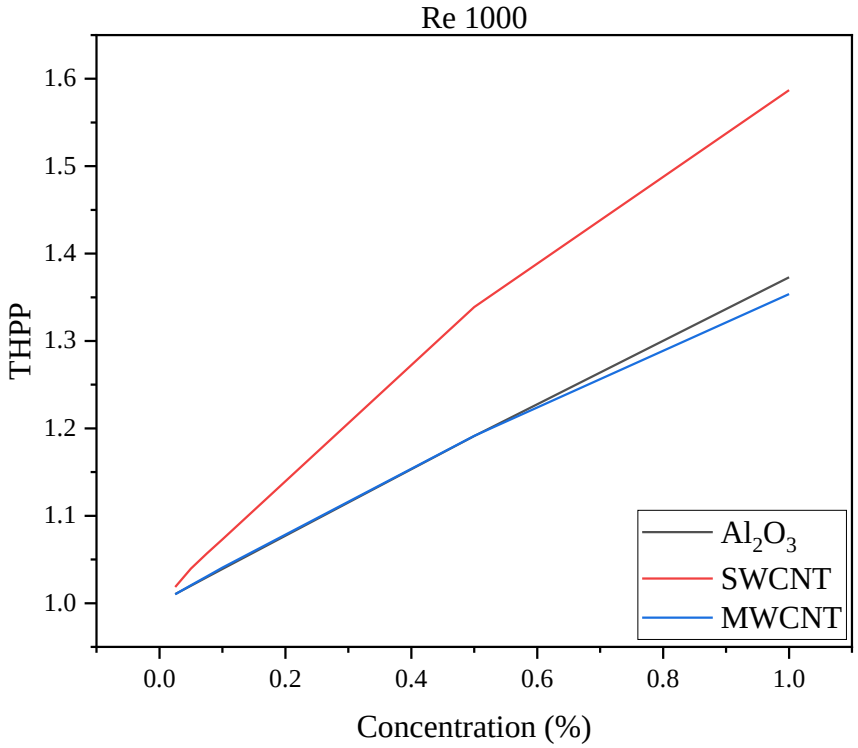
Re 1000
THPP
1.6
1.5
1.4
1.3
1.2
1.1
1.0
0.0
0.2
0.4
0.6
0.8
1.0
Concentration (%)
Al2O3
SWCNT
MWCNT

b)

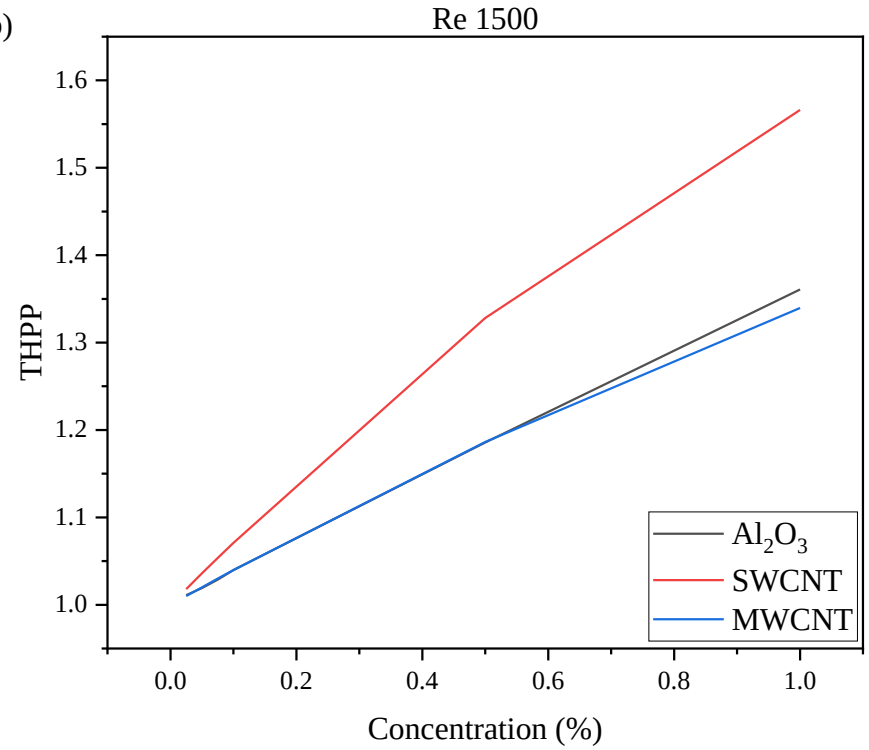
Re 1500
THPP
1.6
1.5
1.4
1.3
1.2
1.1
1.0
0.0
0.2
0.4
0.6
0.8
1.0
Concentration (%)
Al2O3
SWCNT
MWCNT

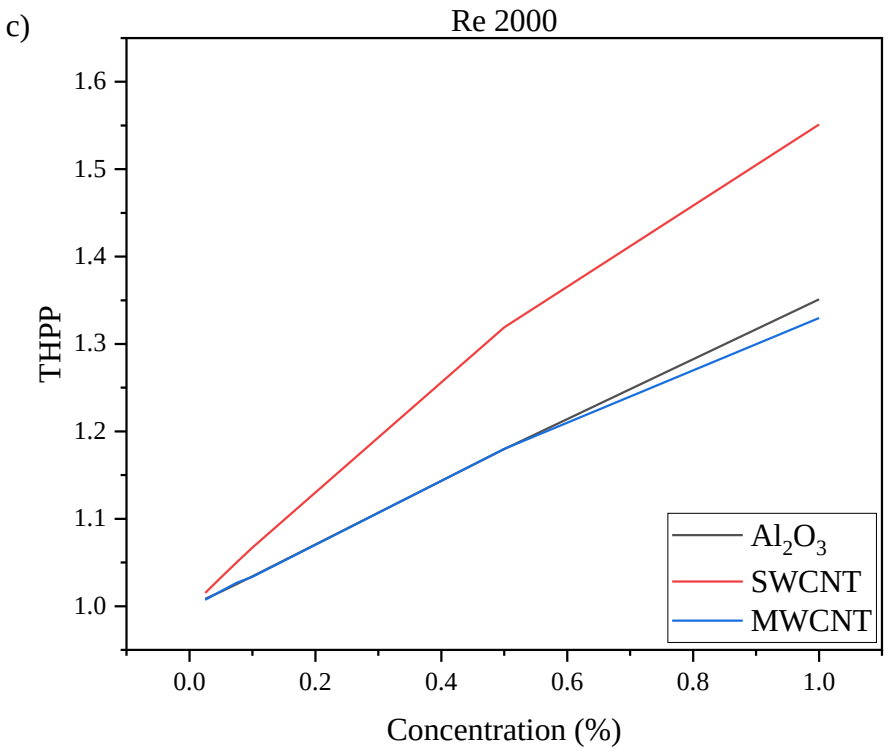

Figure 4.22 Variation of THPP with concentration at 313K. a) 1000 Re, b) 1500 Re and c) 2000 Re

4.9 CONCLUSIONS FROM RESULTS AND DISCUSSION

From the results, SWCNT/water showed the lowest rise in outlet temperature and the highest drop in Nu among the nanofluids. Also, SWCNT/water indicates the highest relative pumping power, followed by MWCNT/water and Al_2O_3/water. Based on these results alone, SWCNT/water seems to be the least preferable nanofluid whereas Al_2O_3/water shows superior performance by generating higher outlet temperature, Nu and lower pumping power. However, the high drop in temperature occurs due to the substantial increase of velocity in a constant Re for SWCNT/water nanofluid. Although SWCNT/water illustrates a lower Nu due to superior augmentation of thermal conductivity, it presents an excellent performance when it comes to the heat transfer coefficient, St and Thermo Hydraulic Performance Parameter. Among Al_2O_3/water and MWCNT/water nanofluids, higher thermal-hydraulic performance was exhibited by MWCNT/water. Subsequently, based on the thermal and hydraulic performance of the nanofluids, SWCNT/water nanofluid indicates superior performance. However, it also requires very high pumping power. Therefore, SWCNT/water nanofluid may exhibit the best performance in a FPSC, but it may not be the best alternative from an economical aspect. On the other hand, MWCNT/water presented a moderate rise in relative pumping power with a substantial increase in thermal-hydraulic performance, albeit quite inferior to SWCNT/water. As a result, it may be a better choice in terms of both cost and performance. Finally, Al_2O_3/water is the most economical among the nanofluids but it showed poor performance compared to carbon-based nanofluids. In conclusion, carbon-based nanofluids exhibit better performance at the expense of higher pumping power. On the other hand, metal-based nanofluids may show poor performance compared to carbon-based nanofluids, they require lower pumping power which makes them economically beneficial.

CHAPTER 5. CONCLUSIONS AND RECOMMENDATIONS

In this study, a computational model was generated for evaluating the performance of metal-based and carbon-based nanofluids at FPSC. The effectiveness of Al_2O_3/water, SWCNT/water, and MWCNT/water nanofluids were observed at 303K and 313K inlet temperatures at Re range of 1000 to 2000. The particle concentration of these nanofluids was kept between 0.025-1%. The computational study showed that:

i. The outlet temperature of FPSC diminishes when both Re and volume concentration increase. Al_2O_3/water showed the lowest decrease in the outlet temperature when the concentration of the nanoparticles was increased.

ii. The friction factor magnitude also depreciates with the increment of the Re, but the nanofluids have a negligible significance on the friction factor.

iii. A higher volume concentration of nanofluids necessitates greater pumping power, though the change in Re and operating conditions do not have any major impact on the pumping power. Among the nanofluids, SWCNT/water required the highest pumping power.

iv. At both inlet temperatures, SWCNT/water showed a higher magnitude of heat transfer coefficient in the range of 740-750 W/m^2K. The magnitude of the heat transfer coefficient was enhanced with the increment of both Re and particle volume concentration.

v. Nu rises at a higher Re, but it decreases when volume concentration increases. At a constant Re, SWCNT/water exhibits the greatest reduction in Nu, followed by Al_2O_3/water and MWCNT/water with the addition of volume concentration.

vi. The St reduces with the rise of the Re. But the improvement in volume concentration has a positive impact on the St. A maximum St was obtained using SWCNT/water nanofluid at 1% volume concentration at 1000 Re.

vii. Though THPP increased with higher volume concentration, Re had a negligible impact on it. At 1% volume concentration, SWCNT/water achieved a maximum THPP value of 1.48 and 1.59 at 303K and 313K inlet temperatures, respectively.

The study indicates SWCNT/water as the best working fluid because of its superior performance in terms of heat transfer coefficient and THPP at the cost of higher relative pumping power. This judgment is in terms of performance basis; the economic feasibility of the utilization is yet to be examined. The developed computational model implies that using carbon-based nanofluids in FPSC is more beneficial than using metal-based nanofluids.

To evaluate the economical aspect of the FPSC with nanofluids, an area reduction study in addition to a payback period analysis should be studied. Another area of future inquiry is the embodied energy analysis and CO_2 emission rate of nanofluids, to assess the environmental effect of FPSC and nanofluids. In addition, to optimize the performance of FPSC, alongside the utilization of nanofluids, change in geometry and flow regime of the collector can be considered for future research purposes. Shifting the flow regime from laminar to turbulent with the addition of turbulent inducing elements has the potential to improve the thermal performance of the FPSC. Furthermore, change in the fluid channel geometry is also an exciting prospect that may enhance the efficiency of a FPSC. In general, FPSCs suffer from high heat losses which reduce their thermal efficiency. Integrating transparent films between the absorber plate and glass cover may be beneficial for the practical implication of FPSC, which calls for further study.

REFERENCES

[1] A. A. Hawwash, A. K. Abdel Rahman, S. A. Nada, and S. Ookawara, "Numerical Investigation and Experimental Verification of Performance Enhancement of Flat Plate Solar Collector Using Nanofluids," *Appl. Therm. Eng.*, vol. 130, pp. 363–374, 2018, doi: 10.1016/j.applthermaleng.2017.11.027.

[2] Y. Li, J. Zhou, S. Tung, E. Schneider, and S. Xi, "A review on development of nanofluid preparation and characterization," *Powder Technol.*, vol. 196, no. 2, pp. 89–101, 2009, doi: 10.1016/j.powtec.2009.07.025.

[3] W. Yu, D. M. France, J. L. Routbort, and S. U. S. Choi, "Review and comparison of nanofluid thermal conductivity and heat transfer enhancements," *Heat Transf. Eng.*, vol. 29, no. 5, pp. 432–460, 2008, doi: 10.1080/01457630701850851.

[4] L. H. Kumar, S. N. Kazi, H. H. Masjuki, M. N. M. Zubir, A. Jahan, and C. Bhinitha, "Energy, exergy and economic analysis of liquid flat-plate solar collector using green covalent functionalized graphene nanoplatelets," *Appl. Therm. Eng.*, vol. 192, no. March, p. 116916, 2021, doi: 10.1016/j.applthermaleng.2021.116916.

[5] F. Cruz-Peragon, J. M. Palomar, P. J. Casanova, M. P. Dorado, and F. Manzano-Agugliaro, "Characterization of solar flat plate collectors," *Renew. Sustain. Energy Rev.*, vol. 16, no. 3, pp. 1709–1720, 2012, doi: 10.1016/j.rser.2011.11.025.

[6] K. M. Pandey and R. Chaurasiya, "A review on analysis and development of solar flat plate collector," *Renew. Sustain. Energy Rev.*, vol. 67, pp. 641–650, 2017, doi: 10.1016/j.rser.2016.09.078.

[7] E. Vengadesan and R. Senthil, "A review on recent development of thermal performance enhancement methods of flat plate solar water heater," *Sol. Energy*, vol. 206, no. May, pp. 935–961, 2020, doi: 10.1016/j.solener.2020.06.059.

[8] N. Ikmal, S. Azha, H. Hussin, and M. S. Nasif, "Thermal Performance Enhancement in Flat Plate Solar Collector Solar Water Heater: A Review," *Processes*, 2020, doi: https://doi.org/10.3390/pr8070756.

[9] M. Edalatpour and J. P. Solano, "Thermal-hydraulic characteristics and exergy performance in tube-on-sheet flat plate solar collectors: Effects of nanofluids and mixed convection," *Int. J. Therm. Sci.*, vol. 118, pp. 397–409, 2017, doi: 10.1016/j.ijthermalsci.2017.05.004.

[10] F. Hossain, M. R. Karim, and A. A. Bhuiyan, “A review on recent advancements of the usage of nano fluid in hybrid photovoltaic/thermal (PV/T) solar systems,” *Renew. Energy*, vol. 188, pp. 114–131, 2022, doi: 10.1016/j.renene.2022.01.116.

[11] M. Sheikholeslami, S. A. Farshad, Z. Ebrahimpour, and Z. Said, “Recent progress on flat plate solar collectors and photovoltaic systems in the presence of nanofluid: A review,” *J. Clean. Prod.*, vol. 293, p. 126119, 2021, doi: 10.1016/j.jclepro.2021.126119.

[12] S. K. Verma, A. K. Tiwari, and D. S. Chauhan, “Performance augmentation in flat plate solar collector using MgO/water nanofluid,” *Energy Convers. Manag.*, vol. 124, pp. 607–617, 2016, doi: 10.1016/j.enconman.2016.07.007.

[13] T. Yousefi, F. Veysi, E. Shojaeizadeh, and S. Zinadini, “An experimental investigation on the effect of Al2O3-H2O nanofluid on the efficiency of flat-plate solar collectors,” *Renew. Energy*, vol. 39, no. 1, pp. 293–298, 2012, doi: 10.1016/j.renene.2011.08.056.

[14] S. A. Sakhaei and M. S. Valipour, “Performance enhancement analysis of The flat plate collectors: A comprehensive review,” *Renew. Sustain. Energy Rev.*, vol. 102, no. May 2018, pp. 186–204, 2019, doi: 10.1016/j.rser.2018.11.014.

[15] S. K. Verma and A. K. Tiwari, “Progress of nanofluid application in solar collectors: A review,” *Energy Convers. Manag.*, vol. 100, pp. 324–346, 2015, doi: 10.1016/j.enconman.2015.04.071.

[16] R. B. Ganvir, P. V. Walke, and V. M. Kriplani, “Heat transfer characteristics in nanofluid—A review,” *Renew. Sustain. Energy Rev.*, vol. 75, no. October, pp. 451–460, 2017, doi: 10.1016/j.rser.2016.11.010.

[17] R. Dobriyal, P. Negi, N. Sengar, and D. B. Singh, “A brief review on solar flat plate collector by incorporating the effect of nanofluid,” *Mater. Today Proc.*, vol. 21, no. xxxx, pp. 1653–1658, 2020, doi: 10.1016/j.matpr.2019.11.294.

[18] R. Dobriyal, P. Negi, N. Sengar, and D. B. Singh, “A brief review on solar flat plate collector by incorporating the effect of nanofluid,” *Mater. Today Proc.*, vol. 21, no. xxxx, pp. 1653–1658, 2020, doi: 10.1016/j.matpr.2019.11.294.

[19] H. K. Gupta, G. Das Agrawal, and J. Mathur, “An experimental investigation of a low temperature Al2O3-H2O nanofluid based direct absorption solar collector,” *Sol. Energy*, vol. 118, pp. 390–396, 2015, doi: 10.1016/j.solener.2015.04.041.

[20] S. S. Khaleduzzaman, M. R. Sohel, R. Saidur, and J. Selvaraj, “Stability of

Al2O3-water nanofluid for electronics cooling system," *Procedia Eng.*, vol. 105, no. August, pp. 406–411, 2015, doi: 10.1016/j.proeng.2015.05.026.

[21] M. Mirzaei, S. M. S. Hosseini, and A. M. Moradi Kashkooli, "Assessment of Al2O3 nanoparticles for the optimal operation of the flat plate solar collector," *Appl. Therm. Eng.*, vol. 134, no. February 2017, pp. 68–77, 2018, doi: 10.1016/j.applthermaleng.2018.01.104.

[22] M. A. Sharafeldin and G. Gróf, "Experimental investigation of flat plate solar collector using CeO2-water nanofluid," *Energy Convers. Manag.*, vol. 155, no. August 2017, pp. 32–41, 2018, doi: 10.1016/j.enconman.2017.10.070.

[23] H. J. Jouybari, M. E. Nimvari, and S. Saedodin, "Thermal performance evaluation of a nanofluid-based flat-plate solar collector: An experimental study and analytical modeling," *J. Therm. Anal. Calorim.*, vol. 137, no. 5, pp. 1757–1774, 2019, doi: 10.1007/s10973-019-08077-z.

[24] P. Michael Joseph Stalin, T. V. Arjunan, M. M. Matheswaran, H. Dolli, and N. Sadanandam, "Energy, economic and environmental investigation of a flat plate solar collector with CeO2/water nanofluid," *J. Therm. Anal. Calorim.*, vol. 139, no. 5, pp. 3219–3233, 2020, doi: 10.1007/s10973-019-08670-2.

[25] M. Moravej *et al.*, "Enhancing the efficiency of a symmetric flat-plate solar collector via the use of rutile TiO2-water nanofluids," *Sustain. Energy Technol. Assessments*, vol. 40, no. June, 2020, doi: 10.1016/j.seta.2020.100783.

[26] L. S. Sundar, A. H. Misganaw, M. K. Singh, A. M. B. Pereira, and A. C. M. Sousa, "Efficiency, energy and economic analysis of twisted tape inserts in a thermosyphon solar flat plate collector with Cu nanofluids," *Renew. Energy Focus*, vol. 35, no. 00, pp. 10–31, 2020, doi: 10.1016/j.ref.2020.06.004.

[27] S. Choudhary, A. Sachdeva, and P. Kumar, "Influence of stable zinc oxide nanofluid on thermal characteristics of flat plate solar collector," *Renew. Energy*, vol. 152, pp. 1160–1170, 2020, doi: 10.1016/j.renene.2020.01.142.

[28] S. Choudhary, A. Sachdeva, and P. Kumar, "Investigation of the stability of MgO nanofluid and its effect on the thermal performance of flat plate solar collector," *Renew. Energy*, vol. 147, pp. 1801–1814, 2020, doi: 10.1016/j.renene.2019.09.126.

[29] E. C. Okonkwo, I. Wole-Osho, D. Kavaz, M. Abid, and T. Al-Ansari, "Thermodynamic evaluation and optimization of a flat plate collector operating with alumina and iron mono and hybrid nanofluids," *Sustain. Energy Technol.*

Assessments, vol. 37, no. January, p. 100636, 2020, doi: 10.1016/j.seta.2020.100636.

[30] S. Choudhary, A. Sachdeva, and P. Kumar, "Time-based analysis of stability and thermal efficiency of flat plate solar collector using iron oxide nanofluid," *Appl. Therm. Eng.*, vol. 183, p. 115931, 2021, doi: 10.1016/j.applthermaleng.2020.115931.

[31] K. Farhana, K. Kadirgama, H. A. Mohammed, D. Ramasamy, M. Samykano, and R. Saidur, "Analysis of efficiency enhancement of flat plate solar collector using crystal nano-cellulose (CNC) nanofluids," *Sustain. Energy Technol. Assessments*, vol. 45, no. February, 2021, doi: 10.1016/j.seta.2021.101049.

[32] A. M. Alklaibi, L. S. Sundar, and A. C. M. Sousa, "Experimental analysis of exergy efficiency and entropy generation of diamond/water nanofluids flow in a thermosyphon flat plate solar collector," *Int. Commun. Heat Mass Transf.*, vol. 120, p. 105057, 2021, doi: 10.1016/j.icheatmasstransfer.2020.105057.

[33] V. P. Kalbande, P. V. Walke, K. Rambhad, Y. Nandanwar, and M. Mohan, "Performance evaluation of energy storage system coupled with flat plate solar collector using hybrid nanofluid of CuO+Al2O3/water," *J. Phys. Conf. Ser.*, vol. 1913, no. 1, 2021, doi: 10.1088/1742-6596/1913/1/012067.

[34] M. Ghalandari, A. Maleki, A. Haghighi, M. Safdari Shadloo, M. Alhuyi Nazari, and I. Tlili, "Applications of nanofluids containing carbon nanotubes in solar energy systems: A review," *J. Mol. Liq.*, vol. 313, p. 113476, 2020, doi: 10.1016/j.molliq.2020.113476.

[35] T. Yousefi, F. Veisy, E. Shojaeizadeh, and S. Zinadini, "An experimental investigation on the effect of MWCNT-H 2O nanofluid on the efficiency of flat-plate solar collectors," *Exp. Therm. Fluid Sci.*, vol. 39, pp. 207–212, 2012, doi: 10.1016/j.expthermflusci.2012.01.025.

[36] R. Das, S. B. Abd Hamid, M. E. Ali, A. F. Ismail, M. S. M. Annuar, and S. Ramakrishna, "Multifunctional carbon nanotubes in water treatment: The present, past and future," *Desalination*, vol. 354, no. November, pp. 160–179, 2014, doi: 10.1016/j.desal.2014.09.032.

[37] D. Anin Vincely and E. Natarajan, "Experimental investigation of the solar FPC performance using graphene oxide nanofluid under forced circulation," *Energy Convers. Manag.*, vol. 117, pp. 1–11, 2016, doi: 10.1016/j.enconman.2016.03.015.

[38] M. Vakili, S. M. Hosseinalipour, S. Delfani, S. Khosrojerdi, and M. Karami, “Experimental investigation of graphene nanoplatelets nanofluid-based volumetric solar collector for domestic hot water systems,” *Sol. Energy*, vol. 131, pp. 119–130, 2016, doi: 10.1016/j.solener.2016.02.034.

[39] F. E. B. Bioucas, S. I. C. Vieira, M. J. V. Lourenço, F. J. V. Santos, and C. A. Nieto de Castro, “Performance of heat transfer fluids with nanographene in a pilot solar collector,” *Sol. Energy*, vol. 172, no. May, pp. 171–176, 2018, doi: 10.1016/j.solener.2018.05.040.

[40] M. Eltaweel and A. A. Abdel-Rehim, “Energy and exergy analysis of a thermosiphon and forced-circulation flat-plate solar collector using MWCNT/Water nanofluid,” *Case Stud. Therm. Eng.*, vol. 14, no. February, p. 100416, 2019, doi: 10.1016/j.csite.2019.100416.

[41] N. Akram *et al.*, “An experimental investigation on the performance of a flat-plate solar collector using eco-friendly treated graphene nanoplatelets–water nanofluids,” *J. Therm. Anal. Calorim.*, vol. 138, no. 1, pp. 609–621, 2019, doi: 10.1007/s10973-019-08153-4.

[42] O. A. Alawi, H. Mohamed Kamar, A. R. Mallah, S. N. Kazi, and N. A. C. Sidik, “Thermal efficiency of a flat-plate solar collector filled with Pentaethylene Glycol-Treated Graphene Nanoplatelets: An experimental analysis,” *Sol. Energy*, vol. 191, no. August, pp. 360–370, 2019, doi: 10.1016/j.solener.2019.09.011.

[43] S. Gupta *et al.*, “Comparative performance analysis of flat plate solar collectors with and without aluminium oxide-based nano-fluid,” *Mater. Today Proc.*, vol. 46, no. xxxx, pp. 5378–5383, 2020, doi: 10.1016/j.matpr.2020.08.797.

[44] W. S. Sarsam, S. N. Kazi, and A. Badarudin, “Thermal performance of a flat-plate solar collector using aqueous colloidal dispersions of graphene nanoplatelets with different specific surface areas,” *Appl. Therm. Eng.*, vol. 172, no. February, p. 115142, 2020, doi: 10.1016/j.applthermaleng.2020.115142.

[45] O. A. Hussein, K. Habib, A. S. Muhsan, R. Saidur, O. A. Alawi, and T. K. Ibrahim, “Thermal performance enhancement of a flat plate solar collector using hybrid nanofluid,” *Sol. Energy*, vol. 204, no. April, pp. 208–222, 2020, doi: 10.1016/j.solener.2020.04.034.

[46] L. A. Tagliafico, F. Scarpa, and M. De Rosa, “Dynamic thermal models and CFD analysis for flat-plate thermal solar collectors - A review,” *Renew. Sustain.*

Energy Rev., vol. 30, pp. 526–537, 2014, doi: 10.1016/j.rser.2013.10.023.

[47] S. K. Verma, A. K. Tiwari, and D. S. Chauhan, "Experimental evaluation of flat plate solar collector using nanofluids," *Energy Convers. Manag.*, vol. 134, pp. 103–115, 2017, doi: 10.1016/j.enconman.2016.12.037.

[48] Y. Tong, X. Chi, W. Kang, and H. Cho, "Comparative investigation of efficiency sensitivity in a flat plate solar collector according to nanofluids," *Appl. Therm. Eng.*, vol. 174, no. April, 2020, doi: 10.1016/j.applthermaleng.2020.115346.

[49] M. Faizal, R. Saidur, S. Mekhilef, and M. A. Alim, "Energy, economic and environmental analysis of metal oxides nanofluid for flat-plate solar collector," *Energy Convers. Manag.*, vol. 76, pp. 162–168, 2013, doi: 10.1016/j.enconman.2013.07.038.

[50] R. Nasrin, M. A. Alim, and S. R. Ahmed, "Comparative study between 2D and 3D modeling of nanofluid filled flat plate solar collector," *Int. J. Heat Technol.*, vol. 34, no. 3, pp. 527–536, 2016, doi: 10.18280/ijht.340326.

[51] E. Farajzadeh, S. Movahed, and R. Hosseini, "Experimental and numerical investigations on the effect of Al2O3/TiO2[sbnd]H2O nanofluids on thermal efficiency of the flat plate solar collector," *Renew. Energy*, vol. 118, pp. 122–130, 2018, doi: 10.1016/j.renene.2017.10.102.

[52] N. K. C. Sint, I. A. Choudhury, H. H. Masjuki, and H. Aoyama, "Theoretical analysis to determine the efficiency of a CuO-water nanofluid based-flat plate solar collector for domestic solar water heating system in Myanmar," *Sol. Energy*, vol. 155, pp. 608–619, 2017, doi: 10.1016/j.solener.2017.06.055.

[53] S. Shamshirgaran, M. K. Assadi, H. H. Al-Kayiem, and K. V. Sharma, "Energetic and exergetic performance of a solar flat-plate collector working with cu nanofluid," *J. Sol. Energy Eng. Trans. ASME*, vol. 140, no. 3, 2018, doi: 10.1115/1.4039018.

[54] S. A. Farshad, M. Sheikholeslami, S. H. Hosseini, A. Shafee, and Z. Li, "Nanofluid turbulent forced convection through a solar flat plate collector with Al2O3 nanoparticles," *Microsyst. Technol.*, vol. 25, no. 11, pp. 4237–4247, 2019, doi: 10.1007/s00542-019-04430-2.

[55] M. R. Saffarian, M. Moravej, and M. H. Doranehgard, "Heat transfer enhancement in a flat plate solar collector with different flow path shapes using nanofluid," *Renew. Energy*, vol. 146, pp. 2316–2329, 2020, doi: 10.1016/j.renene.2019.08.081.

[56] S. P. Aghili Yegane and A. Kasaeian, “Thermal performance assessment of a flat-plate solar collector considering porous media, hybrid nanofluid and magnetic field effects,” *J. Therm. Anal. Calorim.*, vol. 141, no. 5, pp. 1969–1980, 2020, doi: 10.1007/s10973-020-09710-y.

[57] A. Allouhi and M. Benzakour Amine, “Heat pipe flat plate solar collectors operating with nanofluids,” *Sol. Energy Mater. Sol. Cells*, vol. 219, no. October 2020, p. 110798, 2021, doi: 10.1016/j.solmat.2020.110798.

[58] M. Bezaatpour and H. Rostamzadeh, “Simultaneous energy storage enhancement and pressure drop reduction in flat plate solar collectors using rotary pipes with nanofluid,” *Energy Build.*, vol. 239, p. 110855, 2021, doi: 10.1016/j.enbuild.2021.110855.

[59] M. Bezaatpour and H. Rostamzadeh, “Design and evaluation of flat plate solar collector equipped with nanofluid, rotary tube, and magnetic field inducer in a cold region,” *Renew. Energy*, vol. 170, pp. 574–586, 2021, doi: 10.1016/j.renene.2021.02.001.

[60] H. Nabi, M. Pourfallah, M. Gholinia, and O. Jahanian, “Increasing heat transfer in flat plate solar collectors using various forms of turbulence-inducing elements and CNTs-CuO hybrid nanofluids,” *Case Stud. Therm. Eng.*, vol. 33, no. February, p. 101909, 2022, doi: 10.1016/j.csite.2022.101909.

[61] A. Fattahi, “Numerical simulation of a solar collector equipped with a twisted tape and containing a hybrid nanofluid,” *Sustain. Energy Technol. Assessments*, vol. 45, no. April, p. 101200, 2021, doi: 10.1016/j.seta.2021.101200.

[62] J. F. Cerón, J. Pérez-García, J. P. Solano, A. García, and R. Herrero-Martín, “A coupled numerical model for tube-on-sheet flat-plate solar liquid collectors. Analysis and validation of the heat transfer mechanisms,” *Appl. Energy*, vol. 140, pp. 275–287, 2015, doi: 10.1016/j.apenergy.2014.11.069.

[63] L. S. Sundar, M. K. Singh, V. Punnaiah, and A. C. M. Sousa, “Experimental investigation of Al2O3/water nanofluids on the effectiveness of solar flat-plate collectors with and without twisted tape inserts,” *Renew. Energy*, vol. 119, pp. 820–833, 2018, doi: 10.1016/j.renene.2017.10.056.

[64] S. K. Verma, A. K. Tiwari, S. Tiwari, and D. S. Chauhan, “Performance analysis of hybrid nanofluids in flat plate solar collector as an advanced working fluid,” *Sol. Energy*, vol. 167, no. April, pp. 231–241, 2018, doi: 10.1016/j.solener.2018.04.017.

[65] R. Sadri *et al.*, “Study of environmentally friendly and facile functionalization of graphene nanoplatelet and its application in convective heat transfer,” *Energy Convers. Manag.*, vol. 150, pp. 26–36, 2017, doi: 10.1016/j.enconman.2017.07.036.

[66] Z. Huang, Z. Y. Li, and W. Q. Tao, “Numerical study on combined natural and forced convection in the fully-developed turbulent region for a horizontal circular tube heated by non-uniform heat flux,” *Appl. Energy*, vol. 185, pp. 2194–2208, 2017, doi: 10.1016/j.apenergy.2015.11.066.

[67] Y. Cao, H. Ayed, M. Hashemian, A. Issakhov, F. Jarad, and M. Wae-hayee, “Inducing swirl flow inside the pipes of flat-plate solar collector by using multiple nozzles for enhancing thermal performance,” *Renew. Energy*, vol. 180, pp. 1344–1357, 2021, doi: 10.1016/j.renene.2021.09.018.

[68] A. L. Antony, S. P. Shetty, N. Madhwesh, N. Yagnesh Sharma, and K. Vasudeva Karanth, “Influence of stepped cylindrical turbulence generators on the thermal enhancement factor of a flat plate solar air heater,” *Sol. Energy*, vol. 198, no. September 2019, pp. 295–310, 2020, doi: 10.1016/j.solener.2020.01.065.

[69] E. Vengadesan and R. Senthil, “A review on recent developments in thermal performance enhancement methods of flat plate solar air collector,” *Renew. Sustain. Energy Rev.*, vol. 134, no. September, p. 110315, 2020, doi: 10.1016/j.rser.2020.110315.

[70] Y. I. C. Bock Choon Pak, “Hydrodynamic and Heat Transfer Study of Dispersed Fluids With Submicron Metallic Oxide,” *Exp. Heat Transf. A J. , Therm. Energy Transp. , Storage , Convers.*, no. January 2013, pp. 37–41, 2013.

[71] Y. Xuan and W. Roetzel, “Conceptions for heat transfer correlation of nanofluids,” *Int. J. Heat Mass Transf.*, vol. 43, no. 19, pp. 3701–3707, 2000, doi: 10.1016/S0017-9310(99)00369-5.

[72] I. M. Shahrul, I. M. Mahbubul, S. S. Khaleduzzaman, R. Saidur, and M. F. M. Sabri, “A comparative review on the specific heat of nanofluids for energy perspective,” *Renew. Sustain. Energy Rev.*, vol. 38, pp. 88–98, 2014, doi: 10.1016/j.rser.2014.05.081.

[73] F. C. Li, J. C. Yang, W. W. Zhou, Y. R. He, Y. M. Huang, and B. C. Jiang, “Experimental study on the characteristics of thermal conductivity and shear viscosity of viscoelastic-fluid-based nanofluids containing multiwalled carbon nanotubes,” *Thermochim. Acta*, vol. 556, pp. 47–53, 2013, doi:

10.1016/j.tca.2013.01.023.

[74] M. Corcione, “Empirical correlating equations for predicting the effective thermal conductivity and dynamic viscosity of nanofluids,” *Energy Convers. Manag.*, vol. 52, no. 1, pp. 789–793, 2011, doi: 10.1016/j.enconman.2010.06.072.

[75] N. Akram *et al.*, “Experimental investigations of the performance of a flat-plate solar collector using carbon and metal oxides based nanofluids,” *Energy*, vol. 227, 2021, doi: 10.1016/j.energy.2021.120452.

[76] Z. Said, R. Saidur, M. A. Sabiha, A. Hepbasli, and N. A. Rahim, “Energy and exergy efficiency of a flat plate solar collector using pH treated Al2O3 nanofluid,” *J. Clean. Prod.*, vol. 112, pp. 3915–3926, 2016, doi: 10.1016/j.jclepro.2015.07.115.

[77] Z. Said, R. Saidur, M. A. Sabiha, N. A. Rahim, and M. R. Anisur, “Thermophysical properties of Single Wall Carbon Nanotubes and its effect on exergy efficiency of a flat plate solar collector,” *Sol. Energy*, vol. 115, pp. 757–769, 2015, doi: 10.1016/j.solener.2015.02.037.

[78] M. H. Ahmadi, A. Mirlohi, M. Alhuyi Nazari, and R. Ghasempour, “A review of thermal conductivity of various nanofluids,” *J. Mol. Liq.*, vol. 265, no. 2017, pp. 181–188, 2018, doi: 10.1016/j.molliq.2018.05.124.

[79] Y. Xuan and Q. Li, “Heat transfer enhancement of nanofluids,” *Int. J. Heat Fluid Flow*, vol. 21, no. 1, pp. 58–64, 2000, doi: 10.1016/S0142-727X(99)00067-3.

[80] P. C. Mishra, S. Mukherjee, S. K. Nayak, and A. Panda, “A brief review on viscosity of nanofluids,” *Int. Nano Lett.*, vol. 4, no. 4, pp. 109–120, 2014, doi: 10.1007/s40089-014-0126-3.

[81] K. Bashirnezhad *et al.*, “Viscosity of nanofluids: A review of recent experimental studies,” *Int. Commun. Heat Mass Transf.*, vol. 73, pp. 114–123, 2016, doi: 10.1016/j.icheatmasstransfer.2016.02.005.